AN INVESTIGATION INTO THE FLOW OF GASES AROUND LONGWALL TOP COAL CAVING FACES AND GAS DRAINAGE TRIALS AT COAL MINE VELENJE

Sergej Jamnikar

Doctoral Dissertation
Jožef Stefan International Postgraduate School
Ljubljana, Slovenia

Supervisor: Prof. Sevket Durucan, Imperial College, London, United Kingdom
Co-Supervisor: Dr. Simon Zavšek, Premogovnik Velenje, Slovenia

Evaluation Board:
Prof. Milena Horvat, Chair, IPS and Institute Jožef Stefan, Ljubljana, Slovenia
Prof. Nives Ogrinc, Member, IPS and Institute Jožef Stefan, Ljubljana, Slovenia
Prof. Anna Korre, Member, IPS and Imperial College, London, United Kingdom

MEDNARODNA PODIPLOMSKA ŠOLA JOŽEFA STEFANA
JOŽEF STEFAN INTERNATIONAL POSTGRADUATE SCHOOL



Sergej Jamnikar

AN INVESTIGATION INTO THE FLOW OF GASES AROUND LONGWALL TOP COAL CAVING FACES AND GAS DRAINAGE TRIALS AT COAL MINE VELENJE

Doctoral Dissertation

RAZISKAVA PLINSKIH MIGRACIJ OKOLI ŠIROKOČELNIH ODKOPOV IN RAZPLINJEVANJE V PREMOGOVNIKU VELENJE

Doktorska disertacija

Supervisor: Prof. Sevket Durucan

Co-Supervisor: Dr. Simon Zavšek

Ljubljana, Slovenia, September 2016

To my family and friends.

Acknowledgments

This Doctoral Dissertation is a result of doctoral studies at the Jožef Stefan International Postgraduate School Ljubljana with cooperation of the Imperial College London and the research work in Premogovnik Velenje.

I would like to express my greatest and sincere gratitude to my supervisor, Professor Sevket Durucan for his support, scientific discussions and countless advices during research work and Thesis preparation.

At the same place I am especially grateful to Professor Aleksandra Kornhauser Fraser for her encouragement and motivation throughout my Doctoral Studies.

My most sincere thanks go to Dr. Simon Zavšek for his support, guidance and friendship as Industrial supervisor and to Professor Anna Korre for her optimism and all of her supportive thoughts.

I would like to thank to the management of Premogovnik Velenje, d.d. for the financial and overall support of my studies and allowing me to perform numerous experiments, measurements and tests.

Special thanks goes to the Jožef Stefan International Postgraduate School for providing excellent study courses, student conferences and overall study assistance.

Thanks to colleagues and camarades at the Coal Mine Velenje who helped me carry out the research work, experiments, measurements and kept me motivated: Mag. Ludvik Golob, Dr. Jerneja Sedlar, Ivo Zadnik, Robert Lah, Gregor Uranjek, Dragica Smrečnik, Igor Veber, Igor Janžovnik, Anton Firer, Mitja Kamenik, Martin Mravljak and the complete drilling team for their technical assistance, suggestions countless solutions during research work in the mine of Premogovnik Velenje d.d..

I extend my thanks to project partners: Dr. Ji-Quan Shi, Dr. Guanyao Si and Dr. Amer Syed from Imperial College London for data interpretations and guidance into scientific approach, Dr. Grzegorz Mutke, Dr. Adam Lurka and Robert Siata from Central Mining Institute of Poland for undertaking the microseismic measurements, Kerstin Abraham from KUTEC, Germany for performance of seismic tomography measurements, and researchers Dr Miloš Markič and Dr. Tjaša Kanduč for many discussions about geology and coal seam gasses.

The research work was carried out by part funding from the European Commission Research Fund for Coal and Steel (RFCS), Grant No: RFCR-CT-2010-00002. “Development of Novel Technologies for Predicting and Combating Gas Outbursts and Uncontrolled Emissions in Thick Seam Coal Mining (CoGasOUT)” and the Seventh Framework Programme Energy Project, Grant Agreement No. 268194, “Greenhouse Gas Recovery from Coal Mines and Coalbeds for Conversion to Energy (GHG2E)”. The author would like to express his gratitude to the European Commission for funding this research.

My doctoral studies and research were strongly supported and motivated by my family and therefore I express my eternal gratefulness to my mother Sonja, my life companion Nina and my late uncle Matjaž.

Many thanks for keeping me going on also to my dearest friends: Nils, Pavli, Walter, Uroš, Ben and Matej.

Abstract

Underground coal mining has been affected by gas related hazardous events and accidents from the first attempts to excavate economical quantities of coal. Despite the developments in mining engineering technology over the centuries and safety measures taken, mine gas related accidents are still the cause of fatalities in underground mines worldwide.

In the case of Coal Mine Velenje, gas related events (excessive emissions, gas outbursts and methane explosions) caused many accidents in the early and mid-20th century. With the development of mining equipment and strict mining regulations, working environment became less hostile, however, the presence of mine gases in the lignite seam still present a safety risk for the workforce and excessive gas emissions interrupt production for longer periods of time causing an economic loss.

The lignite seam in Velenje has a unique geological characteristic with its 160 metres thickness, covering an area of more than 20 km^2. Another feature is the heterogeneous lithotype composition with a mixture of xylite and detrite in different ratios and at random distribution within the seam. Research has shown that, associated with lithotype and relative position in the lignite seam, gas content of carbon dioxide – methane mixture is relatively high with specific emissions of up to 23 m^3/tonnes of mined coal (12.96 m^3/tonnes CO_2, 9.96 m^3/tonnes CH_4 in the first mining level and 5 – 10 m^3/tonnes on average). Based on the results of ventilation air gas concentration measurements and gas composition sampling in monitoring boreholes, the ratio of mine gasses vary from 1.27:1 to 3.78:1 in favour of carbon dioxide.

Research described in this thesis aimed at improving the understanding of the stress and gas pressure build up conditions which lead to coal and gas outbursts and increased gas emissions in longwall top coal caving (LTCC) faces at Coal Mine Velenje through laboratory and field investigations and theoretical development. The field and laboratory experimental research were designed to generate valuable data to underpin the development of gas outburst monitoring and prevention technologies in and around the production faces. Research led to the development and implementation of seam gas pressure monitoring, improved seam gas composition, rock stress and ventilation gas monitoring methodologies, advanced time-lapse P-S wave tomography and advanced passive microseismic techniques for the monitoring and characterisation of lithology, stress, gas pressure and permeability conditions leading to gas outbursts. Furthermore, the findings of research enabled the use of these space and time dependent characteristics towards the development and testing of gas drainage designs for LTCC faces.

The above listed developments are the novel aspects of this research and have not been previously tested or developed in the context of coal and gas outbursts in ultra-thick coal seams mined using LTCC mining.

Povzetek

Podzemno pridobivanje premoga so od samega začetka organiziranega pridobivanja spremljale težave in nesreče, povezane z premogovimi plini. Ne glede na razvoj rudarstva skozi stoletja ter vpeljavo zakonsko določenih varnostnih ukrepov, je premogov plin še vedno razlog za številne smrtne žrtve v podzemnih premogovnikih po svetu.
V prvi polovici in sredini 20. stoletja so v Premogovniku Velenje dogodki povezani s plinom (presežene emisije, plinski izbruhi, eksplozije metana) povzročili številne nesreče. Delovno okolje v premogovniku je z razvojem rudarske opreme in stroge rudarske zakonodaje postalo manj nevarno, vendar premogov plin v sloju še vedno predstavlja nevarnost za zaposlene in vzrok za izgubo proizvodnje.
Velenjski lignitni sloj je z velikostjo preko 20 km^2 in največjo debelino 160 metrov edinstven v geološkem smislu. Posebnost je tudi izrazita heterogena litotipna sestava z mešanicami ksilita in detrita v različnih razmerjih in naključno porazdelitvijo v sloju. Rezultati raziskav so pokazali, da so vsebnosti plinskih mešanic povezane z litotipom ter relativno lokacijo v sloju Specifična vsebnost plina v premogu znaša do 23 m^3/tono pridobljenega premoga (12.96 m^3/tono CO_2, 9.96 m^3/tono CH_4 na prvem nivoju odkopavanja in 5 – 10 m^3/tono v povprečju). Glede na rezultate spremljave plinskih koncentracij v zračilnem toku in analize vzorčenega plina v vrtinah se razmerje premogovih plinov spreminja, in sicer od 1.27:1 to 3.78:1 v korist ogljikovega dioksida.
Raziskave v obliki teoretičnih osnov, laboratorijskih eksperimentov in meritev v jami premogovnika, opisane v doktorski disertaciji, so bile usmerjene k izboljšanju razumevanja sprememb napetostnega stanja in tlaka premogovega plina, kar lahko privede do plinskih izbruhov in povečanih plinskih emisij pri širokočelnem odkopavanju v Premogovniku Velenje. Eksperimenti in meritve so bile zasnovane z namenom pridobiti kvalitetne podatke, ki predstavljajo temelj za razvoj spremljave plinskih izbruhov in preventivnih ukrepov na in v okolici odkopnih čel. Raziskave so se nadaljevale z razvojem metodologije za spremljavo tlaka plina, izboljšanja metodologij spremljave plinske sestave, hribinskih napetosti in koncentracij plina v zračilnem toku ter s seizmično (P-S valovno) tomografijo in pasivnimi mikroseizmičnimi meritvami za spremljavo in določanje litilogije, hribinskih napetosti, tlaka plina in sprememb permeabilnosti, kar lahko vodi k plinskim izbruhom. Z rezultati raziskav in meritev navedenih časovno in prostorsko pogojenih parametrov je bila kot končni rezultat razvita in testirana metoda razplinjevanja za širokočelne odkope.
Navedeno delo predstavlja nove poglede v razvoju metodologije in še ni bilo uporabljeno v sklopu obvladovanja izbruhov plina in premoga v debelih slojih premoga, kjer se uporablja širokočelna odkopna metoda.

Contents

Acknowledgments vii

Abstract ix

Povzetek xi

Contents xiii

List of Figures xv

List of Tables xix

Abbreviations xxi

Symbols xxiii

1 Introduction and objectives 1
1.1 Objectives 1
1.2 Thesis Structure 3

2 Review of relevant literature 5
2.1 Coal as a reservoir rock 5
2.2 Flow of gases around longwall faces in coal mines 6
2.3 Gas outbursts and excessive gas emissions 6
2.4 Field measurements 7
2.5 Gas emission prediction in coal mines 8
2.6 Active and passive seismic monitoring in coal mines 10
2.6.1 Active seismic tomography 10
2.6.2 Passive seismic tomography 14
2.7 Review of gas drainage methods in coal mining 16

3 Coal Mine Velenje 19
3.1 Coal Mine Velenje outline 19
3.2 Origin and geological structure of the lignite seam 20
3.3 Lithotype composition of Velenje lignite 21
3.4 Velenje Mining Method 23
3.5 Gas emission patterns at Coal Mine Velenje 24
3.5.1 Examples of gas emissions monitoring 25
3.6 Review of previous research at Coal Mine Velenje 28

4 Design and implementation of in situ stress, gas pressure and concentration measurements 29
4.1 General layout and field measurement principles 29
4.2 In situ seam gas concentration measurements 29
4.2.1 Examples of seam gas concentration monitoring 31
4.3 In situ gas pressure measurements 34
4.3.1 Examples of seam gas pressure monitoring results 36
4.4 In situ stress measurements 41
4.4.1 Examples of in situ stress monitoring 44

5 Design and implementation of in situ gas content measurements 47
5.1 In situ gas content measurements 47
5.2 A new in situ gas content interpretation methodology 50

6 Design and implementation of active seismic monitoring campaigns 55
6.1 Active seismic tomography 57
6.2 Active seismic tomography at longwall panel C k.-50 57
6.3 Active seismic tomography at longwall panel B k.-130 61
6.4 Conclusions from the seismic tomography campaigns 65

7 Design and implementation of passive seismic monitoring campaigns 67
7.1 Microseismic monitoring 67
7.2 Microseismic monitoring campaigns at Coal Mine Velenje 68
7.2.1 Use of passive tomography in detecting areas prone to outbursts and uncontrolled emissions 70
7.2.2 Analysis of microseismic monitoring data to predict build-up of uncontrolled emissions 73
7.3 Conclusions from the microseismic monitoring campaigns 75

8 Design and implementation of gas drainage trials at Coal Mine Velenje 77
8.1 Drainage system and monitoring equipment during pilot drainage trials (Longwall panel F k. -65) 77
8.1.1 Pilot gas drainage trials and data analysis 81
8.2 Full scale gas drainage trials (Longwall panel D k. -65) 87
8.2.1 Full scale gas drainage trials and data analysis 91
8.2.2 Conclusions of full scale gas drainage trials 96

9 Conclusions 99
9.1 Main conclusions 100

References 103

Bibliography 109
Publications Related to the Thesis 109
Conference Paper 109

List of Figures

Figure 2.1: Schematic of cleat system and dual-porosity coal structure (after Shi and Durucan, 2005)..... 5
Figure 2.2: Gas transport processes and flow priciples in coal seams (after Ahsan, 2006). 6
Figure 2.3:(a) Numerically simulated maximum and minimum principal stresses, and (b) mean stress and permeability profiles around a 500 m deep longwall face (after Durucan, 1981)..... 9
Figure 2.4: The S-wave velocity field across the longwall coal panel at Velenje coal mine reported from the initial tomographic measurements (grid block size = 5 m).14
Figure 2.5: The distribution of micro-seismological activity during an intensive gas emission event (after Majewska and Marcak, 1989)..... 15
Figure 2.6: Relationship between P-wave velocity and pressure determined in the laboratory (after Dubinski, 1989). 15
Figure 2.7: Gas drainage methods (after Lunarzewski, 2001). 16
Figure 2.8: A schematic representation of different gas drainage techniques used for the drainage of coal seam gas (after Si, 2015) 17
Figure 3.1: Generalised map of Slovenia and location of Velenje 19
Figure 3.2: Geological composition of the Velenje basin and surroundings (after Brezigar, 1986). 20
Figure 3.3: Schematic geological cross section of the Velenje lignite seam in direction SW – NE (after Veber, Premogovnik Velenje). 21
Figure 3.4: Schematic representation of Velenje soft coal lithotypes, coal forming environment and known outburst environments (after Markič, 2009)..... 22
Figure 3.5: Lithotype components of the Velenje lignite as visible in horizontally drilled borehole cores (after Markič, 2009)..... 23
Figure 3.6: Schematic representation of multiple level (multiple slice) longwall top coal caving lignite excavation. 24
Figure 3.7: Schematic of mining sequence in multiple levels within coal seam. Simultaneous mining in levels within parts of mine ensure maximum mining performance and total seam exploitation..... 25
Figure 3.8: Gas concentrations in return ventilation air at longwall face C k. -50..... 26
Figure 3.9: Calculated specific gas emission pattern at longwall face C k. -50..... 27
Figure 3.10:Schematic presentation of CO_2/CH_4 ratio for seismic tomography area (longwall face C k. -50)..... 27
Figure 4.1: Schematic representation of monitoring borehole layout for 2011 - 2013. 30
Figure 4.2: Schematic of the seam gas composition monitoring borehole. 31
Figure 4.3: Gas concentration at borehole jpk 62 (+10°)/12; longwall panel F k. -65. 32
Figure 4.5: Gas concentration at borehole jpk 56 (+10°)/13; longwall panel G3/C..... 33
Figure 4.4: Gas concentration monitoring at borehole jpk 49 (+10°)/12 longwall panel B k.-130. 34
Figure 4.6: Schematic view of the seam gas pressure monitoring borehole..... 35
Figure 4.7: In seam gas pressure monitoring location equipped with a pressure probe, pressure gauge and a temperature probe installed. 35
Figure 4.8: Seam gas pressure measurement data in borehole jpk 34 (+2°)/11; longwall panel C k. -50. 36
Figure 4.9: Seam gas pressure measurement data in borehole jpk 34 (+2°)/11 and rock stress change in borehole jgm 39 (-2°)/11; longwall panel C k. -50..... 37
Figure 4.10:Seam gas pressure measurement data in borehole jpk 39 (+2°)/11; longwall panel A k. -5..... 38

Figure 4.11: Goaf gas pressure measurement data in borehole jpk 40 (+60°)/11; longwall panel A k. -5. 38
Figure 4.12: Seam gas pressure measurement data in borehole jpk 79 (+10°)/14; longwall panel D k. -65. 39
Figure 4.13: Schematic view of gas drainage boreholes E2 (+10°)/13 and E2 (+20°)/13; longwall panel E k. -65. 40
Figure 4.14: Results of gas pressure build up experiments at boreholes E2 (+10°)/13 and E2 (+20°)/13; longwall panel E k. -65. 41
Figure 4.15: Schematic representation of an in situ stress monitoring borehole. 42
Figure 4.16: Generalised representation of stress distribution over the longwall panel and the rib pillar in relation to the longwall face advance based on multiple stress monitoring campaigns. Gas drainage efficiency is significantly affected by the rock stress conditions as they develop. 43
Figure 4.17: Rock stress state development measurements in both orientations (vertical and horizontal) in borehole jgm 55 (-2°)/12; longwall panel B k. -130. 44
Figure 4.18: Rock stress development measurements in both directions (vertical and horizontal) at borehole jgm 60 (-2°)/13; longwall panel F k. -65. 45
Figure 5.1: Modified equipment for desorption experiments; (a) in situ desorption and lost gas content determination equipment, (b) laboratory desorption equipment, at Coal Mine Velenje. 48
Figure 5.2: Details of the newly designed modified equipment for desorption experiments; (a) in situ desorption and lost gas content determination equipment, (b) laboratory desorption equipment, at Coal Mine Velenje. 48
Figure 5.3: Locations of samples for in situ gas content measurements at Coal Mine Velenje. 49
Figure 5.4: Example gas desorption measurement for a lignite sample at Coal Mine Velenje. 49
Figure 5.5: Example gas desorption experiment results for a number of samples tested at Coal Mine Velenje in 2012. 51
Figure 5.6: (a) Pure gas and (b) mixed gas isotherms for lignite from Coal Mine Velenje (Durucan et al., 2014). 52
Figure 5.7: Mixed gas isotherms based upon the measured pure gas isotherms (Durucan et al., 2014). 52
Figure 5.8: Estimation of lost gas volume with the USBM method (Sample JPK 62-1) 52
Figure 5.9: Estimation of lost gas volume with the USBM method (Sample JPK 62-3). 53
Figure 5.10: Estimation of lost gas volume by fitting to a 3rd order polynomial. 54
Figure 6.1: (a) Cross section A-A' along the face line, (b) Longitudinal sections taken along the intake and return gateroads of the longwall district C K.-50. 56
Figure 6.2: Mine outline with longwall panel C k. -50 (Mine Pesje – Coal Mine Velenje). Seismic tomography area is marked with red rectangle. 58
Figure 6.3: (a) Seismic tomography measurement team from the Coal Mine Velenje and K-UTEC), (b) Geophone layout for seismic tomography measurements. 59
Figure 6.4: Longwall panel C k.-50 P-wave velocity tomogram for the 1st measurement during the2011 campaign (x component) (Courtesy of K-UTEC and the CoGasOUT Project). 60
Figure 6.5: Longwall panel C k.-50 P-wave velocity tomogram for the 2nd measurement during the 2011 campaign (x component) (Courtesy of K-UTEC and the CoGasOUT Project). 60
Figure 6.6: Longwall panel C k.-50 P-wave velocity difference between 2nd and 1st measurements in 2011 (x component) (Courtesy of K-UTEC and the CoGasOUT Project). 61
Figure 6.7: Mine outline with longwall panel B k. -130 (Mine Preloge – Coal Mine Velenje). Seismic tomography area is marked with dashed blue rectangle. 61
Figure 6.8: Structural map of longwall B k.-130 showing the faults identified (Scale 1:1,000). 62
Figure 6.9: P-wave velocity tomogram of the 1st measurement at longwall face B k.-130 (y component) (Courtesy of K-UTEC and the CoGasOUT Project). 63
Figure 6.10: P-wave velocity tomogram of the 2nd measurement at longwall face B k.-130 (y component) (Courtesy of K-UTEC and the CoGasOUT Project). 63
Figure 6.11: B k.-130 P-wave velocity difference between 2nd and 1st measurements in 20112 (y component) (Courtesy of K-UTEC and the CoGasOUT Project) 64

Figure 6.12: The Vp/Vs ratio difference tomogram between 2nd and 1st measurements at longwall face B k.-130 taken during the 2012 campaign (Courtesy of K-UTEC and the CoGasOUT Project). 64
Figure 7.1: Microseismic monitoring equipment: (a) The low frequency DLM-2001 geophone probe and (b) DLM-SO surface data receiver. 68
Figure 7.2: The distribution of the seismic stations and the spatial configuration of the sensors used for microseismic study in longwall faces C k.-50 and A k.-130 at Coal Mine Velenje..... 69
Figure 7.3: Schematic of (a) the geophone probe installation, (b) the data transmission system..... 69
Figure 7.4: Daily seismic activity, seismic energy and face advance at the longwall panel K-50/C in coal mine Velenje during the period 7 July to 14 September 2011 (Courtesy of GIG and the CoGasOUT Project). 70
Figure 7.5: Bent-ray tomography P wave velocity images obtained using seismic events recorded during consecutive monitoring periods at longwall C k.-50 in Coal Mine Velenje (units m/s) (Courtesy of GIG and the CoGasOUT Project). 71
Figure 7.6: Bent-ray tomography P wave velocity images for longwall A k.-130 in Coal Mine Velenje during three consecutive months as face retreated towards the SE direction (units m/s) (Courtesy of GIG and the CoGasOUT Project). 72
Figure 7.7: Seismic stations and the configuration of sensors used for microseismic monitoring and ventilation measurements at LTCC panel C k. -50 in Coal Mine Velenje. 73
Figure 7.8: (a) The deployment of monitoring techniques in C k. -50 LTCC panel at Coal Mine Velenje (b) an example plot of the spatial distribution of microseismic events at the longwall panel..... 74
Figure 7.9: Spatial evolution of microseismic events leading to an episode of increased gas emission..... 74
Figure 7.10: Histograms and periodic advance of seismic energy released in a production week. 75
Figure 7.11: (a) Gas flow rate and gas concentrations measured during 22 May – 30 August 2011 period, and (b) evolution of fractal dimension versus the flow rate of emitted gas during 22 May – 28 August 2011 in C k. -50 LTCC panel at Coal Mine Velenje..... 75
Figure 8.1: A schematic of the pilot gas drainage trial system in Coal Mine Velenje..... 78
Figure 8.2: Locations of gas drainage and seam gas pressure-composition,rock stress and deformation monitoring boreholes at LTCC panel F k. -65. 79
Figure 8.3: Schematic representation of a drainage borehole construction. 80
Figure 8.4: Connection between drainage borehole and pipeline with 2'' rubber hose and valves and the gas pressure monitoring equipment. 80
Figure 8.5: (a) Gas vacuum pump Nash 2BE1 203 used in gas drainage trials, (b) the whole drainage control and monitoring system along the main gateroad..... 81
Figure 8.6: Detailed layout of the drainage boreholes at longwall face F k. -65..... 81
Figure 8.7: Gas concentration measurements in the pipeline during drainage trials in borehole R3. 83
Figure 8.8: Flow measurements in the pipeline during drainage trials in borehole R3. 83
Figure 8.9: Flow rate response of different gas components to changes in the suction pressure in borehole R3..... 84
Figure 8.10: Flow rate response of different gas components to changes in the suction pressure in borehole R3..... 84
Figure 8.11: Borehole performance comparison between R3 and R4 85
Figure 8.12: Gas concentration and flow rate measurements in the pipeline during multiple borehole drainage trials. 86
Figure 8.13: Flow rates of drained gas during borehole interference testing (CO_2 and CH_4).87
Figure 8.14: Longwall panel D k. -65 outline with main gas drainage installation locations.88
Figure 8.15: Gas drainage system at longwall panel D k. -65. Drainage includes boreholes in panel and steel perforated needles placed between sections of hydraulic shield support. Needles were placed in the goaf (behind shield support) for collecting released gas from consolidating coal..... 89
Figure 8.16: Gas drainage equipment configuration at longwall panel D k. -65. 90
Figure 8.17: a) Drained gas concentration sensors (from left: CO_2 (0 – 100 %), CH_4 (0 – 100 %), CO (0 – 200 ppm)); b) Drained gas pressure and temperature

monitoring (from left: pressure sensor (-1 to 1 bar), pressure gauge (-1 to 5 bar), temperature sensor (0 - 100°C))....90
Figure 8.18: Gas flow analysis of trials by operating boreholes RD-1, RD-2, RD-3, RD-4, RD-5, RD-6 (1st shift drainage) at longwall panel D k. -65.....94
Figure 8.19: Composition of drained gas during trials of operating boreholes RD-1, RD-2, RD-3, RD-4, RD-5, RD-6 (1st shift drainage) at longwall panel D k. -65.....94
Figure 8.20: Gas flow analysis of trials of operating boreholes RD-3, RD-4, RD-5, RD-6 (1st and 2nd shift drainage) at longwall panel D k. -65.....95
Figure 8.21: Composition of drained gas during trials of operating boreholes RD-3, RD-4, RD-5, RD-6 (1st and 2nd shift drainage) at longwall panel D k. -65.....95
Figure 8.22: Gas flow analysis of trials of operating boreholes RD-3, RD-4, RD-5, RD-6 with activation of borehole RD-4 and longwall face needle drainage system (three shift drainage) at longwall panel D k. -65.....96
Figure 8.23: Composition of drained gas during trials of operating boreholes RD-3, RD-4, RD-5, RD-6 (three shift drainage) at longwall panel D k. -65.....96

List of Tables

Table 1.1: Major gas related accidents in period 2010 – 2015 (Wikipedia, 2016). 2
Table 3.1: Results of continious gas emission monitoring on longwall panels. 26
Table 4.1: Results of gas concentration monitoring in borehole jpk 62 (+10°)/12. 32
Table 4.2: Results of gas concentration monitoring in borehole jpk 56 (+10°)/13. 33
Table 5.1: In situ gas content determination experiments at Coal Mine Velenje in 2012. 50
Table 5.2: Langmuir parameters for pure gas adsorption on coal from Coal Mine Velenje. 51
Table 5.3: Analysis and estimation of lost gas volume. 53
Table 8.1: Drainage bore-hole design parameters. 77
Table 8.2: Details of the drainage cycles implemented and the performance achieved during the pilot trials using boreholes R3 and R4.. 82
Table 8.3: Drainage bore-hole design parameters. 88
Table 8.4: Drainage bore-hole design parameters. 91
Table 8.5: Chronology and organisation of full scale gas drainage trials (Longwall panel D k. -65) 93

Abbreviations

ADEMA	...	Research project Advances in Exploration Methods and Applications
ATEX	...	Directive to protect employees from explosion risk in areas with an explosive atmosphere
CBM	...	coalbed methane
CoGasOUT	...	Research project Development of novel technologies for predicting and combating gas outbursts and uncontrolled emission in thick seam coal mining
EPA	...	United States Environmental Protection Agency
EU	...	European Commission
GHG2E	...	Greenhouse gas recovery from coal mines and unmineable coalbeds and conversion to energy
GIG	...	Główny Instytut Górnictwa
jgm	...	rock stress monitoring borehole
jpk	...	seam gas pressure/ composition monitoring borehole
K-UTEC	...	K-UTEC AG Salt Technologies
LTCC	...	longwall top coal caving
NW	...	northwest
P-S	...	longitudinal and shear seismic wave
RFCS	...	Research Fund for Coal and Steel
SE	...	southeast
SOS	...	Seismic Observation System
SW	...	southwest
USBM	...	United States Bureau of Mines
VELGASPREVENT	...	Research project Model for preventive recognition of the geodynamic phenomena in coal mines based on geophysics borehole measurements

Symbols

$\varnothing$	. . . diameter
σ_1	. . . principal stress (vertical component)
σ_3	. . . principal stress (horizontal component)
$<U_{Pm}^2>$	. . . mean value for P-wave
$<U_{Sm}^2>$	. . . mean value for S-wave
a	. . . half length of the crack
A	. . . surface area of the fault
D	. . . matrix of seismic ray path
D	. . . average fault slip
dX	. . . detro-xylite
E	. . . Young's modulus
E_c	. . . potential energy released from failure
E_f	. . . released potential energy
E_r	. . . radiated seismic energy
fD	. . . fine detrite
G	. . . shear modulus
k	. . . seam permeability
K	. . . bulk modulus
L	. . . length
M	. . . number of grids
N	. . . rated speed, span
P	. . . electro-motor power
P_L	. . . Langmuir pressure
P_{x2}-P_{x1}	. . . longitudinal seismic wave velocity difference in x direction
P_{y2}-P_{y1}	. . . longitudinal seismic wave velocity difference in y direction
r	. . . distance between the seismic source and receiver
S	. . . slowness vector
T	. . . seismic wave travel time
t_1, t_2	. . . times bounding a group of P-wave and S-wave
U_P^2, U_S^2	. . . radiation pattern terms
v	. . . excavation height
V_i	. . . gas volume for chosen gas component
V_L	. . . Langmuir volume
Vp	. . . longitudinal seismic wave velocity
V_p/V_s	. . . ratio between longitudinal and shear seismic wave velocity
Vs	. . . shear seismic wave velocity
X	. . . xylite
xD	. . . xylo–detrite
Y_i	. . . gas concentration for chosen gas component
$\Delta\sigma$	. . . stress drop between initial stress and final stress
μ	. . . Poisson's ratio
ρ	. . . rock density, density of medium
σ_f	. . . stress after faulting

σ_n . . . normal stress acting on the crack

Chapter 1

Introduction and objectives

1.1 Objectives

Coal mining has been accompanied by gas related hazardous events since the early activities nearly three centuries ago. Accidents, caused by increased mine gas emissions or sudden gas outbursts, grew in the number together with development of underground mining. Increased production caused larger gas emissions and technologies to provide safety against gas explosions or other gas related accidents did not develop as fast as the production technologies.

Until the middle 20th century, mine gas hazard prevention research mostly included the development of ventilation improvements and equipment upgrades in a way to limit the presence of explosive gas mixtures and possibility of gas explosions. Later on, several attempts towards efficient gas monitoring were undertaken with research in methodologies for gas content determination in coal seams, detection of gas accumulations, rock stress influenced gas behaviour and gas drainage.

Mining with the application of a variant of the Longwall Top Coal Caving (LTCC), mostly in descending slices, experience quite different and unique stress and gas pressure fields around the working coal faces, which lead to uncontrolled emissions and/or outbursts of gas with serious safety and health consequences. Despite all the safety measures implemented, and the targeted research efforts of the last few decades, coal mine gas outbursts, uncontrolled emission and methane explosions are still claiming many lives, and result in significant loss of production in many coal mines worldwide. Indeed, mines exploiting relatively thick and/or steep seams using longwall top coal caving or sublevel caving methods have been experiencing such accidents in particular.

Coal Mine Velenje experienced its last major coal and gas outburst in 2003, when two miners were killed, and the longwall district in question lost one month's worth of production. This loss of production was worth €4.5 million and 4% of the total income of the mine in that year. Besides such major incidents, Coal Mine Velenje experiences at least one uncontrolled gas emission related stoppage each year, losing approximately 5 days-worth of production (35,000 tonnes of coal) per event on average.

Such losses are worth around €1 million and 1% of the annual production each year. During the last five years, excessive gas emissions and resultant stoppages reduced production by 5% and cost the mine €5.25 million in total. High gas emission rates at the production faces require high rate of ventilation and energy consumption. The mine estimates that 10-15% reduction in ventilation costs as a result of reduced gas emissions would save in the region of €1.2 million/year. Furthermore, the seam gas at Velenje is a mixture of CO_2 and CH_4 and, any reduction in the emission of these gasses at this mine, and in other mines in Europe and worldwide, by means of predicting outbursts and uncontrolled emissions and capturing the gasses in advance, would reduce the emissions of greenhouse gases to the atmosphere significantly.

Table 1.1: Major gas related accidents in period 2010 – 2015 (Wikipedia, 2016).

Mine	Country	Year	Fatalities	Mine	Country	Year	Fatalities
Muchonggou mine	China	2000	159	Tunlan	China	2009	77
Chengzihe mine	China	2002	124	Xinfeng mine	China	2009	7
Daping mine	China	2004	148	Shouzhou	China	2009	11
Chenjishan mine	China	2004	166	Tonghua mine	China	2009	30
Sunjiawan mine	China	2005	214	Henan mine	China	2009	67
Xishui mine	China	2005	72	Xinxing mine	China	2009	108
Shenlong mine	China	2005	83	Raspadskaya mine	Russia	2010	66
Dongfeng mine	China	2005	171	Pike river mine	New Zealand	2010	29
Liuguantun mine	China	2005	54	Suhodolskaya -Vostochnaya mine	Ukraine	2011	17
Wayaobao mine	China	2006	27	Sukhodilska–Skhidna mine	Ukraine	2011	17
Linjiazhuang mine	China	2006	50	Xiaojiawan mine	China	2012	45
Jiaojiazhai mine	China	2006	40	Machang mine	China	2013	25
Nanshan mine	China	2006	24	Babao	China	2013	53
Halemba mine	Poland	2006	23	Taozigou	China	2013	28
Ulyanovskaya Mine	Russia	2007	108	Nueva Mina mine	Spain	2013	6
Yubileynaya Mine	Russia	2007	38	Soma	Turkey	2014	302
Hongtong	China	2007	105	Zasyadko mine	Ukraine	2015	23
Zasyadko mine	Ukraine	2007	101	Vorkuta Mine	Russia	2016	36
Huludao	China	2008	16				

In thick seam coal mining, such as tat at Coal Mine Velenje, the primary source of gas emissions and, in most cases, the source of gas outbursts experienced is the coal seam being mined, since both the roof and the floor strata are the thick seam itself. In these operations, the pressure field, gas flow characteristics and gas outburst conditions generated during mining of the virgin sections of the coal differ significantly from conventional flat lying and relatively thinner seam longwall workings. As a result, the thick seam mining methods do not benefit from the application of the well-researched and developed gas drainage techniques widely applied in many European coalfields.

The research presented in this thesis aimed at improving the understanding of the stress and gas pressure build up conditions which lead to coal and gas outbursts and increased gas emissions in LTCC through laboratory and field investigations and theoretical development. Both the field and laboratory experimental research were designed to generate valuable data to underpin the development of gas outburst monitoring and

prevention technologies in and around thick seam coal faces mined using the LTCC method at Coal Mine Velenje.

The research involved the development and implementation of seam gas pressure, improved seam gas composition and rock stress and ventilation gas monitoring methodologies, advanced time-lapse P-S wave tomography and advanced passive microseismic techniques for the monitoring and characterisation of lithology, stress, gas pressure and permeability conditions leading to gas outbursts in coal mines. Furthermore, the findings of research enabled the use of these space and time dependent characteristics towards the development and testing of underground gas drainage designs for LTCC faces.

The above listed developments are the novel aspects of this research and have not been previously tested or developed in the context of coal and gas outburst research in thick coal seams mined using LTCC. In summary, research aimed to investigate:

- lignite deposit geology and lithotypes, seam gas properties and behaviour and rock stress distribution;
- the development of monitoring systems for seam gas pressure, improved monitoring for seam gas composition and rock stress and gas content determination methodology.
- the potential for the use of time lapse seismic tomography techniques for the identification of lithofacies, stress states and gas pressure/volume conditions that are indicators of gas outburst conditions in coal seams;
- the potential for the use of advanced passive microseismic techniques for the monitoring and prediction of coal and gas outburst conditions in coal mines;
- the development and piloting of gas drainage methodology to combat gas outbursts and uncontrolled gas emissions at Coal Mine Velenje.

1.2 Thesis Structure

The research presented in this Thesis was carried out as theoretical background studies and experimental field work underground at Coal Mine Velenje. The field work was carried out with the funding from the EU Commission projects CoGasOUT and GHG2E, partly in collaboration with international partners.

Review of relevant literature is presented in Chapter 2, which includes main objectives and state of the art knowledge associated with the research work. A comprehensive review of coal seam gas properties and dynamics are presented, followed by research into known methods for gas emissision prediction, gas accumulation investigations and gas drainage techniques and methodologies.

Chapter 3 introduces Coal Mine Velenje, where research for the purpose of this Thesis was carried out. A detailed decription of the lignite deposit is presented, followed by descriptions of the Velenje lignite lithotypes, the Velenje longwall top coal caving mining method, gas emission patterns at longwall faces and a review of previous research at Coal Mine Velenje relevant to the research topic.

In Chapter 4, the underground research that was carried out at Coal mine Velenje is described. This Chapter includes implementation of newly designed seam gas pressure monitoring boreholes, improved rock stress measurements, coupled with seam gas pressure monitoring and modified seam gas composition measurements. The results of monitoring campaigns and experimental measurements are presented and discussed in relation to the longwall face advance.

The development of a modified methodology for in situ gas content determination of Velenje lignites is described in Chapter 5. Based on previous experience and an unsatisfactory historical data, a newly developed methodology was tested on lignite samples for direct gas content measurements. The complete methodology for total gas

content determination utilised laboratory experiments carried out at Imperial College London, which were performed for the purposes of project CoGasOUT.

Active and passive seismic monitoring campaigns carried out at three longwall panels as a part of the CoGasOUT project are described in Chapters 6 and 7 respectively. The equipment used in these campaigns were supplied by the research partners who also processed and reported the results. The author of this thesis designed the field installations underground and prepared the necessary technical and safety documents, as well as supervising the work by the partner institutions underground. The processed data provided by the partners were further analysed and interpreted for gas dynamics and rock stress zones to help the design of seam gas drainage layouts trialled at Coal Mine Velenje.

Chapter 8 presents the field research carried out towards the main objective of thesis – the development and implementation of underground seam gas drainage methodology. The seam gas drainage procedures were developed and tested using all the results obtained from field based research described in previous chapters. Initial pilot trials of the gas drainage system were performed as small scale experiments with promising results, which were followed by full scale trials, performed as an additional activity at operating LTCC face.

Finally, Chapter 9 presents the overall conclusions of the research carried out and discuss its accomplishments.

Chapter 2

Review of relevant literature

2.1 Coal as a reservoir rock

Coal structure is a result of distinctive coalification process, which has been influenced by tectonic processes, temperature and strata pressure over the geological periods.

Origin and genesis of the coal deposit has, as a result, a significant role in coal structure and consequently in stored accumulations of coal seam gas.

Coal structure is defined as a system of micropores and macropores, what is often described as dual-porosity system. Micropores in matrix are associated with molecular range and consist of capillaries and cavities in which a significant share of coal seam gas is stored as adsorbed gas (Rogers et al., 2007).

Macroporosity is related to the cleat system as shown in Figure 2.1. Cleats are oriented as two-dimensional system, where continuous face cleats follow the bedding planes and butt cleats connect face cleats as primary fractures in coal.

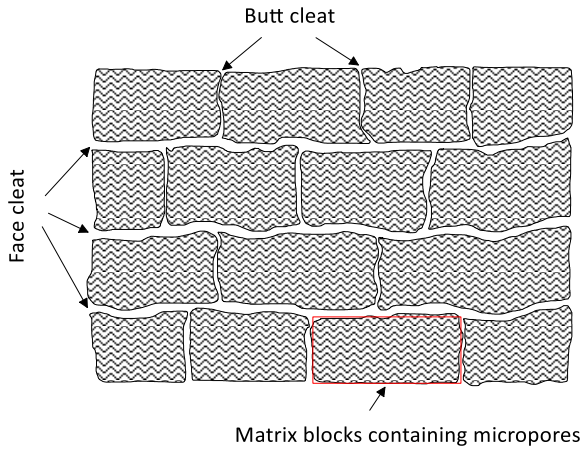


Figure 2.1: Schematic of cleat system and dual-porosity coal structure (after Shi and Durucan, 2005).

Permeability of coal matrix to gas is low. On the other hand, the cleat system permeability is associated with larger volumes of cleat size and represents a path for gas migration.

Ahsan (2006) proposed a model for coal seam gas release and flow in different pore sizes in coal seams, describing the flow principle in every stage (Figure 2.2). Gas flow within the matrix it is limited to desorption and diffusion processes from the internal coal surface and micro pores. Flow characteristics change a gas migrates in the cleat system and main fracture network where it is described by Darcy flow. The process illustrated in Figure 2.2 below describes the gas release mechanism from coal structure when it is being affected by the influence of an advancing longwall face.

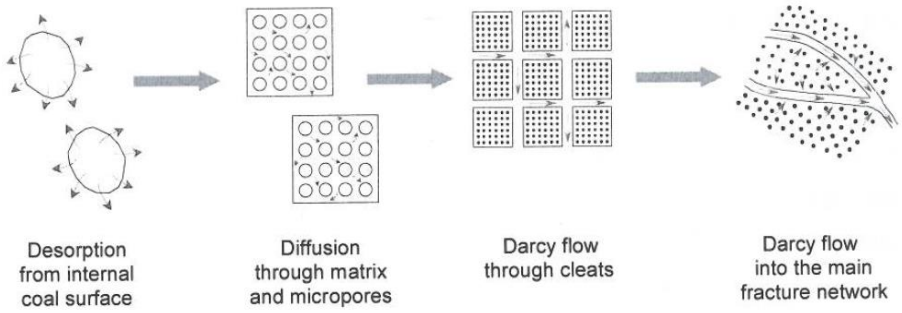


Figure 2.2: Gas transport processes and flow priciples in coal seams (after Ahsan, 2006).

2.2 Flow of gases around longwall faces in coal mines

Gas flow around longwall faces in coal mines relates to the natural properties of coal and is influenced by dynamics of coal excavation. Natural permeability of coal is a function of its heterogeneity, fracture system, porosity, pore size distribution and overall connectivity. It is often assumed that coal represents a dual-porosity reservoir (Pan and Connell, 2012), where gas is stored in the coal matrix (after Harpalani, 1999) and in natural fracture system with different fluid flow properties. According to number of fluid components in the rock, permeability depends on fluids behaviour and composition, therefore, gas effective permeability is related to absolute permeability, fluid saturation and sorption capacities.

Porosity and permeability change as a result of mechanical impacts or sorption processes was studied by many authors, mostly testing stress dependent cleat compressibility (Durucan and Edwards, 1986; Shi and Durucan, 2010) and sorption cleat space swelling and shrinkage (Durucan at al., 2009; Karacan, 2003). Furthermore, several models were developed for understanding stress and/or sorption induced influence on coal compressibility and permeability changes (Gray, 1987; Palmer and Mansoori, 1996, 1998; Shi and Durucan, 2005).

Coal permeability increases after failure due to mechanical effects. As a consequence, migration of coal seam gas is enhanced and desorption process is established.

2.3 Gas outbursts and excessive gas emissions

Since the first documented coal and gas outburst occurred in the Issac Colliery in France (1843), as many as 30,000 outbursts have occurred in the world coal mining industry (Lama and Bodziony, 1998). Taylor (1852–1853), as reported by Lama and Bodziony (1998), was the first to study the phenomenon of sudden gas and coal outbursts, while investigating methane explosions in the Northumberland and Durham coalfields of Northern England.

Outbursts were observed to occur in the immediate vicinity of tectonic disturbances, and the coal involved was soft and of different texture from the nearby coal. Hargraves and Upfold (1985) have also concluded that microstructurally altered coal will lead to higher outburst tendency. Farmer and Pooley (1967) suggested that outbursts only occur in districts subject to severe tectonic movement, hence their association in many places with anthracite and in association with such deformation and depositional structures as folds, faults, rolls and slips and in particular with rapid fluctuations in the seam thickness. Shepherd et al. (1981) reported on outburst occurrences in Australia, North America,

Europe, and Asia, and found that probably over 90% of significant outbursts have been concentrated in the narrow strongly deformed zones along the axes of structures such as asymmetrical anticlines, the hinge zones of recumbent folds, and the intensely deformed zones of strike-slip, thrust, reverse, and normal faults.

An essential element in outbursts is the gas content, which contributes to outbursts in producing gas pressure. Normally, methane or carbon-dioxide pressure provides the energy to propel coal particles from the face during an outburst. Thresholds of 9 m^3/tonne for CH_4 and 6 m^3/tonne for CO_2 are used in the Sydney Basin, Australia, to indicate outburst prone conditions (Beamish and Crosdale, 1998). In China, 10 m^3/tonne methane is used as the outburst threshold and the gas contents in the mines experiencing outbursts are higher than 10 m^3/ton, and generally range from 15 to 25 m^3/tonne coal (Cao et al., 2001).

It is suggested that outburst-prone coal exhibits low permeability. Lama and Bodziony (1998) found that coal seams with in situ permeability >5 mD are not liable to outburst. Other studies (Hargraves, 1993; Lama and Bodziony, 1998) have concluded that stress is an additional contributing factor to outbursts. Kidybinski (1980) took into consideration the gas content and flow, stress, and coal failure to explain his theory of gas outbursts. Williams and Weissmann (1995) referred to the outbursts frequently encountered Australian conditions and stated that "the most important parameter is gas desorption rate, in conjunction with the gas pressure gradient ahead of the face".

In recent years, the CSIRO in Australia carried out a series of research projects investigating coal and gas outbursts. Wold and Choi (1999) developed a coupled geomechanical-flow model and applied to field conditions at a number of Australian coal mines. They concluded that pore fluid pressure and its gradient, which is a function of the reservoir pressure, desorption pressure/isotherm, absolute permeability and relative permeabilities rather than gas content is a key determinant of outburst initiation risk. In a follow up application of the same model (Choi and Wold, 2002) found that, contrary to expectations, coal seams rich in CO_2 were not more outburst prone than seams rich in CH_4. It was suggested that, because of the higher adsorption capacity of coal to CO_2 relative to CH_4 at the same partial pressure, outbursts tend to be initiated at higher gas contents for CO_2 compared to CH_4. In a more recent report and a summary publication (Wold et al., 2008) have reported a numerical study into gas outbursts and suggested that permeability plays a key role in the formation of the pressure gradients within the coal that can lead to failure and gas outbursts. Furthermore, it was concluded that gas outbursts are strongly sensitive to the spatial variation of permeability in the coal seam and moderately sensitive to coal strength variation.

Using in situ borehole pressure measurements, Diaz Aguado and Gonzalez Nicieza (2007) have concluded that the gas outburst occurrences in the Asturias coal basin of Spain were controlled by the mining stresses and gas pressure build up in virgin areas. Except for one outburst incident which occurred in 2003, all other incidents at Coal Mine Velenje were of similar nature, taking place at the longwall face during production, and the majority of these occurring under virgin coal mining conditions (no previous over mining within ~25 metres of the face), indicating stress and pressure build up related mixed gas (CH_4 and CO_2) outbursts.

2.4 Field measurements

Field measurements are a crucial part of research into gas flow around longwall faces where many factors come to play. Understanding this behaviour requires field measurements of seam gas and rock parameters.

2.5 Gas emission prediction in coal mines

Methane drainage or pre-drainage and gas pressure relief around mining operations can partly alleviate the risk of outbursts if the drilling and gas drainage programme is designed based on the understanding of the conditions leading to outbursts. In flat lying and relatively thinner seam longwall coal mine operations methane is emitted from the coal seam being mined and from the surrounding coal seams above and below the mined seam because of increased fracturing and caving into areas of lower pressure. The size of the de-stressed zone, which defines the gas emission zone and the subsequent rate of gas flow into the workings, is dependent on coalface length and height, seam depth and the mechanical and elastic properties of the rock strata.

In thick seam coal mining, the primary source of gas emissions and, in most cases, the source of gas outbursts experienced is the coal seam being mined, since both the roof and the floor strata is the thick seam itself. In these operations, the pressure field, gas flow characteristics and gas outburst conditions generated during mining of the virgin sections of the coal differ significantly from conventional flat lying and relatively thinner seam longwall workings. As a result, the thick seam mining methods do not benefit from the application of the well-researched and developed gas drainage techniques widely applied in many European coalfields.

The European methods of methane prediction used in coal mining mostly adopt the same basic principles and utilise the degree of gas emission function which may vary from country to country depending on the coalfield characteristics they represent. Initially, these methods were based on empirical principles. Later on, Europe wide theoretical developments, field validation and harmonisation efforts were funded mainly through the ECSC funding of collaborative projects during the 70's (MRDE, 1980) and 80's. Each of these methods consider (a) the stratigraphy above and below the worked seam, (b) desorbable gas content of the coal seams, (c) zone of gas emission in the roof and floor strata, and (d) the degree of gas emission.

In the UK, Airey's (1968) experimental investigations into the emission of methane from broken coal, and his mathematical interpretation of this with respect to the state of stresses around longwall faces, formed the basis to the MRDE method of firedamp prediction. This method was progressively fine tuned using extensive field observations. Further details of all European prediction methods based on the degree of gas emission principle can be found in Curl (1978). In a more up to date publication, Noack (1998) described further the principles as applied to methane prediction, drainage systems and outburst control in Europe. The extension of the gas emission zone in the German prediction method is dependent on a parameter quantifying the strength of the strata (Curl, 1978). In practice, the emission zone extends between 164 m to 212 m into the roof and 41 m to 85 m into the floor. In the UK, Airey (1971) estimated a degassing zone of up to 140-160 metres above and 60 metres below the longwall. Noack (1998) suggested that the effect of mining on the strata could extend up to 260 m above and 100 m below the worked seam, the interval from 130 m above to 50 m below being the most affected.

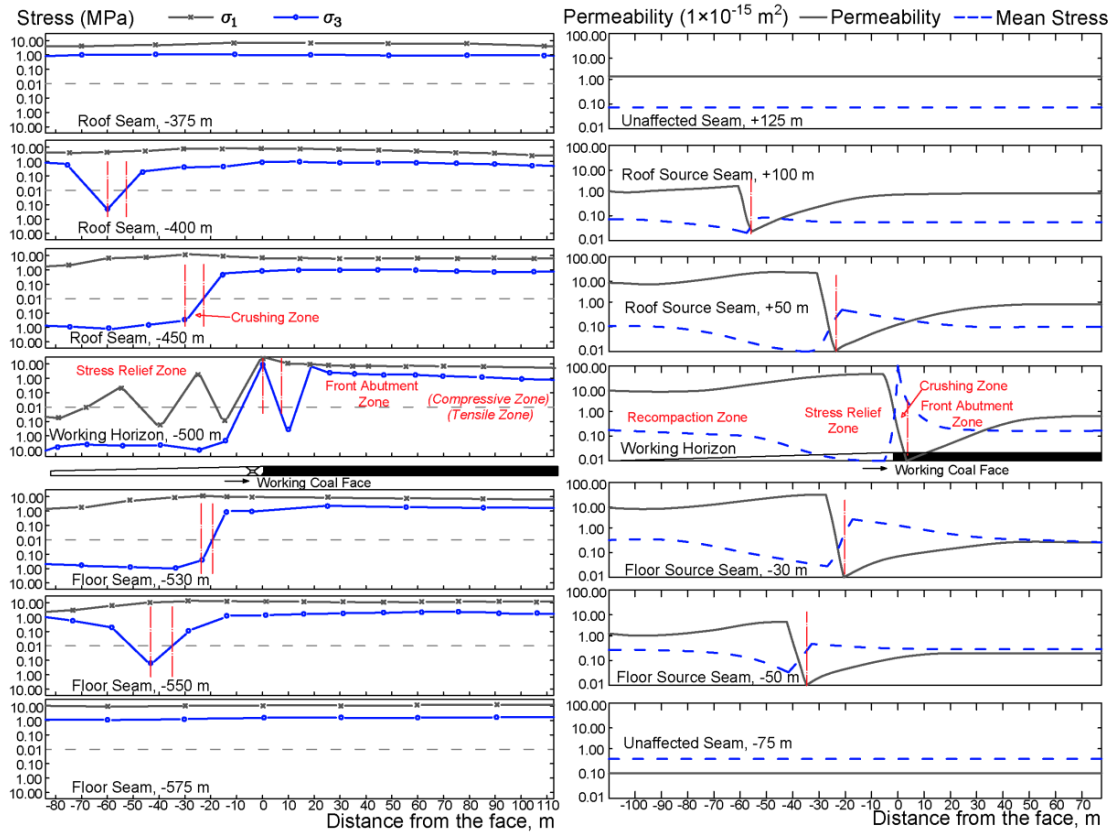
However, these methods were specifically designed for longwall extraction methods in relatively thinner coal seams (generally up to 4m thick) where the coal seams mined are overlain/underlain by coal measure rocks. Therefore the above estimates of gas emission zones are not applicable to ultra-thick or steeply dipping thick seam coal mining cases where the LTCC method is applied, and where both the roof and floor strata are predominantly coal.

Although the empirically developed methane prediction methods have successfully been applied in most coalfields, these methods are not necessarily portable and may not be applied accurately at every coalfield. An alternative approach to gas flow and outburst prediction involves stress analysis and the use of coupled geomechanical and fluid flow

simulators, the application of which helps to improve our understanding of the mechanisms that control these processes.

As a background to such geomechanical models, a conceptual description of the state of stresses and stress abutments formed around a longwall faces was proposed (Whittaker, 1974) and later validated through numerical studies by several researchers (Durucan, 1981; Ren and Edwards, 2000; Whittles et al., 2006). Durucan (1981) used his numerically derived stress states to further describe the resulting permeability zones and gas flow paths around longwall faces (Figure 2.3).

Esterhuizen and Karacan (2005) described the application of a finite difference model to develop a geomechanical model that predicts permeability changes within the rock mass. The calculated permeabilities were used as input to a reservoir simulator which models methane desorption from the coal matrix, methane release from the layers and flow towards the mine excavations. This approach was applied to a number of coal mines operating in the Northern Appalachian Coalfield and the findings were published as Guidelines for the Prediction and Control of Methane Emissions on Longwalls by the US National Institute for Occupational Safety and Health (NIOSH) (Schatzel et al., 2008). Another recent publication worth referring to is by Unver and Yasitli (2006) which describes a numerical modelling study on strata movement and fracture zone development around thick seam Top Coal Caving Longwall faces.



(a) (b)

Figure 2.3:(a) Numerically simulated maximum and minimum principal stresses, and (b) mean stress and permeability profiles around a 500 m deep longwall face (after Durucan, 1981).

2.6 Active and passive seismic monitoring in coal mines

Seismic velocity tomography is a noninvasive technology. Seismic methods are an established tool to investigate geological formations. By transmission of acoustic waves through the rock, lithological parameters and structural information can be gained. Velocity tomography is accomplished by propagating seismic waves through a rock mass to measure velocity distribution of the rock mass. The main information is the spatial distribution of the wave velocity. Tomograms are created by mapping this velocity distribution and relative stress in the rock mass can be inferred. From seismic velocities other petrophysical parameters can be derived under good conditions and depending on the lithology.

While seismic tomography has been applied frequently in oil and gas exploration and in earthquake studies the application is far less prevalent in the mining industry. In the early days, seismic tomography measurements have been used in coal mines mainly to detect voids, to image structures and/or old workings from one general location in the mine (e.g., face areas of mains and panel developments) well ahead of planned developments (Hanson et al., 2002). This reduced the need to drill probe-holes. However, most studies used P-waves for the tomography.

2.6.1 Active seismic tomography

Active seismic tomography is a special seismic method, whereby the transmitters and the receivers of the seismic waves can be placed on different sides of a longwall panel. The result of the measurement is the distribution of the seismic velocity in a plane. Seismic tomography allows for inference of stress distribution through a velocity image. Measurements in the past have been concentrated to P-waves. In the EU RFCS funded CoGasOUT project, P-waves (compressional waves) and S-waves (shear waves) were measured. The measurement of P-wave and S-wave velocities can give even more information, since their response to many rock parameters is different.

When seismic tomography is applied to mining, active sources are generally used. Active sources have also been implemented repeatedly to image individual pillars in underground mines (Scott and Williams, 2004; Watanabe and Sassa, 1996). Tunnels have also been imaged to determine stress distribution around an excavation implementing both passive (Maxwell and Young, 1996) and active sources.

The aforementioned studies were conducted on a relatively small scale where active sources and optimum source-receiver placement are fairly easy to implement. There are fewer large scale mine studies in the literature. Friedel et al. (1997) used active sources to span drifts and image high velocity in working faces. Roof bolt mounted receivers have been implemented with a longwall shearer as a source to image a section of a longwall panel (Westman et al., 2001). An earlier study was able to image velocity on a longwall panel and show that high velocity areas advanced with the longwall face (Kormendi et. al., 1986).

The energy released in an outburst is from accumulated strain energy in the coal, roof or floor. Numerous factors have been stated to influence the occurrence of bumps, including properties of coal, geology (joints, folds, faults, etc.), mining induced stresses, strong sandstone beds in the roof, pillar size and shape, mining technique and mining rate (Westman et al., 2001). Seismic tomography carried out in the past in the mining industry has been used to image geological features as well as stress-related features. More recently it was started to investigate whether the diverse information could be used to increase understanding of mining-induced stress redistribution in coal mines. The method has been adapted to image stress concentrations ahead of a longwall face by a unique application of the longwall mining equipment as the seismic source.

Westman et al. (2001) reports a seismic tomography study which was carried out in a longwall coal mine in the western United States. Results from this were correlated with data from pressure measurements on the longwall shield legs across the face and data form a seismic monitoring network in an effort to increase understanding of mining-induced stress redistribution and bump potential. The study showed a correlation between averaged tomogram values and seismically active areas and demonstrated that the tomography system is capable of imaging heavy shield-leg loading and outburst-prone conditions prior to them disrupting the face operation.

In Westman's study the longwall shearer was used as seismic source and geophones were mounted on roof bolts in the gate roads. Mine personnel generated 3 tomograms each day. Therefore the tomograms are representative of conditions in the strata above the coal seam. The tomograms displayed geological features in the roof. The target of research in CoGasOUT was the coal seam itself, not the roof rock. However, this study indicated clearly that high stress areas correlate to areas with high P-wave velocities. And the high stress areas indicated in seismic tomograms correlate very well with the most seismically active areas indicating by the monitoring network. The disadvantage for using a shearer as seismic source is that this is only one of the seismic noises generated in an operating mine (as well as the belt conveyer, shearer itself, shields, machines…).

Usually P-waves were measured in seismic tomography. Westman (1994) described one case study in which the stress distribution in a portion of an underground longwall coal mine was imaged with compressional and shear wave travel time tomography. Two surveys were completed across a 215 m wide panel of coal, the first when the working face was 25 m from the survey area, and the second after the face was within 8 m of the survey area. Sources were placed on one side of the panel and receivers at 6 m intervals each on the other. Three very interesting results were reported:

1. The in-situ shear wave velocity distributions correlated very well with stress measurements taken at point locations with conventional mining instrumentation.
2. The in-situ shear wave velocity tomogram displayed the distribution of stresses very well.
3. The in-situ P-wave velocity tomogram did not correlate as well with the theoretical and measured stresses indicating a lower sensitivity to in situ stress changes.

Laboratory testing of rocks have shown that P-wave velocity increases slightly with initial axial stress. Prior to the peak stress the elastic wave velocity begins to decrease rapidly as microcracks propagate (Paterson and Wong, 1978), so that an increase in velocity would be indicative of an increase in stress, but a decrease in velocity is not necessarily indicative of failure; it may be a pre-failure indicator. This indicates changes in P-wave velocity are largely due to changes in fractures and porosity (Thill, 1973). Other factors also affect the P-wave velocity, including fluid saturation which can increase the wave velocity (Thoksoz et. al., 1976) and preferred orientation of cracks/fractures which can give rise to velocity anisotropy. It is vital that the velocity-stress relationship is carefully considered when using velocity tomograms to make inferences about relative stress in a mine. Laboratory ultrasonic wave velocity measurements of different types of coal have demonstrated that their dynamic elastic properties depend on coal rank and applied effective pressure.

Zheng et. al. (1991) measured ultrasonic velocities on relatively “undisturbed” coal samples concurrently with triaxial and hydrostatic compression. The coal used in this research was surface mined and hence was assumed to be degassed. Effects of saturation on coal static-dynamic behaviour were also examined. P-wave velocity increases as the level of saturation increases. S-wave velocities decreased as the level of saturation increased. It is hypothesized that this is due to the cleat/fracture system in the coal, arguing that the pore fluid damped S-wave propagation by reducing the solid-solid contact area. With higher cleat porosity, more reduction in S-wave velocity might be expected,

when pore fluid is present. At constant confining stress, an increase in pore pressure also reduces the S-wave velocity because higher pore pressure can induce more separation of fracture surfaces and less contact area. Based on elastic equations from which dynamic Young's modulus and Poisson's ratio were derived, an increase in V_P and a decrease in V_s with increasing saturation yielded an increased value for Poisson's ratio and either an increased or decreased value for elastic modulus, depending on the degree of change in P and S wave velocities. Limited evidence suggested that the most significant reduction in shear wave velocity may take place at relatively low saturation levels. When saturation reaches a certain level, reduction in the S-wave velocity levels out. On the low porosity coal tested, this saturation level is speculated to be less than 42%.

Yu et. al. (1993) described laboratory measurements of P- and S-waves on Permian coals from Wollongong, New South Wales, Australia. They pointed out that Ultrasonic compressional- and shear-wave velocities in coal specimens are sensitive to confining pressure changes, with increases in dry specimens typically 20 percent for P-waves and by 13 percent for S-waves as confining pressure increases from 2.0 MPa to 40 MPa. P-wave velocities are also strongly affected by water saturation, while S-wave velocities are barely affected by water saturation. On average, compressional wave velocity increases by 23 percent and shear wave velocity decreases by 1.5 percent with water saturation at atmospheric pressure. This behaviour is attributed to the presence of thin cracks, particularly through the influence of pore medium bulk modulus on the effective bulk modulus and P-wave velocity of the material. Measurements of P-wave velocity in water-saturated coal specimens as functions of changes in hydrostatic confining pressure and pore pressure indicate that the changes in confining pressure are not entirely cancelled by equivalent changes in pore pressure. This may be caused by the influence of total pressure on the intrinsic moduli of the coal framework (Yu et. al., 1993). There are large increases of amplitude and peak frequency of P-waves, and smaller increases in the energy and peak frequency of S-waves, with increasing confining pressure and with water saturation. Both P-wave and S-wave attenuation decreases significantly with increasing confining pressure in dry and water-saturated coal specimens, apparently caused by the low, predominantly crack-like, porosity of coal. There is marked P-wave attenuation decrease and small S-wave attenuation increase in fully water-saturated coal specimens. Velocity measurements across, at 45 degrees to, and along bedding planes, show that weak, transversely isotropic, velocity anisotropy exists in coal specimens. P-wave and SH-wave velocities parallel to bedding planes are 10-15 percent and 4-8 percent higher than velocities perpendicular to bedding planes, respectively. The velocity difference with specimen orientation in both air dried and water saturated coal specimens is virtually independent of confining pressure up to 40 MPa, indicating that it is the result of intrinsic anisotropy of the coal structure rather than of anisotropic crack distribution. Velocity dispersion across bedding planes is much smaller than along bedding planes (Yu et. al., 1993).

In a laboratory study by Morcote et. al. (2010) velocities were measured in core plugs parallel and perpendicular to lamination surfaces as a function of confining pressure up to 40 MPa in loading and unloading cycles. P- and S-wave velocities increased as coal rank increased. Bituminous coal and cannels have shown lower velocities than higher ranked coals such as semi anthracite and anthracite. The V_p-V_s relationship for dry samples was found to be linear and covers a relatively wide range of effective pressures and coal ranks. There is a pressure dependence on the elastic properties of coal for confining pressures below 5 MPa. This pressure sensitivity is related to the presence of microcracks. Morcote et. al. (2010) pointed out that the data show an intrinsic anisotropy at confining pressures above 5 MPa, the closing pressure for most of the microcracks. This anisotropy at high pressures might to be due to fine lamination and preferred orientation of the macerals.

Xue (2005) took coal samples from Kushiro coal mine, Northeast Hokkaido in Japan and carried out laboratory experiments on coal matrix swelling strain and P-wave velocity changes during CO_2 injection. In a fractured sample the P-wave velocity increased up to 12.7% due to the coal matrix swelling. The increase of P-wave velocity was larger compared to 9.4% which was observed when the sample was subjected to hydrostatic pressure up to 2.5 MPa. The results suggest that the coal matrix swelling caused the cleat closure during CO_2 injection and consequently the coal permeability reduced. The experimental results show that the volumetric swelling strain was about 0.15% due to the CO_2 adsorption and the permeability decreased by about 50% associated with coal matrix swelling in an intact sample.

Previous gas outburst experience and existing data at Coal Mine Velenje (Zavšek et al., 2008) has shown that the gas outbursts are associated with special coal lithotypes that exist in the thick coal deposit. In a previous Eureka Project VELGASPREVENT (3211-06-000386), the application of seismic methods for the detection of lithotypes that are related to the gas outburst have been investigated by Coal Mine Velenje in cooperation with K-UTEC. This project aimed at developing, testing and applying geophysical measurement procedures in long, horizontal, research boreholes to identify different coal lithotypes which relate to coal and gas outbursts. One element of this research involved an investigation into a possible correlation between P-wave velocity and coal properties, such as lithotypes, RQD etc. Seismic P-wave velocity was measured on core samples taken from different parts of the coal seam in the mine. Furthermore, the potential of cross longwall seismic tomography in identifying coal seam properties (which may lead to gas accumulations and/or outburst conditions) was tested and found to be technologically feasible.

Since it is more promising to measure both P-wave and S-wave velocities, these two parameters were determined in the previous research. The drawback of many seismic S-wave sources is their low energy emission and restrictions when used under mining conditions. Therefore, a borehole S-wave vibrator has been developed and tested by K-UTEC. Figure 2.4 below shows the S-wave velocity field in the coal panel in the Velenje coal mine from the initial tomographic measurements. The velocities determined by the tomography measurements agreed remarkably with those determined on core samples in the laboratory.

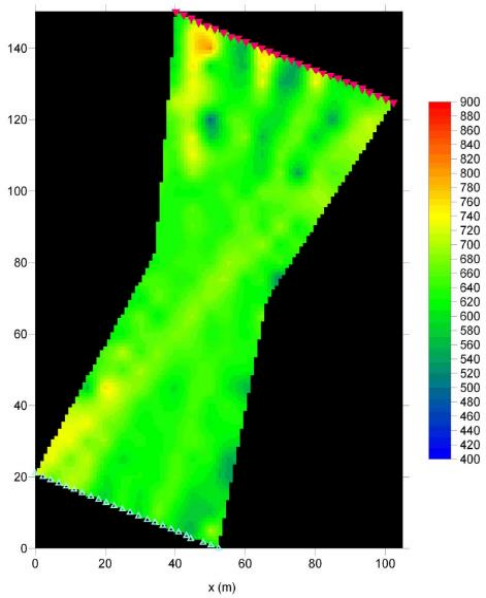


Figure 2.4: The S-wave velocity field across the longwall coal panel at Velenje coal mine reported from the initial tomographic measurements (grid block size = 5 m).

2.6.2 Passive seismic tomography

Fracture formation in rocks is a source of seismo-acoustic waves. It is commonly assumed that the centre of the frequency band, in which seismo-acoustic recordings are performed, is inversely proportional to the length of the fracture which is the source of the seismo-acoustic signal. Therefore, the selection of the frequency band, in which the seismo-acoustic recordings are conducted in coal should be selected very carefully (McKavanagh and Enever, 1977).

Seismo-acoustic activity and permeability of sandstone samples taken from the outburst prone Nowa Ruda mine subjected to traxial state of stresses was measured in the laboratory by Majewska and Marcak (1989). The experiments were carried out in the frequency band 1 to 100 kHz and have shown that fracture formation and propagation, accompanied by a significant increase in permeability, also increased seismo-acoustic emission as a result of fracturing.

Field monitoring of seismo-acoustic emissions in the former Thorez mine, which was classified as gas and rock outburst hazard Category III mine, was conducted at the upper frequency bands of 1 kHz and 16 kHz respectively. Boreholes of approximately 3 m were drilled and sensors installed. The results of these investigations, conducted in two frequency bands, have shown that a large number of seismic signals were recorded in the high frequency band, representing sources as small as the macro-pores in coal (Majewska and Marcak, 1989). Figure 2.5 illustrates that the seismo-acoustic activity takes place irregularly, and that periods of increased activity are preceded by the periods of silence. This example confirms that micro-seismological recording is a good indicator of changes in the thermo-dynamic and hydraulic regime in the rock medium. These measurements have also confirmed that, with increased gas flow, the micro-seismological activity was also much higher than that observed when gas flow/emissions were much smaller.

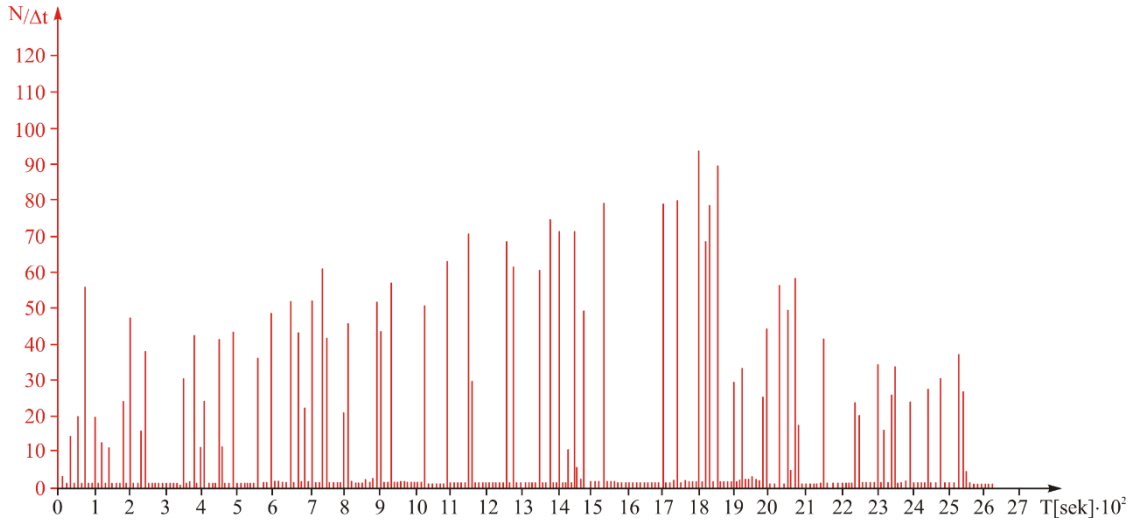


Figure 2.5: The distribution of micro-seismological activity during an intensive gas emission event (after Majewska and Marcak, 1989).

As shown in Figure 2.6, P-wave velocity increases with increase in stress (Kowalczuk and Szwejkowski, 1975), therefore, the measurements of seismic wave velocities are made to estimate the seismic hazards (Dubinski, 1989).

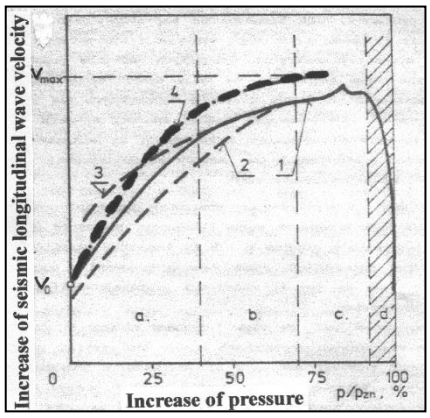


Figure 2.6: Relationship between P-wave velocity and pressure determined in the laboratory (after Dubinski, 1989).

The main observation from the analysis of tomographic P-wave velocity images in the previous RFCS Project ADEMA (RFCR-CT-2005-00001) was the increase of P-wave velocity with an increase of pressure in the rock mass. ADEMA project established a positive correlation between zones of highest P wave velocity (zones of higher stresses) and zones of highest seismic activity and rock burst events. The flameproof automated Seismic Observation System (SOS) and software developed by the Polish Central Mining Institute (GIG) was used to study seismicity and rock-bursts hazard in mines (Mutke et al., 2009). During the RFCS funded COGASOUT project, the P-wave field around a coal production district (LTCC and/or SLC) was studied in space and time, using passive tomography, in order to develop a methodology to monitor and predict stress and gas pressure build up which is believed to lead to gas outbursts.

2.7 Review of gas drainage methods in coal mining

Coal seam gas drainage has been practised in many coal mines since the early 20th century as a safety precaution and, in some cases, the extracted gas is utilised as an energy source. Parallel to the development of mining, gas drainage methods were developed and adopted for distinctive type of coal mine operations.

Drainage of coal seam gas is amongst most common approaches towards mine safety and energy saving improvements, as well as providing an energy source for gas fuelled engines. Several studies (Dunn, 1995, U.S. Environmental Protection Agency, 2009) report widely used methane drainage methodologies within coal deposits prior to and during conventional mining. On the other hand, examples of enhanced coalbed methane (CBM) recovery and CO_2 storage without the involvement of mining where methane is used solely as energy source is also widely discussed in the literature (Ozdemir, 2009).

Surface gas drainage requires drilling of surface boreholes and installation of perforated casing sections to provide sufficient gas flow from coal formations to the drainage boreholes. Generally, surface gas drainage targets mostly methane drainage as its presence represents greater risk for mining operations, which also provides valuable energy source.

Selection of a gas drainage method is based on coal deposit geology and tectonic conditions, seam gas content, coal permeability and economical aspects (Wang and Xue, 2008). In theory, several guidelines for gas drainage are proposed which offer the most appropriate approach for gas drainage according to the geological properties, stage of coal mine development and technical limitations (Lunarzewski, 2001). In general, suggested methods are categorised in two main groups: pre-drainage and post-drainage operations by drilling surface and inseam boreholes and wells. Figure 2.7 below summarises the most commonly used gas drainage techniques in coal mining. Figure 2.8 illustrates these methods schematically.

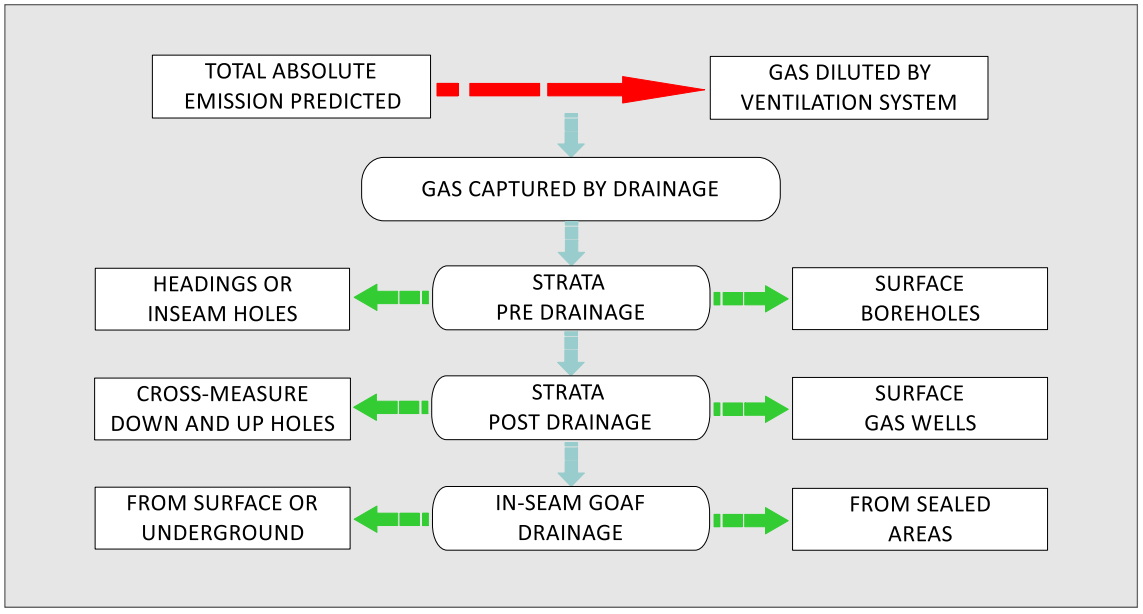


Figure 2.7: Gas drainage methods (after Lunarzewski, 2001).

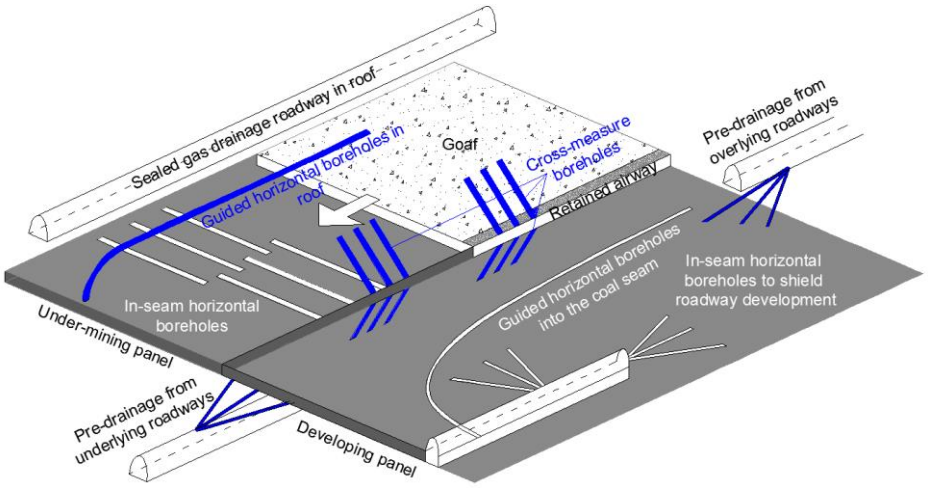


Figure 2.8: A schematic representation of different gas drainage techniques used for the drainage of coal seam gas (after Si, 2015) .

Contrary to surface mining, underground gas drainage is preferably used as safety increase approach towards high gas emission reductions, especially by gate road driving and also during mining (Xia and Xu, 2004, U.S. Environmental Protection Agency, 2009). Gas drainage prior excavation of developed excavation panels reduces uncontrolled gas emissions and possible gas outbursts during long-wall face advance. Varieties of coal types with respect to its distinctive rock mechanics conditions define possibilities of direct or stimulated way of gas drainage which is mostly dependent on coal permeability properties which are often a subject of stress-strain conditions. Dynamic rock stress influence, caused by mining activity usually causes coal permeability increase and accelerates gas migrations.

Chapter 3

Coal Mine Velenje

3.1 Coal Mine Velenje outline

Lignite deposit in the Šalek valley is located North-Western of the town of Velenje in North-central part of Slovenia (Figure 3.1). First written reports of the lignite findings in the Šalek valley are found in Austrian governmental achieves from 1766 and 1767. Historical data of organised coal deposit research for possible production dates in 1875, when systematic research drilling begun after geologists logged nearby rock formations and geothermal water source. In the same year, the main coal seam was proved by drilling.

Mining at Velenje Coal Mine started to develop moderately in the early 20th Century; at the time the consumption of lignite was relatively low. Lignite was used in the thermal power station, local manufacture and as a domestic heating source.

After World War II, as the town of Velenje started to develop and expand in growing population and industry, the need for lignite was increased. Annual production grew rapidly and peaked in 1985, when 5 million tonnes of lignite were excavated. In recent years, the production varies around 4 Mt/a with an average calorific value of around 10.5 MJ/kg.

Currently, the entire annual lignite production is consumed by the nearby 600 MW Šoštanj thermal power plant (TEŠ), which meets around one third of national power supply (Seher, 1995; Žerdin, 2003).

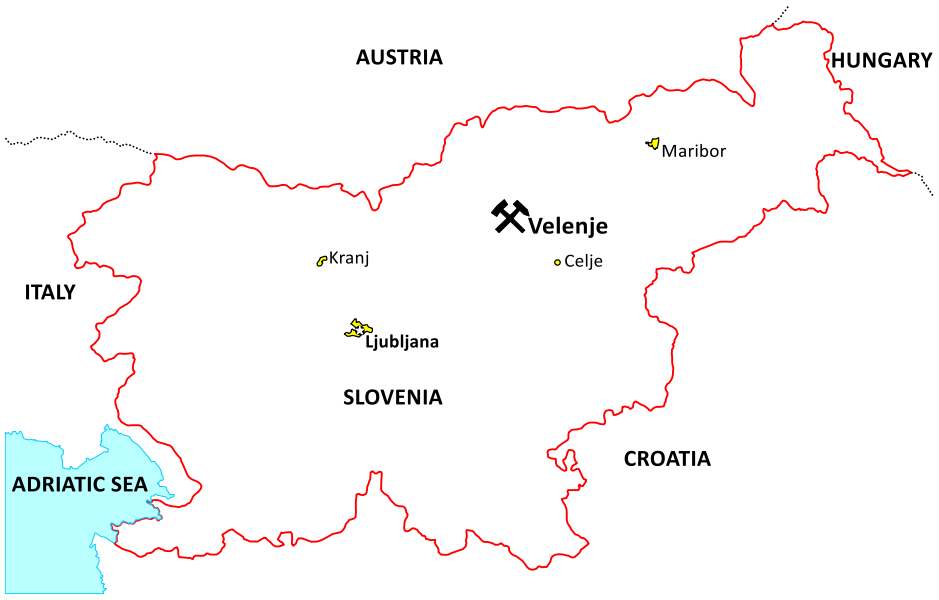


Figure 3.1: Generalised map of Slovenia and location of Velenje

3.2 Origin and geological structure of the lignite seam

The coal basin lies in synclinal valley which extends between the Šoštanj and Smrekovec faults. Coal as well as roof layer of isolative clay and sand were formed in the Pliocene era, which are followed by several layers of younger rock materials. The sequence was caused by subsidence of the area between faults and simultaneous backfilling by continuous alluvial deposits (sand, silt, marl).

Figure 3.2 shows major geological composition of the coal seam and surrounding rock formations in the area which was crucial for coal seam formation. Tectonic depression has been re-modified with several faults in different directions and ages. With its subsidence and constant material (organic, alluvial) accumulations, the depression was formed in its present shape.

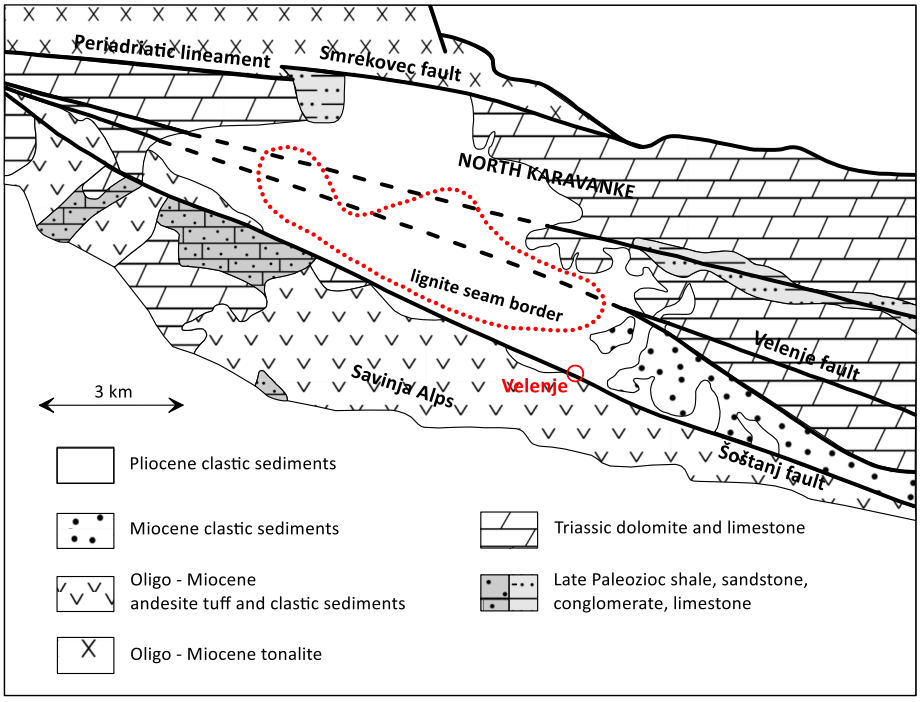


Figure 3.2: Geological composition of the Velenje basin and surroundings (after Brezigar, 1986).

Lignite, as a representative of low rank coal with a limited stage of coalification process, forms the coal deposit in the Velenje basin, which was defined by several investigations and analysis of pollen and mastodont remains in the lignite layers by Šercelj and Rakovec (1968).

The lignite seam is lens shaped with 8.3 km in length and 2.5 km in width and up to 160 m thick. Depth of the lignite seam varies from 200 to 500 m (shallow on seam limits, deeper in the centre), with low quality minor outcrops on eastern border of the seam. Mining concept with longwall top coal (LTCC) caving method in multiple levels was chosen as the most efficient due to extreme seam thickness, depth and geotechnical conditions.

More than 160 surface exploration boreholes were drilled in area of coal seam in order to investigate complete strata distribution. Besides surface drilling, continuous underground drilling is used to prove micro-local geology of lignite seam and the surrounding rock materials, especially aquifers. The complete geological composition (geological column)

over a characteristic cross section over part of lignite seam, where majority of mining operations are held, is shown in Figure 3.3.

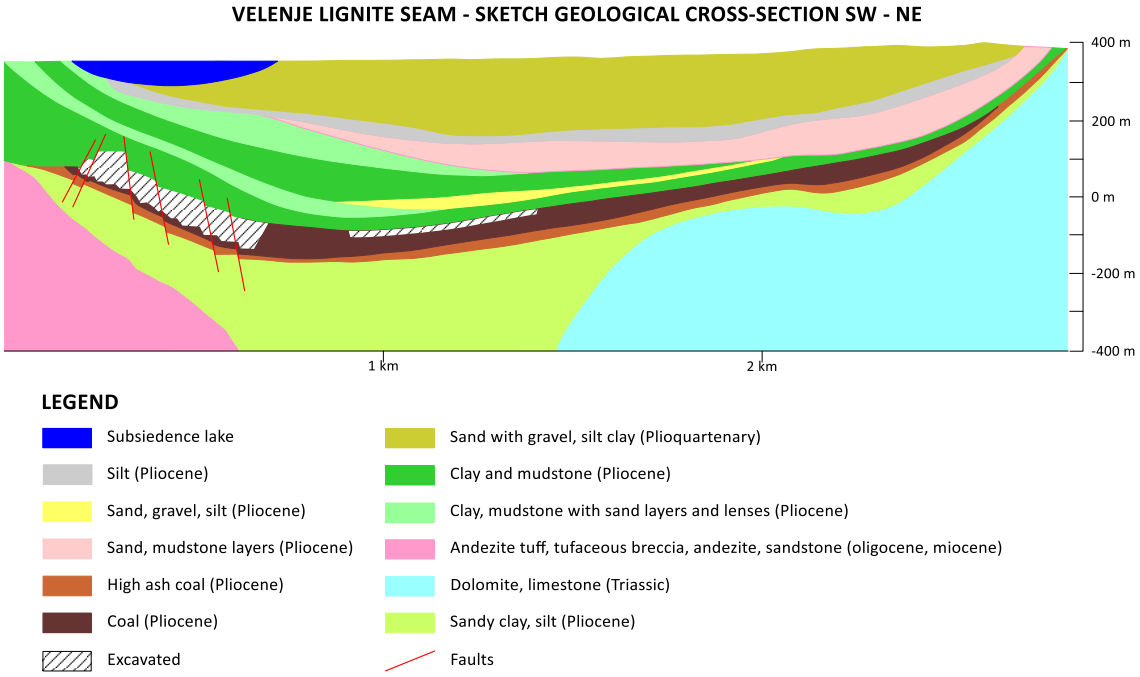


Figure 3.3: Schematic geological cross section of the Velenje lignite seam in direction SW – NE (after Veber, Premogovnik Velenje).

Different depression accumulations represent complete sedimentary cycle, from dry land phase over to swampy phase to lake-phase and return, over swampy phase to dry land. Described sequence has been disturbed by several fluvial sediments (sand and gravel), transported from north and north-east. Onto pre-pliocene beds, which are represented by Triassic dolomite in the North and oligo-miocenic sediments in central and Southern part (lythotamnian limestone and andezite with tuff and breccia), strata of sandy silt and sand and above Triassic strata, red and grey clay has been deposited.

Lignite quality differs according to position in the seam. In lower section, coal-clay represent the border between floor strata and the lignite seam. Therefore, lignite quality in lower part of the seam is relatively low. In the middle and upper sections of the seam the lignite quality (calorific value) increases.

The border between the coal seam and roof strata is clean and consists mostly of marl with fossil intrusions. Upper roof strata are followed by mudstone, clay and silt, which represent water isolation and protection against water inflow from sand and gravel layers above the isolation layer.

Upper roof strata towards the surface consist of clay and mudstone layers with sand and gravel inclusions, sandy mudstone with sand and gravel. The surface layer is represented by alluvial accumulations and weather-beaten materials.

3.3 Lithotype composition of Velenje lignite

Spatial facies analysis and interpretation of coal genesis are almost unimaginable without the lithotype study. Also, a range of problems referring to mining, rock mechanics and gas-dynamics can be effectively described by lithotype treatment of coal because different

lithotypes have different properties. The different lithotypes of the Velenje lignite have different rock-mechanical properties as well as different properties with regard to gas content, sorption, permeability etc.

The main macropetrographic features of the Velenje lignite in terms of ratios between xylitic fragments of very variable dimensions and shapes and fine detrital homogenous matrix are shown in Figure 3.4, which also illustrates the petrographic characteristics in areas where gas outbursts and rock bursts have been observed.

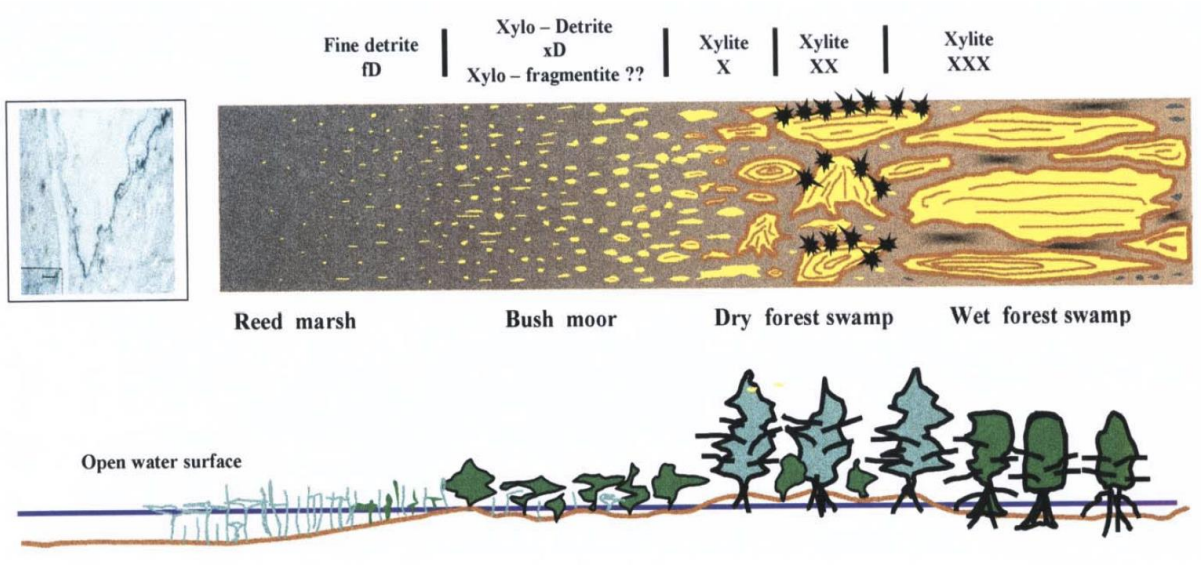
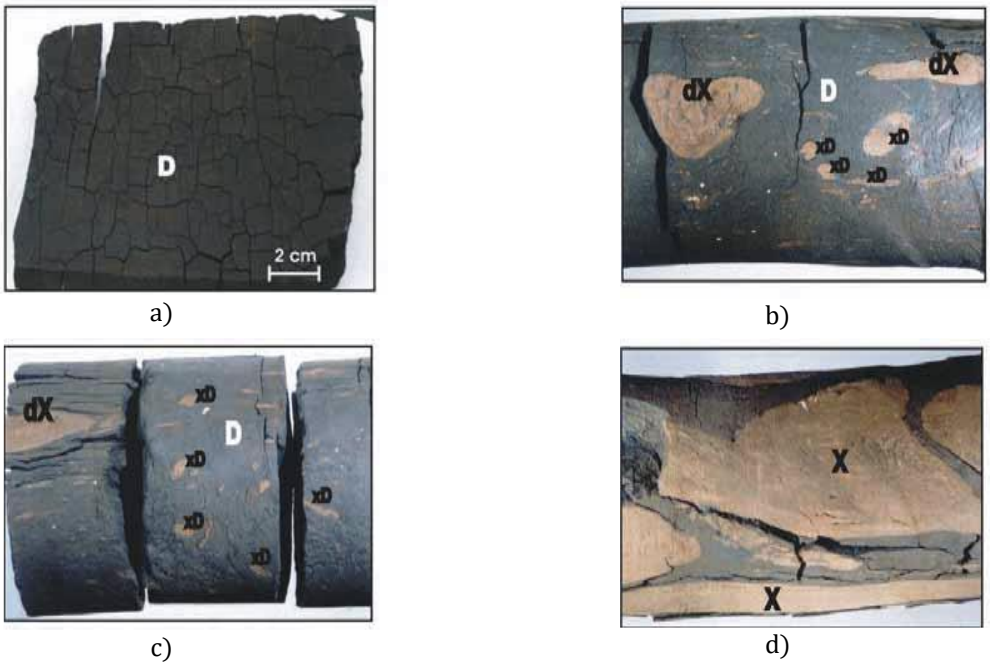


Figure 3.4: Schematic representation of Velenje soft coal lithotypes, coal forming environment and known outburst environments (after Markič, 2009).

The Velenje coal is a type of lignite, more or less rich in xylite fragments, fusinite, and mineral matter. Its matrix is fine-detrital, dark brownish in colour. Petrographic heterogeneity is furthermore expressed by very different sizes, shapes, and orientations of xylitic fragments and by different degrees of gelification affecting more severely the fine-detrital matrix.

Figure 3.5 shows the lithotype components of the Velenje lignite as observed in borehole cores. The macerals and/or microlithotypes of the Velenje lignite are typical as for the soft brown coals or lignites (Markič, 2009).



a) Detrite (D) fine lignite typically crushed and cracked due to desiccation.
b) Xylo-detrite (xD) composed of xylitic pieces smaller than the half of the core diameter.
c) detro-xylite (dX) composed of xylitic pieces bigger than the half of the core diameter within the fine detrital matrix.
d) Xylite (X) as xylitic pieces bigger than the core diameter

Figure 3.5: Lithotype components of the Velenje lignite as visible in horizontally drilled borehole cores (after Markič, 2009).

3.4 Velenje Mining Method

Velenje (longwall) mining method is a variation of known longwall top coal caving mining methods where major coal exploitation is concentrated on top coal mining by means of natural coal fracturing caused by changes in stress and deformation state.

The mining method was developed after observations during coal excavation by conventional longwall mining, equipment testing, in-situ measurements and coupled analysis and technical design on which safety criteria (Kočar et al., 1987) was used as a basis for currently used Velenje Mining Method (Lenart et al., 1996).

The unique lignite seam geometry allows multiple level excavation and top coal caving by a pre-defined sequence in the direction from top layers of seam to the economic border of mineable coal (8.4 MJ/kg calorific value). Distinctive features of different areas (overburden clay seam thickness, water pressure in sand above the lignite layer, relative position of the production panel in lignite seam) dictate the design of planned panel excavation heights. In the current mine design the maximum working heights allowed range between 4 – 15 metres, with a special emphasis on local conditions and limitations.

Figure 3.6 illustrates a generalised conceptual mining layout where excavated coal represents previously mined levels with already consolidated roof strata and mining levels representing the sequence of multiple level coal excavation.

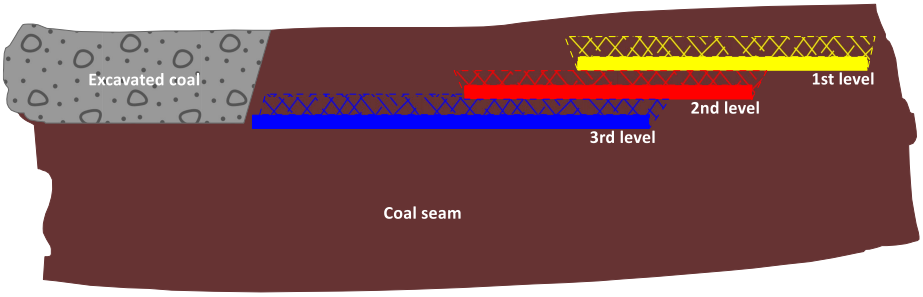


Figure 3.6: Schematic representation of multiple level (multiple slice) longwall top coal caving lignite excavation.

The efficiency of Velenje Mining Method is based on the top coal caving in the upper section of the longwall level/slice (Figure 3.7). Top coal caving from the upper section follows a pre-designed number of face cuts with the shearer and shield support movements. With mining equipment currently used at Coal Mine Velenje, 1 to 2 cuts in solid and 2 to 3 cuts in crushed and deformed coal are required. The rate of longwall face advance is strongly dependent on mine plans and geomechanical conditions of a given location in the seam.

Controlled top coal caving from the upper section is achieved by the breaking of coal over the roof beam and lowering of the hydraulic shield support sections. At the longwall face, coal is transported to the main gateroad by a chain conveyor, where further transport is provided by a belt conveyor.

3.5 Gas emission patterns at Coal Mine Velenje

During the two EU funded research projects CoGasOUT and GHG2E, continuous monitoring of gas emission as a result of coal production at the longwall face was performed at all longwall panels (2009 – 2012). Measurements in all parts of the mine were performed with permanent gas and air velocity sensors placed at the end of return gateroads. Recorded data were stored and processed together with other technological parameters (daily face advance and coal production rate).

Measurements of gas emissions during 2012, during the most extensive campaigns, were carried out at longwall faces A k. –65, B k. –130, F k. –65 and G3/C. The methodology of monitoring and sensors locations on longwall C k. –50 as a representative example are presented in Figure 3.7. This was also the longwall face where the first seismic tomography trial was carried out. Monitoring data in 2012 displayed a common feature where methane concentration in the gas released in to the ventilation air represented a relatively larger share of the total gas emitted when the coal block extracted is located under solid coal as compared to waste rock roof immediately above the Top Coal. The carbon dioxide percentage was much higher at the lowermost levels of the Velenje coal seam.

Historical data have shown that gas concentrations at longwall faces in virgin areas (longwall faces under solid coal roof) exceed gas concentrations at faces in the lower levels by factor of 1.5 – 2.0. Another difference is observed in the CO_2/CH_4 ratio, where the share of carbon dioxide usually exceed the concentration of methane because of extensive top coal caving and increased production. Nevertheless, the location of the longwall panel within the coal seam (the level of mining) generally defines the overall gas emission rates and gas ratios in the ventilation air.

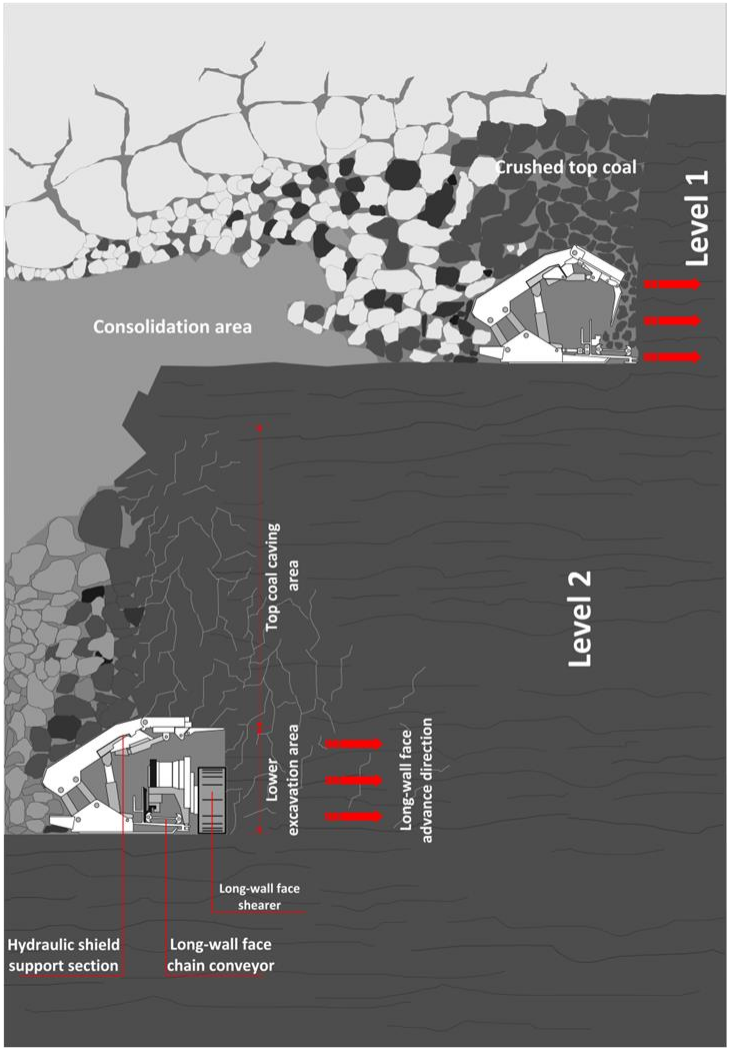


Figure 3.7: Schematic of mining sequence in multiple levels within coal seam. Simultaneous mining in levels within parts of mine ensure maximum mining performance and total seam exploitation.

The specific emissions calculated for each component of released gases per ton of mined coal are the most representative results for the gas emission pattern analysis. Table 3.1 clearly shows that gas emission at longwall panels in virgin and near-virgin areas exceed that experienced bottom level panels when LTCC is applied. Seam gas content in lower levels is reduced as a result of upwards gas migration during the mining of upper levels which results in reduced specific emission as mining moves in to the lower levels.

3.5.1 Examples of gas emissions monitoring

As an example of gas emission monitoring, the setup, methodology and results of the monitoring campaign at operating longwall face C k. -50 is described below. The gas emission rates were monitored over the mining period with sensors placed in the return gateroad and used for further analysis.

Figure 3.8 presents concentrations of methane and carbon dioxide against daily longwall face advance and production over the mining period. The weekly gas release pattern, where gas concentrations rise during the working week and reaching a concentration peak by the end of the week (overall maximum CO_2 5 vol. %, CH_4 3 vol. %), is clearly evident in the figure.

Table 3.1: Results of continious gas emission monitoring on longwall panels.

	Mining level	CO_2 (vol. %)	CH_4 (vol. %)	CO_2/CH_4	CO_2 * (m^3/t)	CH_4 * (m^3/t)	Production (tones)
A k. –5	Seventh	0.85	0.23	3.78	5.95	1.49	6,821.9
A k. –50	Fifth	1.09	0.37	2.93	6.29	2.02	8,685.5
B k. –50	Fourth	1.10	0.32	3.44	4.51	1.11	9,772.4
C k. –50	First/Second	1.79	0.57	3.14	10.81	3.28	7,929.7
A k. –65	Sixth	1.02	0.36	2.83	3.11	1.16	8,874.1
D k. –65	First	1.35	1.06	1.27	12.96	9.96	6,218.2
F k. –65	First	1.53	0.75	2.04	10.91	5.25	4,421.9
A k. –130	Seventh	0.98	0.54	1.81	5.74	3.06	7,257.0
B k. –130	Sixth	1.05	0.37	2.84	4.51	1.64	7,528.5
G2/B	Second	0.67	0.39	1.72	3.08	1.45	2,803.4
G2/C	Second	0.74	0.43	1.72	2.44	1.27	6,931.1
G3/B	Third	0.80	0.40	2.00	3.50	1.50	5,996.4
G3/C	Third	0.80	0.56	1.43	3.13	2.01	6,019.6

* Specific emission rate for each gas is calculated as a ratio of the volume of component gas released to the average daily production rate during production.

Figure 3.9 shows gas capacities, calculated from average daily gas concentrations and daily coal production. Specific gas emissions mostly follow the pattern of gas concentrations with exceptions in cases of major gas release into the longwall area from overmined gob zone when performing intense top coal caving. Average specific gas emissions for the excavation period of longwall face C k. -50 were 3.28 m^3/ton for methane and 10.81 m^3/ton for carbon dioxide.

Figure 3.10 presents the gas concentrations (CO_2/CH_4) ratio for a limited area, where calculated ratios ranged from 2.1 to 3.9 in favour of CO_2. Calculations in Table3.1 prove the ratio for the whole excavation period with an average of 3.14.

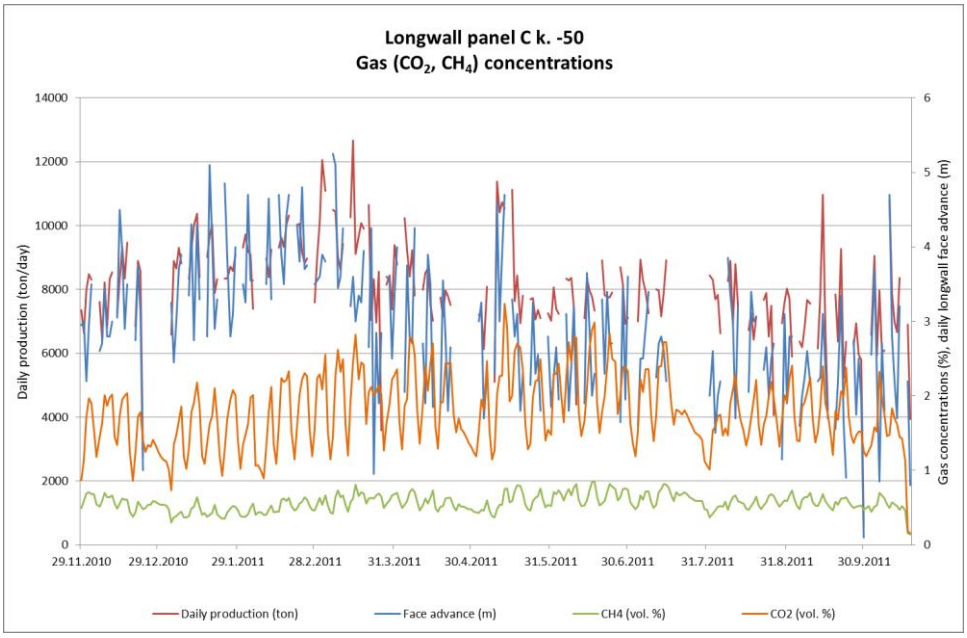


Figure 3.8: Gas concentrations in return ventilation air at longwall face C k. -50.

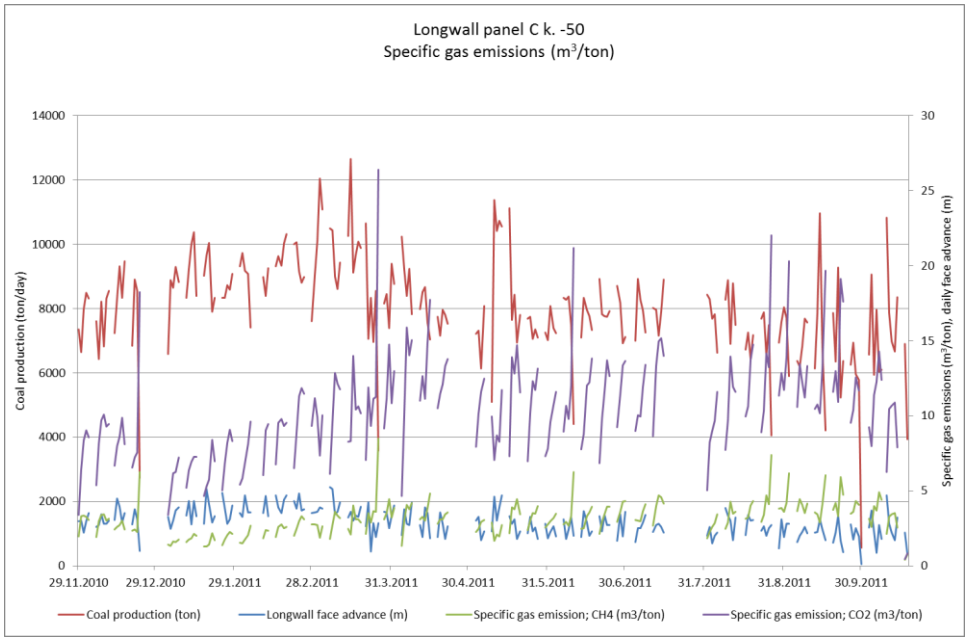


Figure 3.9: Calculated specific gas emission pattern at longwall face C k. -50.

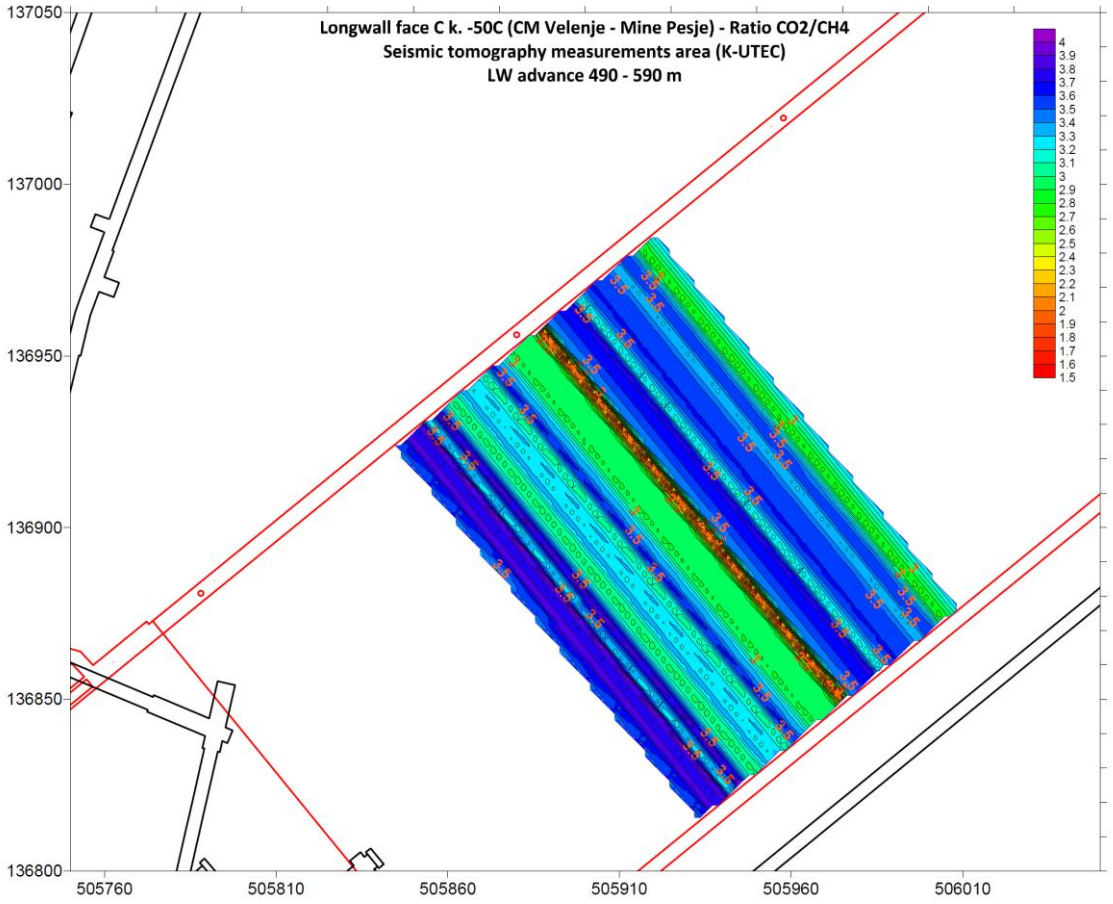


Figure 3.10: Schematic presentation of CO_2/CH_4 ratio for seismic tomography area (longwall face C k. -50).

3.6 Review of previous research at Coal Mine Velenje

Previous research at Coal Mine Velenje, related to this thesis included in situ measurements and monitoring of the seam gas dynamics, gas composition and the effect of geomechanic on seam gas behaviour around the LTCC faces.

Kočar et al. (1987) investigated elements of safe LTCC under water bearing strata at Coal Mine Velenje. Research into dynamics of longwall excavation and its effects on overburden strata resulted in the *Criteria of Safe Excavation* under water bearing strata.

Extensive research into the petrography and structural properties of the Velenje lignite at different stress states and gas presence (Zavšek, 2004) resulted in better understanding of mechanisms of coal and rockburst events. The research included laboratory experiments (stress-strain) on different lithotype lignite samples, which were later used in model creation.

Likar (1995) studied the mechanisms of sudden outbursts (coal and gas) on the basis of preliminary measurements and historical data. The analysis included geological, physical and stress-strain dependent factors for outburst events.

In both studies, modelling approach towards gas outburst prevention technologies was investigated by using mathematical methods and applying to areas of coal seam with variable natural parameters (depth, lignite lithotype, stress state and stage of development).

Analysis of overall interaction between stresses and deformations by LTCC in the coal seam, overburden and floor strata was investigated by Jeromel (2010). On the basis of historical geomechanical monitoring and coal production results, a comprehensive study and numerical modelling of the effect of advancing longwall panels on surrounding structures was published. Numerical modelling and a large number of simulations involving multiple overburden strata failure and consolidation resulted in novel approaches towards improved stability of underground constructions and safety measures.

The origin of coal gases and its distribution in Coal Mine Velenje were researched during late 1990's by gas sampling for concentration, composition and isotopic composition analysis of carbon isotopes in carbon dioxide and methane. Kanduč and Pezdič (2005) published their results which determined major coal gasses in the seam as carbon dioxide and methane, some evidence of nitrogen in certain areas of the deposit and traces of other gasses. Another important finding of this research was its characterisation of methane as the low adsorbed free gas component and carbon dioxide as the stored gas in the coal matrix structure.

An improved understanding of macropetrographic composition of the Velenje lignite was established by Markič over nearly 20 years by detailed lithotype composition logging of coal samples from the coal seam (Markič, 2009). Velenje lignite is a composition of different contents of two major lithotypes; fine detrite (fD) and xylite (X) in ratios of 0-100 % in favour of both types. Fine detrite has higher capacity for gas storage due to its higher specific surface area and porous volume.

Chapter 4

Design and implementation of in situ stress, gas pressure and concentration measurements

The objective of design and implementation of in situ stress, gas pressure and concentration measurements was to investigate the principles of their behaviour around the LTCC faces and to understand the interaction between them.

The methodology involved drilling and instrumenting in seam horizontal boreholes; collecting fresh cores and gas samples for further analysis; installing borehole pressure monitoring equipment and monitoring pressure build-up for in seam gas pressure and permeability calculations; and a preliminary assessment of the effects of stress on gas pressure and permeability in different parts of the coal seam due to LTCC mining.

4.1 General layout and field measurement principles

During the research period, a number of boreholes were drilled and used for the measurements of seam gas composition, seam gas pressure and rock stress over a period of time to analyse the effect of face advance and distance to the longwall face at Coal Mine Velenje. These investigations were carried out at the longwall panels in all mining districts, including the panels where the seismic monitoring work was performed. The layout of in-situ drilling and monitoring involved the use of specific design boreholes with the following characteristics:

- Seam gas composition (25 m long boreholes, +10° from horizontal (initially +2°))
- Seam gas pressure (30 m long boreholes, +10° from horizontal (initially +2°))
- Strain measurements using extensometers (30 m long boreholes, -2° from horizontal)
- Stress measurements – pressure cell (+2° from horizontal)

An example of monitoring borehole layout from years 2011 - 2013 mining activities is shown in Figure 4.1.

4.2 In situ seam gas concentration measurements

Monitoring of seam gas composition at Coal Mine Velenje begun in mid 1990s' as a part of a research programme where the main objective was to investigate the effect of longwall face advance on seam gas composition. Initial monitoring and gas sampling investigated the presence of gasses in the seam and their migration principles caused by longwall face advance rate. The first results defined presence of methane and carbon dioxide as major components, followed by nitrogen and traces of sulfur gases and higher hydrocarbons

(Kanduč and Pezdič, 2005). Another finding of this research was on gas emissions, which suggested earlier migration of methane, followed by delayed release of carbon dioxide from the coal structure.

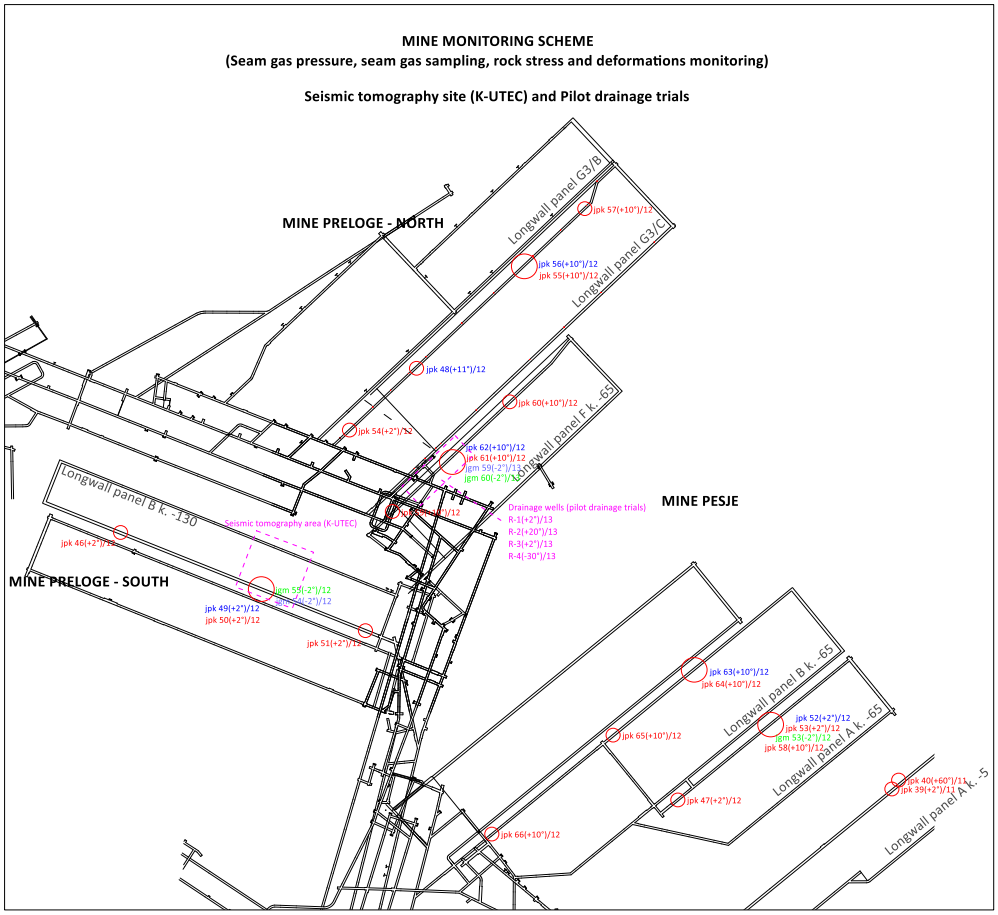


Figure 4.1: Schematic representation of monitoring borehole layout for 2011 - 2013.

In 2009, monitoring of seam gas composition and gas sampling was expanded to all operating longwall faces as a part of a combined seam gas/rock mechanics monitoring. A modified borehole design was proposed and tested with the purpose to ensure full coupling with coal and to prevent seam gas contamination by the ventilation air. The borehole length was increased to 25 m and drilled by coring to obtain core sections from the whole depth. All the cores were logged and used for possible further research.

The technical details of the seam gas composition monitoring borehole are presented in Figure 4.2 and consists of the following: steel casing (L = 20 m, ∅ = 128 mm) for stability, antistatic plastic tube (L = 25 m, ∅ = 25.4 mm) with perforation for sampling tube and copper sampling capillary tube. All intersections were sealed with cement-fly ash mixture or expandable foam.

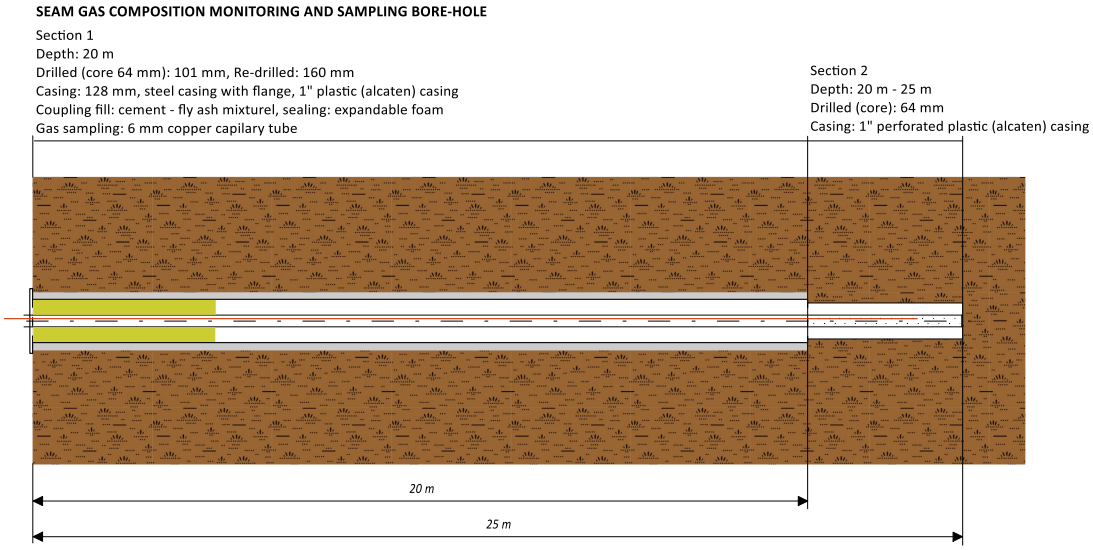


Figure 4.2: Schematic of the seam gas composition monitoring borehole.

Samples of coal seam gas, often contaminated with minor proportions of ventilation air were collected and recorded against distance of the monitoring borehole from the advancing longwall face. A set of two samples were taken in a sampling bag and a depressurised sampling ampoule for simple analysis by a laboratory gas sensor at Coal Mine Velenje and by more accurate laboratory analysis.

4.2.1 Examples of seam gas concentration monitoring

Examples of seam gas concentration and composition monitoring from monitoring boreholes jpk 62 (+10°)/12 at longwall panel F k. -65 (virgin area), jpk 49 (+10°)/12 (A k. -130) in an overmined area and jpk 56 (+10°)/12 (G3/C) in a moderately affected area by two levels of single slice caving (Figure 4.1) are presented in Tables 4.1 and 4.2 and Figures 4.3, 4.4 and 4.5 respectively.

It is observed that the seam gas is generally rich in CO_2, with the exception of panel F k.-65 (Figure 4.3), which, being the first level longwall panel to be mined, had not been disturbed by previous mining/caving above. The measured concentration for CH_4 and CO_2 remained largely stable throughout the face advance for the borehole at longwall panel B k. -130. This was also the case for longwall panel F k. -65 until the longwall approached within 40 m from the borehole.

Table 4.1: Results of gas concentration monitoring in borehole jpk 62 (+10°)/12.

Date	Distance of LW to Borehole m	CH_4 vol. %	CO_2 vol. %
29.11.2012	268.20	58.1	41.9
4.1.2013	190.00	42.5	57.5
9.1.2013	174.40	43.3	56.7
15.1.2013	156.20	43.2	56.8
22.1.2013	131.30	44.9	55.1
28.1.2013	112.10	43.3	56.7
6.2.2013	70.90	42.9	57.1
11.2.2013	59.80	53.0	47.0
19.2.2013	34.70	24.5	75.5
20.2.2013	31.20	24.0	76.0
21.2.2013	27.40	19.4	80.6
22.2.2013	25.00	15.9	84.1
23.2.2013	21.40	19.7	80.3
25.2.2013	17.90	19.0	80.9
26.2.2013	14.40	19.8	80.2
27.2.2013	11.10	20.4	79.6
1.3.2013	4.60	17.7	82.3
4.3.2013	1.80	13.6	86.4

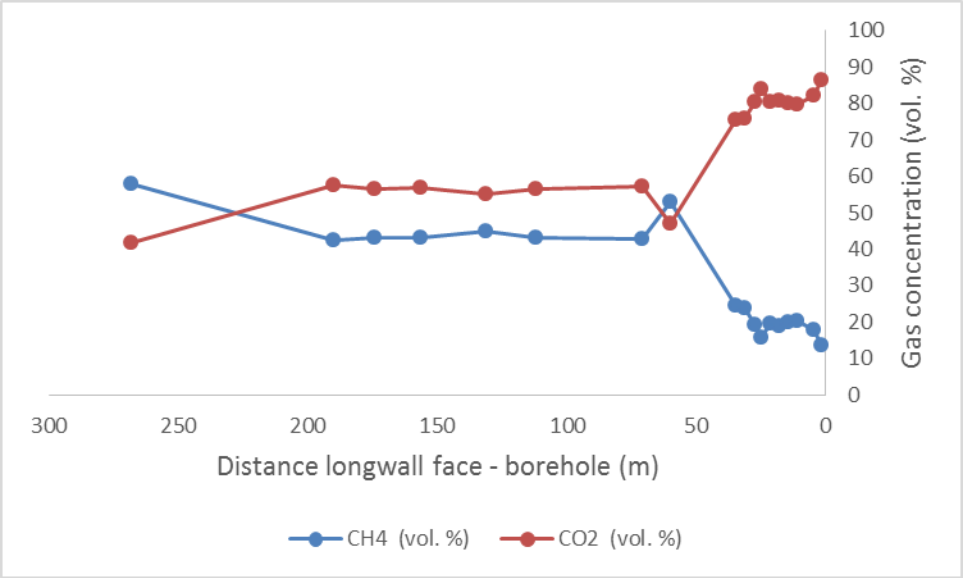


Figure 4.3: Gas concentration at borehole jpk 62 (+10°)/12; longwall panel F k. -65.

Table 4.2: Results of gas concentration monitoring in borehole jpk 56 (+10°)/13.

Date	Distance of LW to Borehole m	CH_4 vol. %	CO_2 vol. %
22.2.2013	189.90	63.6	36.3
25.2.2013	179.60	63.9	36.1
8.3.2013	125.40	22.2	77.8
13.3.2013	104.90	22.4	77.6
27.3.2013	60.00	41.5	58.5
4.4.2013	37.40	61.9	38.1
15.4.2013	19.60	36.4	63.6
17.4.2013	13.90	33.8	66.2
19.4.2013	7.30	12.0	88.0
22.4.2013	3.90	40.8	59.2

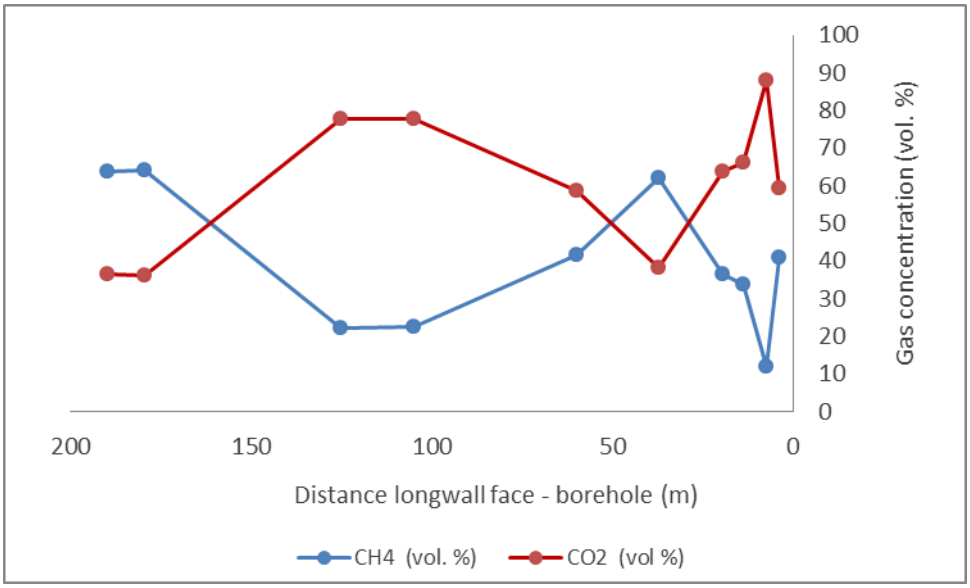


Figure 4.45: Gas concentration at borehole jpk 56 (+10°)/13; longwall panel G3/C.

Lonwall panel B. k-130 was located at the bottom of lignite seam and has been influenced by overmining due to longwall panels in upper levels. Gas sampling borehole jpk 49 (+2°)/12 illustrates the effect of stress on gas composition change. Before the peak, a relatively stable gas composition was observed (Figure 4.4). As the stress peaks formed, methane as free gas migrated from the coal block monitored and its concentration in the borehole seam gas mixture reduced significantly, with a corresponding increase in the CO_2 concentration. At approximately middle of the observation period, the longwall face becoming closer to the borehole and the deformations in the longwall panel created a connection between the borehole and the face/gateroads; methane escaped freely, carbon dioxide remained attached (adsorbed) in the coal matrix. This newly established gas ratio stayed the same until the end of monitoring period.

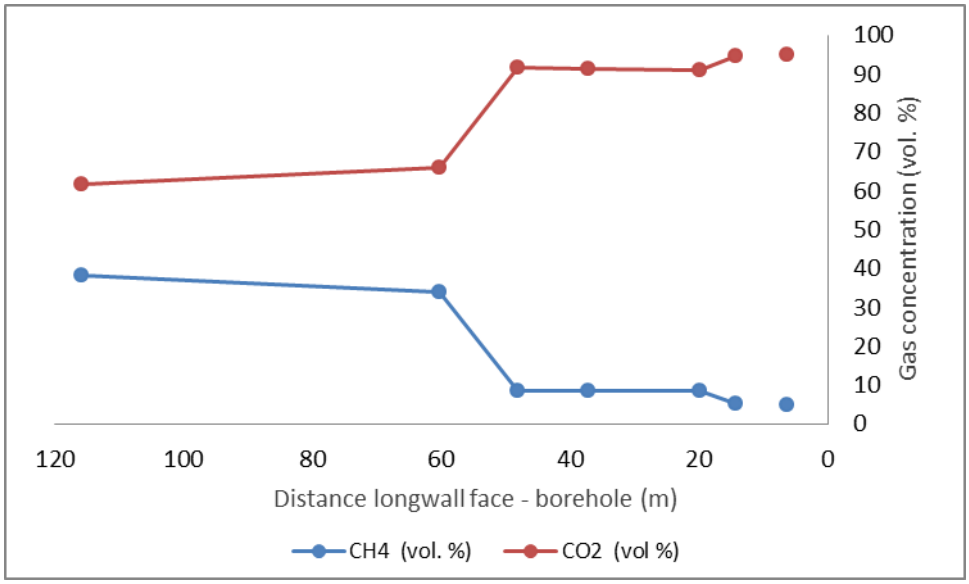


Figure 4.54:Gas concentration monitoring at borehole jpk 49 (+10°)/12 longwall panel B k.-130.

On the other hand, the gas concentration measured at panel G3/C displayed considerable fluctuations against the advance of longwall face (Figure 4.3). At the start of sampling 64 vol. % of methane was in the samples. When the longwall face started to approach to borehole (around 120 m from the borehole) the percentage of CO_2 increased. The last peak of CO_2 (88 vol. %) was observed when the face was 7 m from the borehole.

In the frame of research projects CoGasOUT and GHG2E funded by the European Commission monitoring data obtained by the author once again confirmed the earlier observations that in virgin and moderately disturbed areas methane stored in the Velenje lignites readily releases and migrates due to mining associated stress and permeability changes, however, the CO_2 stored in the coal remains in the seam and requires further fracturing and significantly more enhanced flow paths in order to start its release and migration. Therefore, gas outburst risk at Velenje would be higher in areas of higher CO_2 concentration as the seam gas, as well as in areas of increased stress disturbance due to mining or geological features (Durucan et al., 2012; Durucan et al., 2013).

4.3 In situ gas pressure measurements

Inseam gas pressures monitoring in parallel with seam gas concentration and longwall stress parameters started in 2009 with the purpose to investigate and confirm the earlier observations that showed certain dynamics of rock stresses which are dependent on the distance to the working longwall face.

In-seam gas pressure monitoring allows the correlation between gas pressure behaviour with the advance rate of longwall face, and the evaluation of the effect of resulting stress abutment on permeability and gas release. Seam gas pressure measurements were conducted using long boreholes (Figure 4.6). The borehole length was designed as 30 m and drilled by coring to obtain core sections from the whole depth. All the cores were logged and used for possible further research.

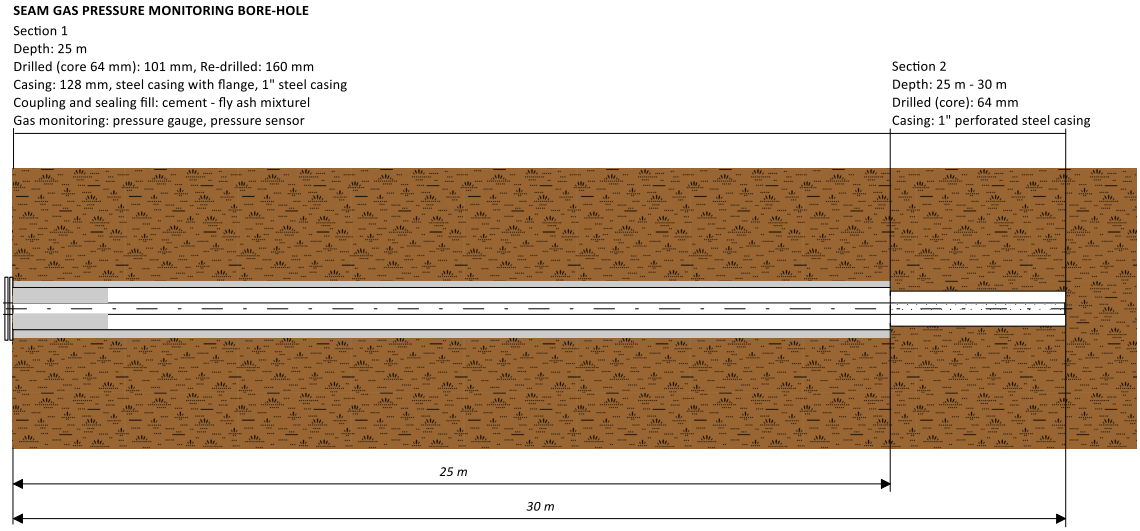


Figure 4.6: Schematic view of the seam gas pressure monitoring borehole.



Figure 4.7: In seam gas pressure monitoring location equipped with a pressure probe, pressure gauge and a temperature probe installed.

The design of gas pressure monitoring boreholes is presented in Figure 4.6 and consists of the following: steel casing (L = 25 m, ∅ = 128 mm) for stability and steel tube (L = 30 m, ∅ = 25.4 mm) with perforation for gas connectivity, mounted by a flange of steel casing. All intersections were sealed with cement-fly ash mixture.

All gas pressure monitoring boreholes were equipped with a gas pressure sensor, optionally temperature sensor and a mechanical pressure gauge (Figure 4.7). The sensors used are passive electrical elements encased in an ATEX certified explosion proof construction in order to achieve real time continuous monitoring and data transfer to the office computers. Gas pressure was measured and recorded both by continuous digital sensors as well as manually by pressure gauges. Longwall face advance and position was

also recorded and compared with the gas pressure measurements. Since 2009, seam gas pressure monitoring boreholes were drilled in every longwall panel which resulted in more than 30 monitoring boreholes in all mining areas (Figure 4.1).

4.3.1 Examples of seam gas pressure monitoring results

Figure 4.8 presents the in-seam gas pressure measurement data obtained in borehole jpk 34(+2˚)/10 at longwall panel C k.-50 in the early stages of the gas pressure monitoring programme. As the face line approached the gas pressure monitoring borehole, at around 70 metres from the face line, the abutment pressure built up and a sharp increase in seam gas pressure was observed. At around 40 metres from the face line, the gas pressure started to decline again, indicting enhanced gas flow in the area due to fracturing and loss of gas from the sealed borehole, ultimately reaching the flowing gas pressure at around 5 metres from the face line.

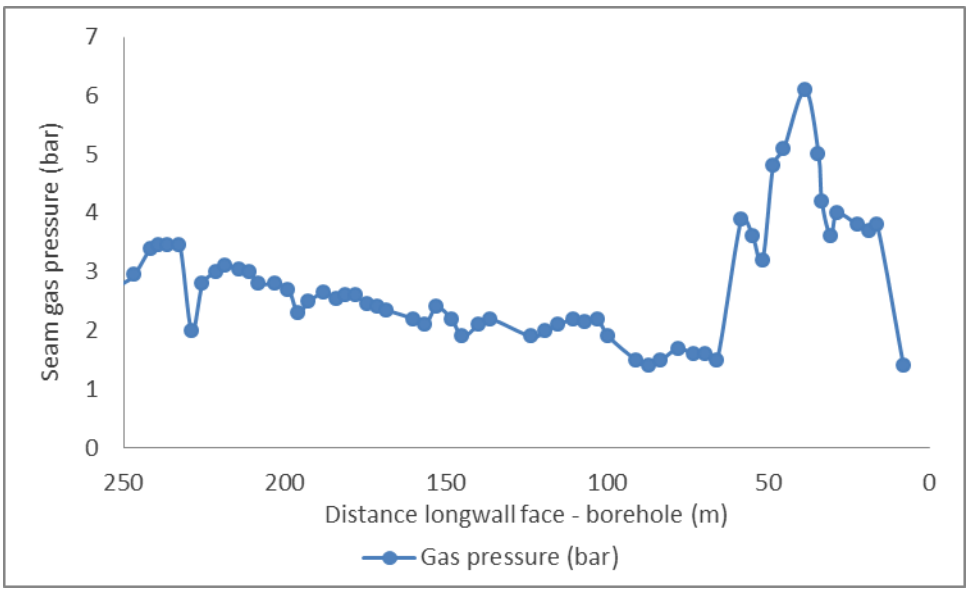


Figure 4.8: Seam gas pressure measurement data in borehole jpk 34 (+2°)/11; longwall panel C k. -50.

The first assessment of the correlation between rock stress, seam permeability changes and gas pressure dynamics were made after seam gas pressure monitoring at borehole jpk 34(+2˚)/10. Combined presentation of results of seam gas pressure measurement and rock stress measurements is given in Figure 4.9. A pair of stress cells at 25m depth, which gave a better response to dynamic stress changes ahead of the advancing longwall face was used. Results from rock stress monitoring (jgm 39 (-2°)/10) and seam gas pressure monitoring (jpk 34 (+2°)/10) are combined together on a single chart.

The stress cells used in coupled monitoring systems measure only the differential stresses in the field. Combining the changes in stress with gas pressure it can be shown that the front abutment pressure build up decreases permeability and the in seam gas pressure increases. It is clear that at around 40 metres from the face line the abutment stresses peaks, initiating fractures and increasing permeability in the coal, and this also initiates flow out/through the borehole and gas pressure starts decreasing. It is also notable that the in seam pressures react first to the mining related changes in the coal seam. Maximum stress levels are reached at a distance of 25-20 metres from the face line, after which point both stresses and gas pressure fall rapidly to near 0 values.

As discussed before, the gas pressure reached a peak at the distance of 40m and then started to decrease towards normal air pressure of 1 bar at a distance to the long-wall face round 10m. As expected gas pressure reacts to the changes in the formations first. The vertical and horizontal stress components reacted to the changes with a delay of 30m distance to the longwall face. Maximum stress change was achieved at a distance of 20-25m just before both rock stresses and gas pressure simultaneously decreased to 1 MPa and 0 bars respectively.

The effect of stress state changes and gas pressure dynamics presented In Figure 4.9 can be explained as “cleat system opening and closing”. When long-wall face distance to monitoring point is more than approximately 70 metres, stress changes cause several in-seam deformations. Seam gas is allowed to move freely through the seam and measured gas pressure decreases. As the longwall face approaches towards the monitoring point, rock stress rises, the cleats are closing and seam gas is trapped into the closed volume. This phenomenon is recorded as seam gas pressure rise. Seam gas pressure rises until the peak abutment stress is reached (50 – 30 m). After that point (30 – 0 m), the section of the longwall panel ahead of the face deforms significantly and the seam gas escapes from the cleat system and the fractures created.

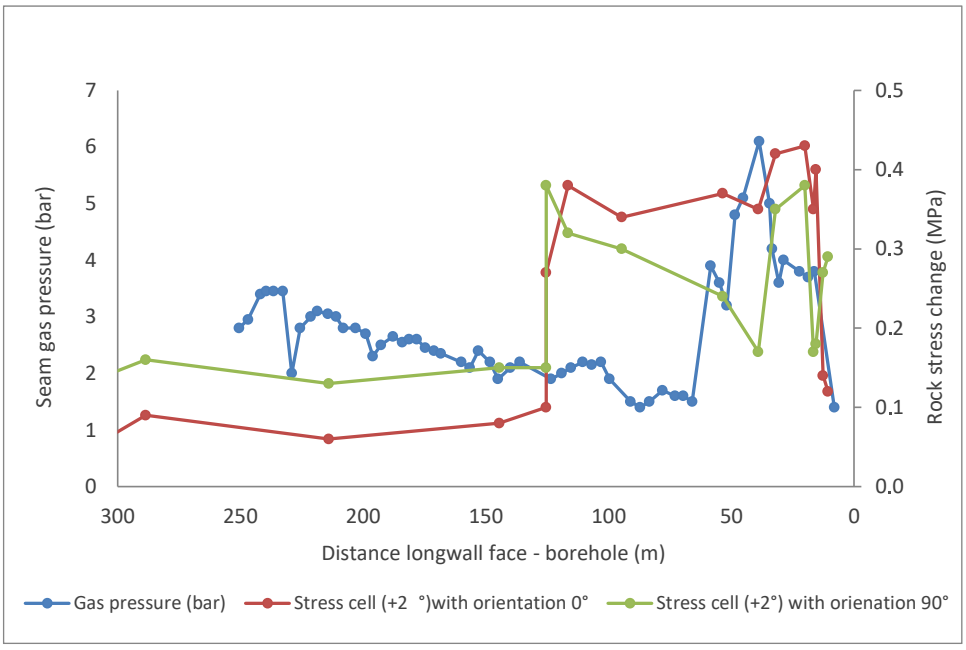


Figure 4.9: Seam gas pressure measurement data in borehole jpk 34 (+2°)/11 and rock stress change in borehole jgm 39 (-2°)/11; longwall panel C k. -50.

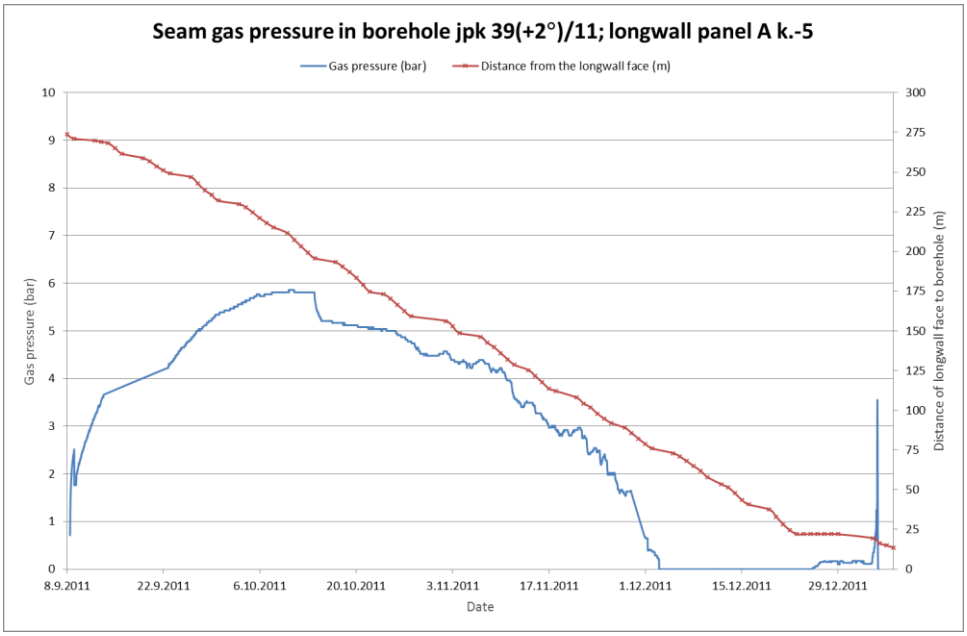


Figure 4.10: Seam gas pressure measurement data in borehole jpk 39 (+2°)/11; longwall panel A k. -5.

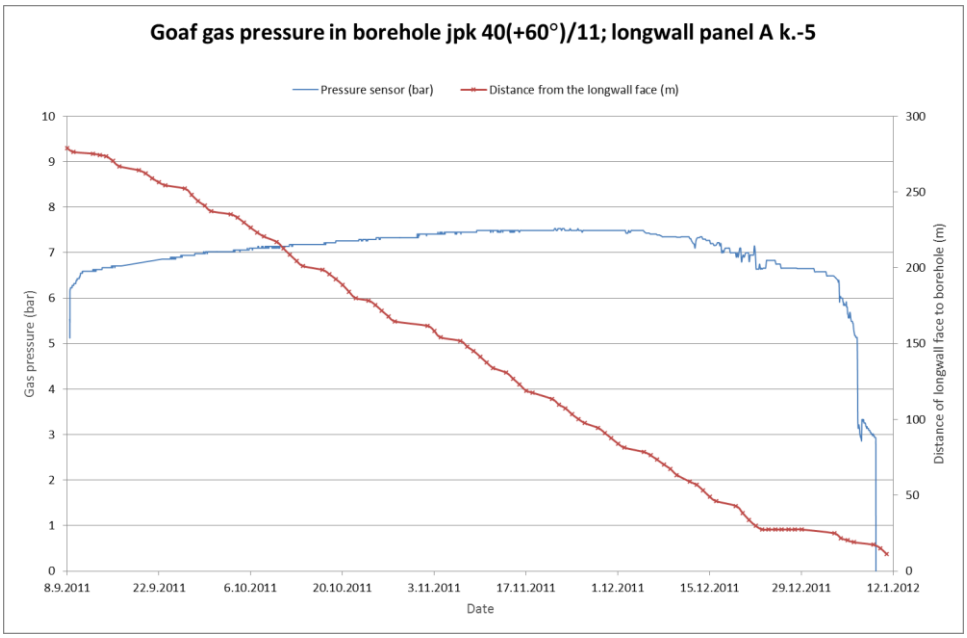


Figure 4.11: Goaf gas pressure measurement data in borehole jpk 40 (+60°)/11; longwall panel A k. -5.

Two other sets of seam gas monitoring data are presented in Figures 4.10 and 4.11. Figure 4.10 presents seam gas pressures measured in borehole jpk 39(+2°)/11, drilled in solid coal beneath an overmined area, as the face line approached it. Borehole jpk 40(+60°)/11 in Figure 4.11 was drilled into the pre-mined area above long-wall face A k. -5 in order to investigate gas pressure dynamics in an area which may be a source for gas emissions

while the LTCC faces are operating. A noticeable difference between the gas pressure behaviour of the two zones was observed as shown in Figures 4.10 and 4.11. While the gas pressure in the solid coal is definitely affected and reduced by the face advance, gas pressures in the goaf above the LTCC district seem to remain constant, providing a steady source of gas emission to towards the operating longwall.

During preparations for second gas drainage trials (Chapter 8) at longwall panel D k. -65, a seam gas pressure monitoring borehole jpk 79 (+10°)/14 was prepared in the longwall panel. Unlike previous observations in gas pressure monitoring boreholes, values of seam gas pressure (pressure build-up) increased steadily after the borehole was closed and reached 22 bars. After the longwall face started production at 450 m distance from the monitoring borehole, a noticeable pressure drop to 16 bars was observed, which recovered and built up to 26 bars at 150 m distance from the longwall face, which represents the highest measured seam gas pressure since 2009 (Figure 4.12).

In general, in seam gas pressures measured in the boreholes varied between 4-6 bars gauge and an increased pressure zone is observed at around 70 to 30 metres from the face, after which the pressure started to decline and reached the flowing gas pressure at around 5 metres from the longwall face. In the case of borehole jpk 79 (+10°)/14, the monitoring borehole was surrounded by xylite (core log), which provides a locally isolated area, similar to those where gas is stored under even higher pressures and can cause gas outburst by affecting the sealing coal mass.

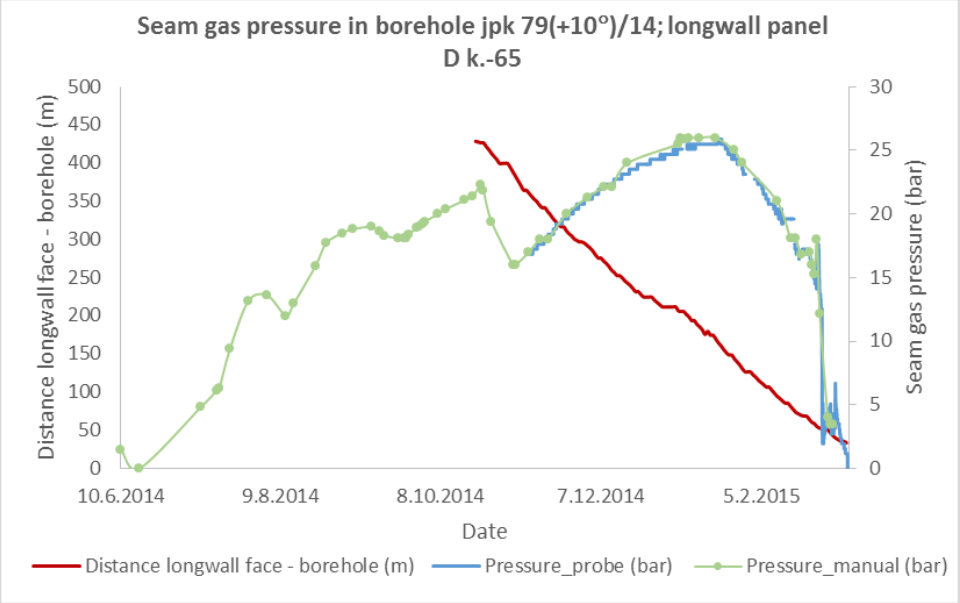


Figure 4.12: Seam gas pressure measurement data in borehole jpk 79 (+10°)/14; longwall panel D k. -65.

In conclusion, the pressure decline zone suggests extensive fracturing and failure of coal around the borehole due to changing stress conditions. This usually is accompanied by a sharp increase in stress measured in all the cells monitored, where the increased abutment stresses peak.

Two additional in-seam gas pressure monitoring boreholes, E2 (+10°)/13 and E2 (+20°)/13, were drilled during the preparation of a gas drainage trial site at longwall panel E k. -65. The first, borehole E2 (+20°)/13 was drilled as a gas drainage borehole at a steep angle and finished in clay layer above the coal at a distance of 25 m. E2 (+10°)/13

was drilled as a backup gas drainage borehole from the same location and finished with a full length of 40 m in coal (Figure 4.13).

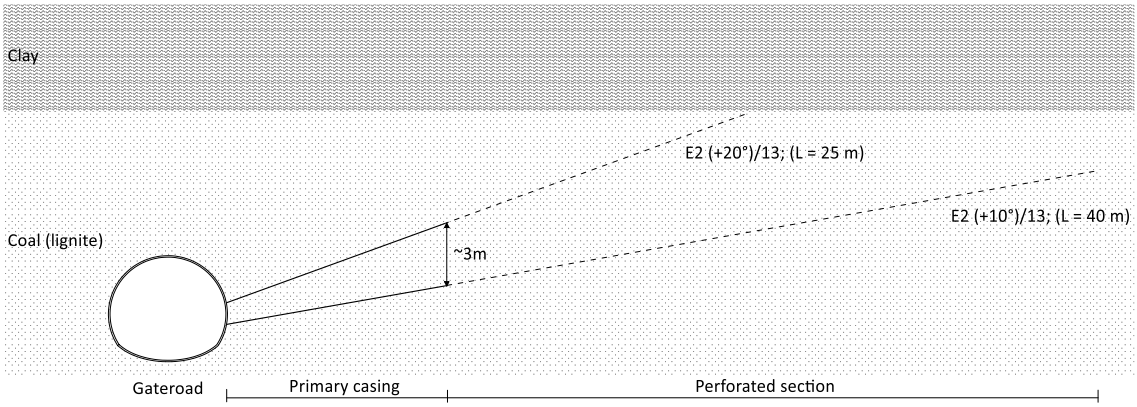


Figure 4.13: Schematic view of gas drainage boreholes E2 (+10°)/13 and E2 (+20°)/13; longwall panel E k. -65.

The gas drainage trials planned for longwall panel E k. -65 were later moved to another panel due to operational requirements by the mine, however, these boreholes were still used for gas pressure monitoring. Research plan included monitoring of seam gas pressure at both boreholes, similar to the cases described above, opening of the boreholes and releasing the trapped gas, followed by pressure build-up experiments at different stages of longwall advance towards the boreholes. The objective was to observe the behaviour of coal mass between the perforated sections of the two boreholes (which were 3 m apart) and the development of a permeable zone between them (fracture development), as well as pressure build-up behaviour due to longwall face advance. Initial gas pressure measurements in the two boreholes showed different in-seam pressure values.

Durucan et al. (2014) report that interference between the drainage boreholes was not recorded until the longwall face was 5 m from the drainage boreholes. Permeability calculations for the seam sections have shown that the initial seam permeability was very low ($k = 0.69$ mD), which increased to $k = 141.2$ mD when the face advance fractured the seam section between boreholes.

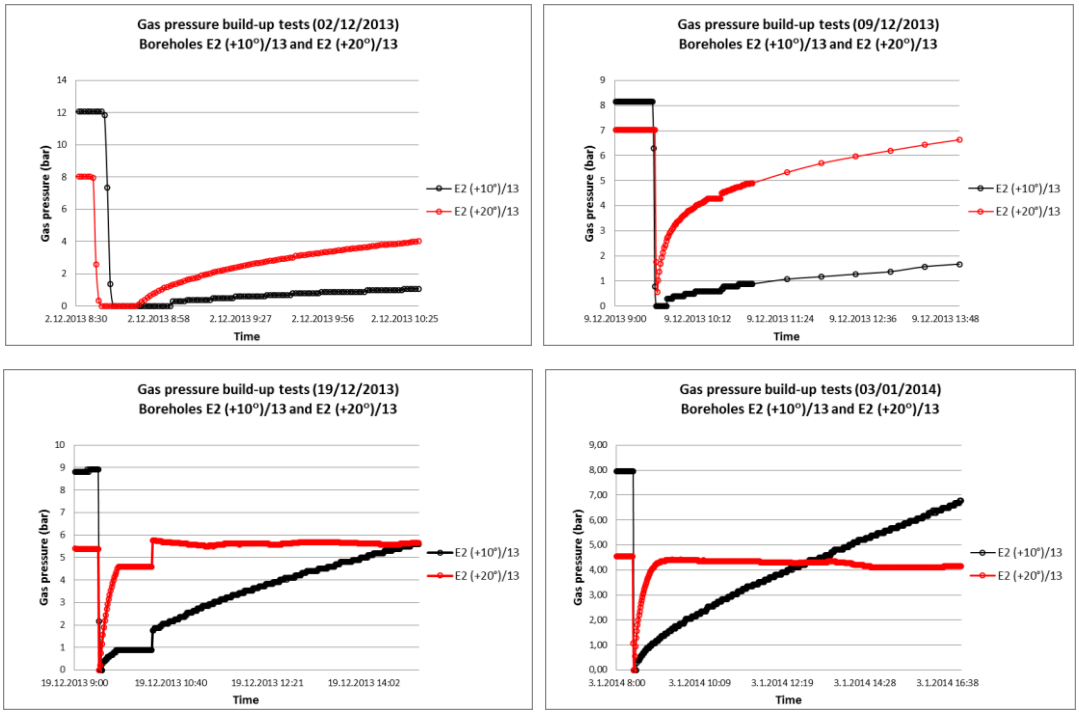


Figure 4.14: Results of gas pressure build up experiments at boreholes E2 (+10°)/13 and E2 (+20°)/13; longwall panel E k. -65.

Figure 4.14 shows pressure build up in both boreholes for a number of longwall face positions as the face moved towards the borehole location. Initial experiment (02/12/2013) was performed when the longwall face was at 88.6 m distance from the borehole location. Pressure values in boreholes were 12 bar (E2(+10°)/13) and 8 bar (E2(+20°)/13). During the period of experiments, pressure values changed significantly, with a drop in the maximum pressure value, and the pressure drop was higher at borehole (E2(+20°)/13) to 4 bar.

4.4 In situ stress measurements

Geotechnical monitoring at Coal Mine Velenje over the research period has confirmed the dynamic behaviour of stresses with distance from the longwall face. Gas pressure changes monitored in the boreholes depended on the position of the longwall face with respect to depth below surface (thus depth within the thick seam) as a result of over/under mining. Mining history affected the intensity of fracturing in the coal seam mined and gas pressure changes in boreholes situated in highly fractured areas due to over/under mining were minimum.

However, regardless of the gas pressure changes observed, increased stresses ahead of the longwall face due to mining caused changes in permeability of the coal seam and, depending on the location of the reference point, this has manifested itself as “opening and closing” of the fracture system and thus a change in gas flow dynamics.

Rock stress changes were monitored by the Coal Mine Velenje proven methodology by using Gloetzl hydraulic stress cells, placed into boreholes in two separate depths. Experience of measuring stress changes in vertical (0°) and horizontal (90°) direction

were used in all cases of in situ stress monitoring. Cells used are pillow shaped elements which are filled with hydraulic fluid and connected by rigid plastic tubes with measuring point in the gateroad. Stress cells were coupled with surrounding coal mass with cement and fly-ash mixture in a required ratio that matches the strength properties of coal for better transmission of rock stress changes. Usually two pairs of cells were installed in 20 and 30 meters depths in the boreholes (Figure 4.15).

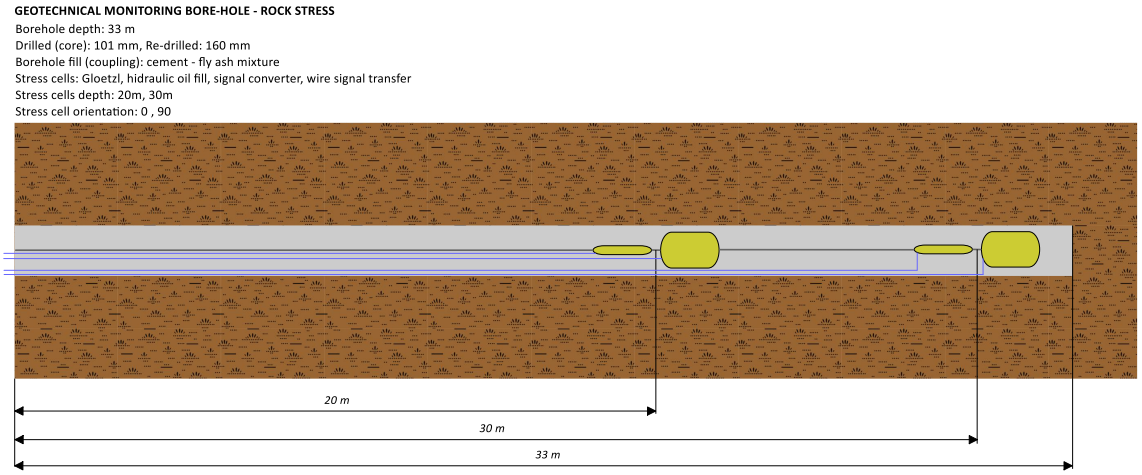


Figure 4.15: Schematic representation of an in situ stress monitoring borehole.

Rock stress distribution is commonly expressed in three-dimensional components in the rock mass. Most relevant component concerning stress conditions is the vertical component, which varies in relative to the position in coal seam, dependent on depth from surface. Observations, interpretations and design background in mining usually utilise the vertical (σ_1) and one of the horizontal components (σ_3). Based on the observations and experience at Coal-mine Velenje, the relationship between stress components can be represented by the ratio $\sigma_1 = 0.8\sigma_3$.

Therefore, the current monitoring campaigns normally set the stress cell orientation as 0° (vertical component, σ_1) and 90° (horizontal component, σ_3). While drilling and cell installation, special emphasis was placed on proper coupling mixture injection that matched the approximate strength properties of surrounding coal and was later tested in the laboratory for uniaxial compressive strength. Monitoring of stress state changes in the longwall panels is interpreted as additional secondary vertical stress development and distribution over the longwall panel dependent on the effects of advancing longwall face.

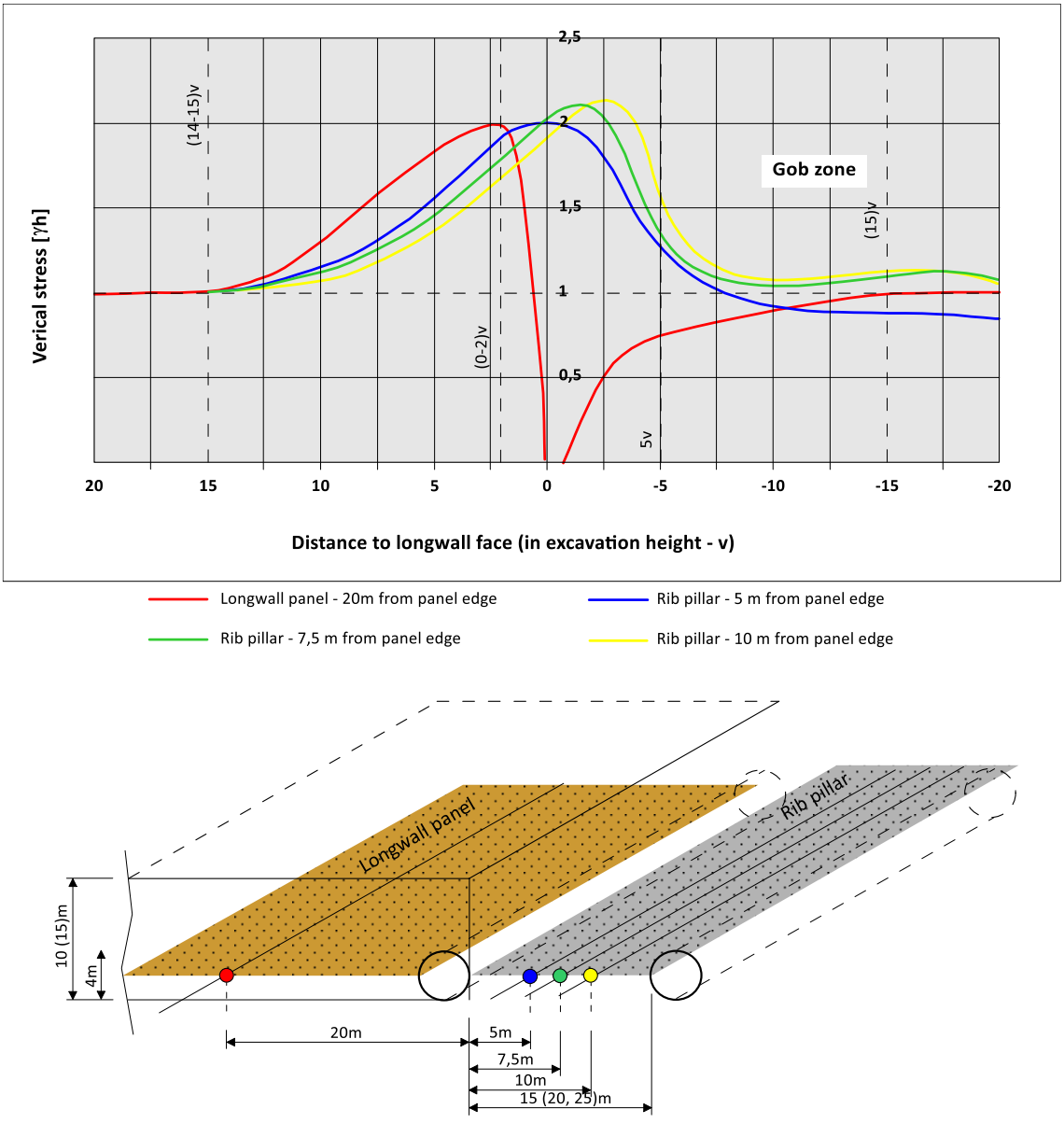


Figure 4.16: Generalised representation of stress distribution over the longwall panel and the rib pillar in relation to the longwall face advance based on multiple stress monitoring campaigns. Gas drainage efficiency is significantly affected by the rock stress conditions as they develop.

Figure 4.16 presents a generalised representation of secondary vertical stress development due to longwall face advance as an additional load to primary stress ($\sigma_1 = \gamma$ x h), which varies according to the relative position within the coal seam. Observations have shown relatively constant secondary stress development, which reached a peak value similar to the primary stress, leading to a total applied stress. Development of secondary stress is best described with s wave shaped curve which constantly moves in front of the longwall face line at a distance of 2 – 2.5v. Stress peak is followed by a section of stress relief and deformation development, which is limited by the longwall face line. Stress relief is recorded even behind the line of longwall face and results in a completely destressed zone, which gradually increases to reach the primary stress value at some distance behind the face line.

4.4.1 Examples of in situ stress monitoring

The stress measurements in borehole jgm 55 (-2°)/12, have shown notable stress changes as the longwall face advanced towards the borehole location. Stress cells at borehole jgm 55 (-2°)/12 recorded stress changes during face advance which peaked at around 50 m distance between longwall face and borehole (Figure 4.17). Stress development curve at monitoring location displays behaviour which can be correlated with historical measurements at Coal Mine Velenje by reaching nearly 100% of additional stress at peak point due to the effect of advancing longwall face.

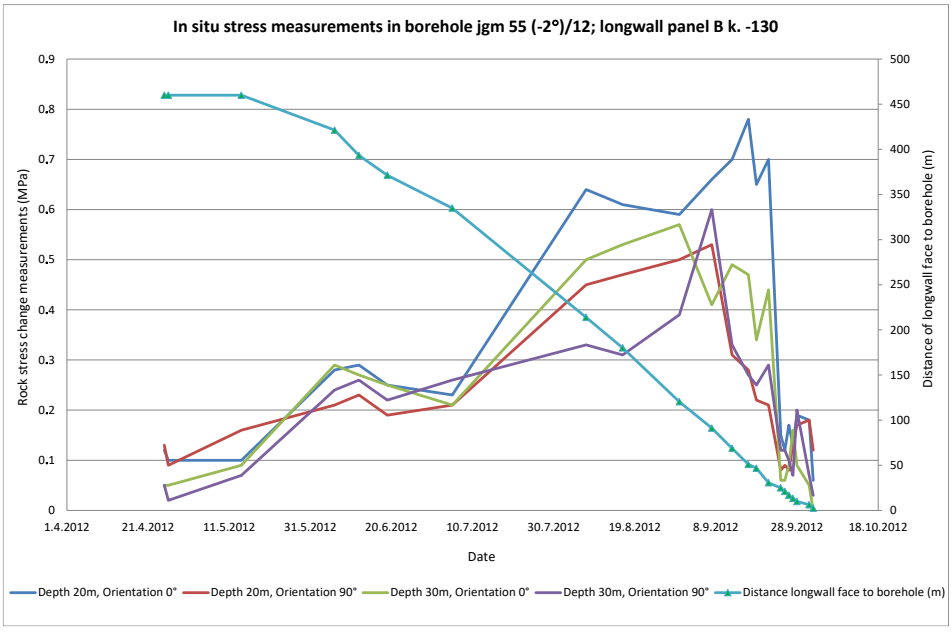


Figure 4.17: Rock stress state development measurements in both orientations (vertical and horizontal) in borehole jgm 55 (-2°)/12; longwall panel B k. -130.

Borehole jgm 60 (-2°)/13 was drilled and equipped with the purpose of coupled monitoring of gas drainage trials at longwall panel F k. -65. Despite its limited time duration, monitoring showed expected results, especially by the vertical stress measurements at a depth of 20 m, where the vertical stress was increased by nearly 100 %. Recordings in other measuring points showed stress abutment development at a distance of approximately 70 meters in front of the long-wall face, similar to the vertical stress records at a depth of 20, but with less intensity (Figure 4.18).

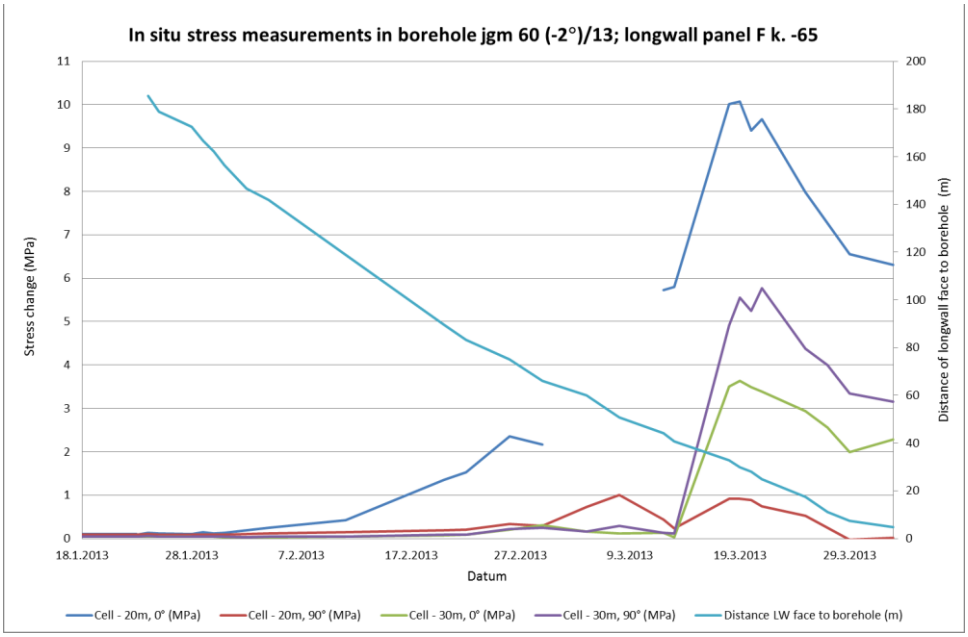


Figure 4.18: Rock stress development measurements in both directions (vertical and horizontal) at borehole jgm 60 (-2°)/13; longwall panel F k. -65.

The common feature of stress conditions is the presence of a destressing zone behind the stress peak in which is reached at distances less than 30 meters between long-wall face and drainage bore-hole. However, stress development as a consequence of longwall face advance is crucial for the longwall panel macro-permeability growth and the application of gas drainage technologies.

Chapter 5

Design and implementation of in situ gas content measurements

At Coal Mine Velenje, procedures for determining the in situ gas content of coal seams using a modified version of the US Bureau of Mines direct method (Kissel et al., 1973; Diamond and Schatzel, 1998; Diamond et al., 2001) was set up after the domestic methodology by using large sample canisters and common laboratory equipment has led to unsatisfactory results. The in situ gas content measurements were performed following the US Bureau of Mines Method and the Australian Standards for direct gas content measurements with some modifications that have been implemented to cater for the specific desorption properties of the lignites at Coal Mine Velenje.

Unlike measurements taken from most bituminous coals, the initial gas desorption from the solid lignite samples in the canister was very rapid and, as a result, the conventional USBM method was found to underestimate the lost gas volume. Therefore, significant modifications both to the equipment used and the measurement methodology were found to be necessary. The initial measurements of seam gas composition have suggested that, in Velenje lignites, methane is either held in the pore space in a free state (not adsorbed) or the gas desorption runs much faster than that observed in hard coal. On the other hand, the pressure rise in the large canisters was very low, making the measurements both underground and in the laboratory rather difficult and complicated. Therefore, the system was modified further to utilise the vacuum created by the water column in a graduated cylinder.

Accordingly, both the underground desorption measurement and consequent laboratory measurement equipment were re-designed as shown in Figures 5.1 and 5.2, which lend themselves to total sealing, simple maintenance and reduced trapped air volumes. Furthermore, the canisters and the graduated cylinders used for lost gas determination were adapted for the mining conditions underground and the core sample size taken.

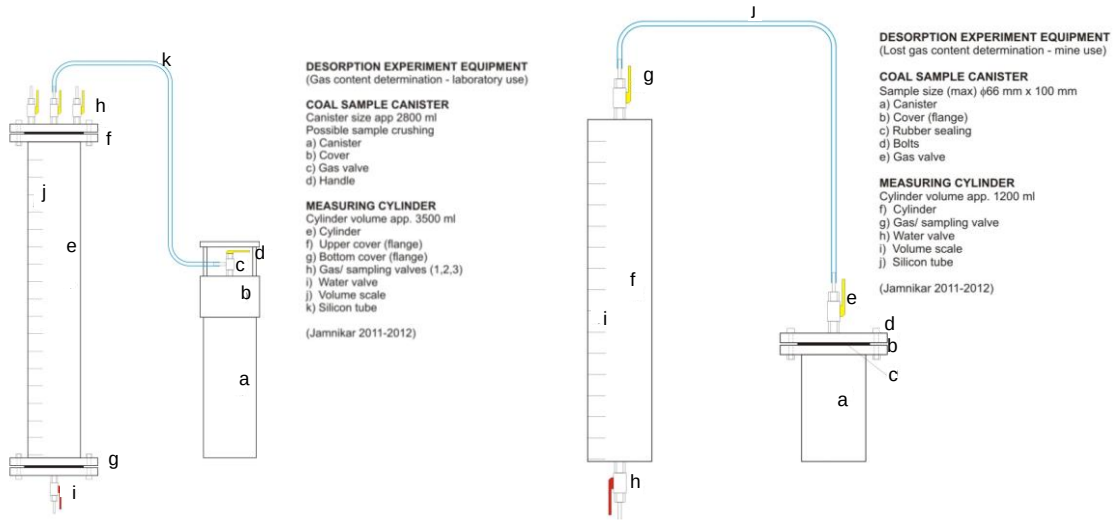
5.1 In situ gas content measurements

At Coal Mine Velenje, a total of 25 experiments for in situ gas content determination were performed for the COGASOUT project using the modified equipment during 2012. Experiments included samples taken from different mine locations as indicated in Figure 5.3. Figure 5.4 presents the total gas desorbed from one of the samples taken. Due to very fast rate of gas release observed in Velenje lignites, special attention was paid to the lost gas content determination aspect of the experiments and a new methodology applicable to Velenje lignites was developed. Table 5.1 presents the gas content measurement data from the 2012 measurements.



(a) (b)

Figure 5.1: Modified equipment for desorption experiments; (a) in situ desorption and lost gas content determination equipment, (b) laboratory desorption equipment, at Coal Mine Velenje.



(a) (b)

Figure 5.2: Details of the newly designed modified equipment for desorption experiments; (a) in situ desorption and lost gas content determination equipment, (b) laboratory desorption equipment, at Coal Mine Velenje.

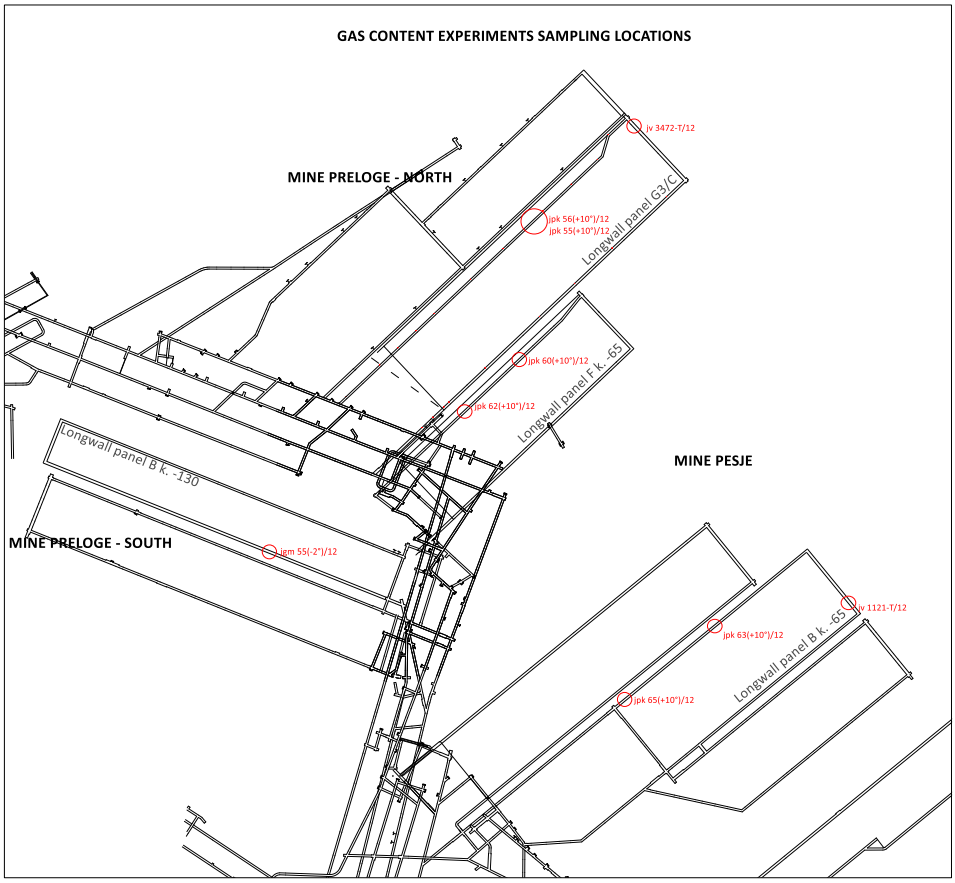


Figure 5.3: Locations of samples for in situ gas content measurements at Coal Mine Velenje.

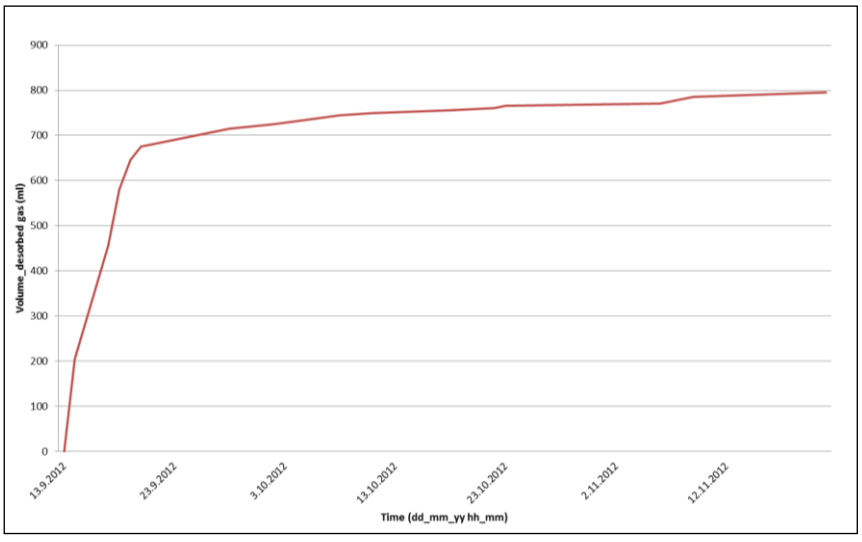


Figure 5.4: Example gas desorption measurement for a lignite sample at Coal Mine Velenje.

Table 5.1: In situ gas content determination experiments at Coal Mine Velenje in 2012.

	Sample	Start Date	End Date	Section (m)	Weight (g)
1	DES jgm 55-1	24.4.2012	26.6.2012	30.90 - 31.00	370.6
2	DES jgm 55-1a	24.4.2012	24.4.2012	30.70 - 30.80	357.6
3	DES jgm 55-2	24.4.2012	21.6.2012	30.80 - 30.90	342
4	JPK 60-1	21.6.2012	21.8.2012	4.60 - 4.70	390.6
5	JPK 60-2	21.6.2012	21.6.2012	4.50 - 4.60	257.2
6	JPK 56-1	3.10.2012	3.10.2012	16.30 - 16.40	317.9
7	JPK 56-2	3.10.2012	3.1.2013	16.40 - 16.50	292
8	JPK 55-1	8.10.2012	3.1.2013	8.90 - 9.00	335
9	JPK 55-2	8.10.2012	8.10.2012	9.00 - 9.10	280
10	JPK 55-3	10.10.2012	10.10.2012	22.40 - 22.50	318
11	JPK 55-4	10.10.2012	10.10.2012	22.50 - 22.60	288
12	jv 3472-T	10.11.2012	10.11.2012	14.80 - 14.90	/
13	jv 3472-T	10.11.2012	10.11.2012	14.90 - 15.00	/
14	JPK 65-1	26.11.2012	29.11.2012	26.60 - 26.70	294
15	JPK 65-2	26.11.2012	28.1.2013	28.10 - 28.20	314
16	JPK 63-1	28.11.2012	28.1.2013	10.60 - 10.70	354
17	JPK 63-2	28.11.2012	28.1.2013	13.70 - 13.80	215
18	JPK 63-3	30.11.2012	30.11.2012	24.35 - 24.45	307
19	JPK 63-4	30.11.2012	30.11.2012	25.80 - 25.90	322
20	JPK 63-5	6.12.2012	6.12.2012	27.10 - 27.20	/
21	JPK 63-6	6.12.2012	6.12.2012	28.60 - 28.70	274
22	JV 1121T-1	12.12.2012	12.12.2012	16.70 - 16.80	294
23	JV 1121T-2	12.12.2012	12.12.2012	18.00 - 18.10	289
24	JV 1121T-3	14.12.2012	14.12.2012	45.40 - 45.50	214
25	JV 1121T-4	14.12.2012	14.12.2012	54.40 - 54.50	229

According to the developed methodology, samples were first tested for in situ gas content at the drilling site underground. After coring and retrieving the core barrel, samples were stored in sampling canister and connected to a graduated cylinder. Measurements of released gas were taken until the release rate dropped; detrite samples in comparison to xylite samples required measurements for longer time due to larger specific surface area.

5.2 A new in situ gas content interpretation methodology

Unlike measurements taken from most bituminous coals, the initial gas desorption from the solid lignite samples in the canister was very rapid and, as a result, the conventional USBM method was found to underestimate the lost gas volume. Figure 5.5 presents an example gas desorption experiment results for a number of samples tested in 2012.

Using the laboratory determined sorption isotherms for CO_2 and CH_4 (Figure 5.6) and the fitted Langmuir parameters (Table 5.2), the isotherm for the binary gas mixture may be obtained using the extended Langmuir equation.

$$V_i = \frac{pY_i V_{Li} b_i}{1 + p(Y_{CH_4} b_{CH_4} + Y_{CO_2} b_{CO_2})} \tag{5.1}$$

where subscript i denotes CH_4 or CO_2, Yi is the gas concentration of component i in the free gas phase and $b = 1/P_L$. Figure 5.7 presents the computed isotherms ($Y_{CO2} = 0.7$) for the two components and the sum of the two. The in situ gas pressure was found to range from 6 to 8 bar, therefore the corresponding total gas content lies between 4.55 and 5.87 m^3/tonne.

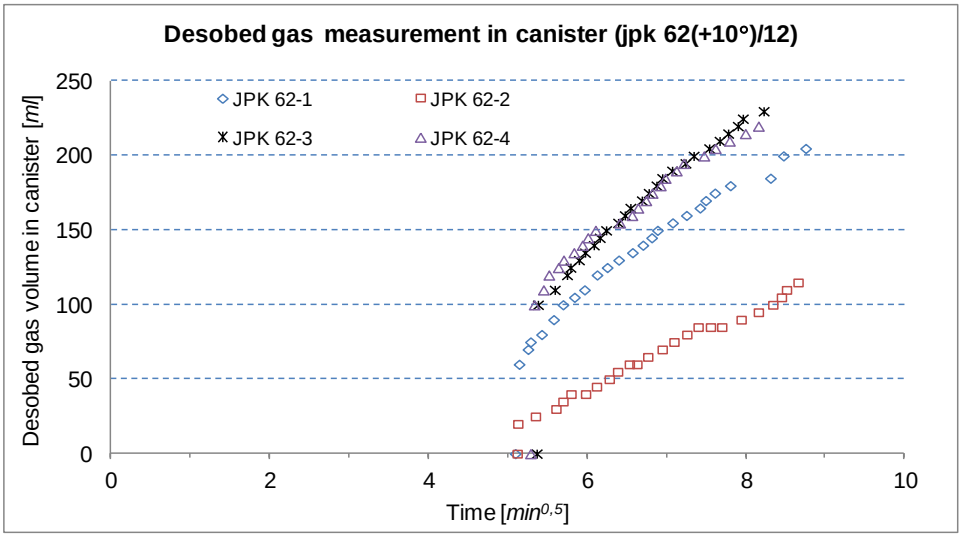


Figure 5.5: Example gas desorption experiment results for a number of samples tested at Coal Mine Velenje in 2012.

Table 5.2: Langmuir parameters for pure gas adsorption on coal from Coal Mine Velenje.

	Langmuir parameters	
Gas	P_L (MPa)	V_L (m^3/t)
Nitrogen	7.5	12
Methane	7.5	25
Carbon dioxide	4.7	50

Using the USBM method, a lost gas of between 114 and 245 ml was estimated for the four samples shown in Figure 5.5. This would give rise to a gas content between 2.91 and 3.52 ml/g for the three samples (Table 5.3), which is considerably lower than that estimated from the isotherms (4.55 - 5.87 m^3/tonne). Examples of the application of the USBM method to the measured desorption data are given in Figures 5.8 and 5.9.

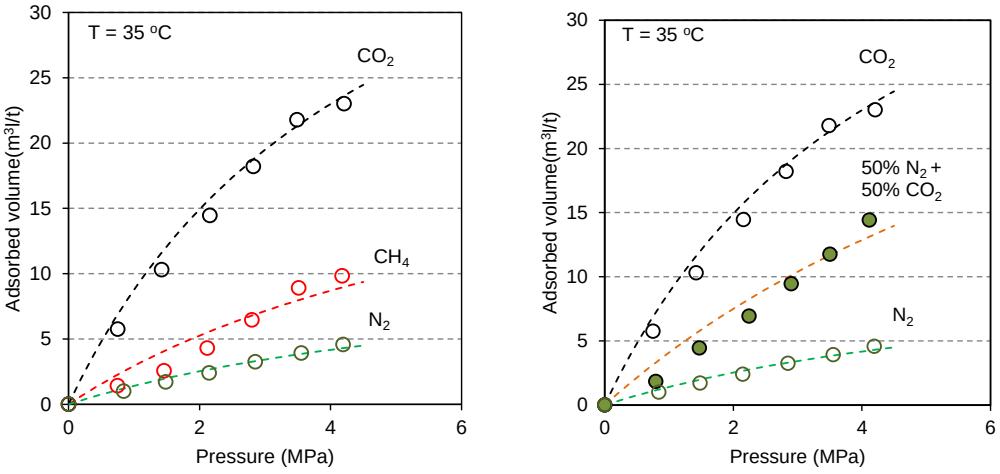


Figure 5.6: (a) Pure gas and (b) mixed gas isotherms for lignite from Coal Mine Velenje (Durucan et al., 2014).

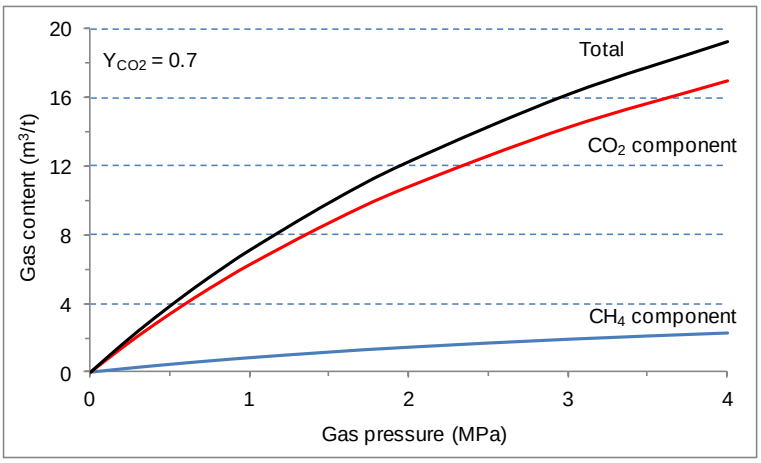


Figure 5.7: Mixed gas isotherms based upon the measured pure gas isotherms (Durucan et al., 2014).

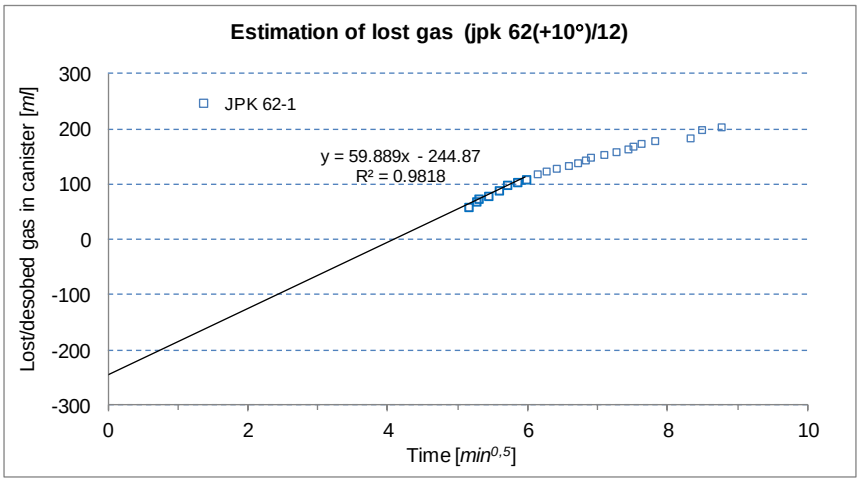


Figure 5.8: Estimation of lost gas volume with the USBM method (Sample JPK 62-1)

Table 5.3: Analysis and estimation of lost gas volume.

Sample	JPK 62-1	JPK 62-2	JPK 62-3	JPK 62-1
Section, m	22.0 – 22.1	22.1 – 22.2	23.5 – 23.6	23.6 – 23.7
Weight, g	354	314.1	334	287
Time (coring)	13/9/2012 8:29	13/9/2012 8:31	13/9/2012 10:16	13/9/2012 10:18
Time (sampling)	13/9/2012 8:54	13/9/2012 8:57	13/9/2012 10:44	13/9/2012 10:46
Sampling canister	MK 2	MK 4	MK 1	MK 4
Desorbed gas in canister + laboratory, ml	795	115*	755	780
Estimated lost gas (USBM method), ml	900 (245)	239 (114)	583 (218)	782 (230)
Total, ml	1,695 (1040)		1,338 (973)	1,562 (1010)
Estimated gas content, m^3/tonne	4.79 (2.94)		4.01 (2.91)	5.44 (3.52)
Estimated gas content based on mixed gas isotherm ($Y_{CO2} = 0.7$), m^3/tonne	4.55 – 5.87 (gas pressure 6 – 8 bar)			

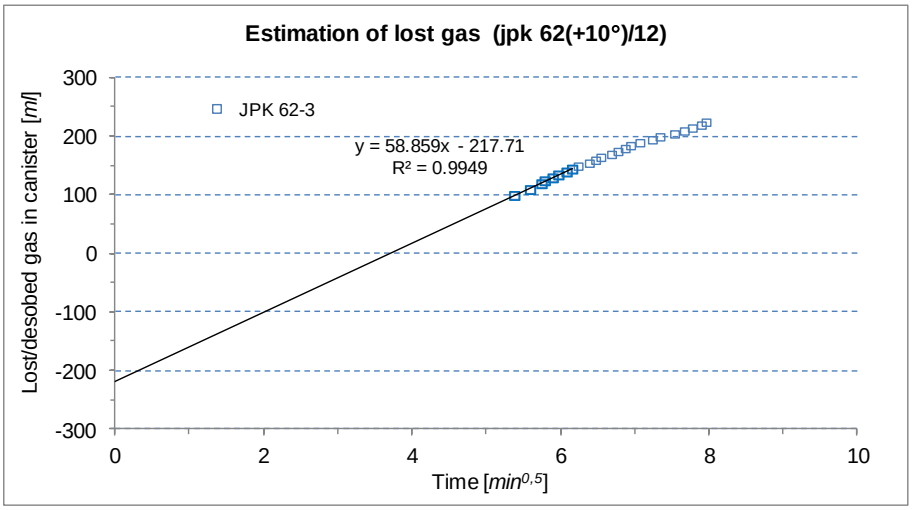
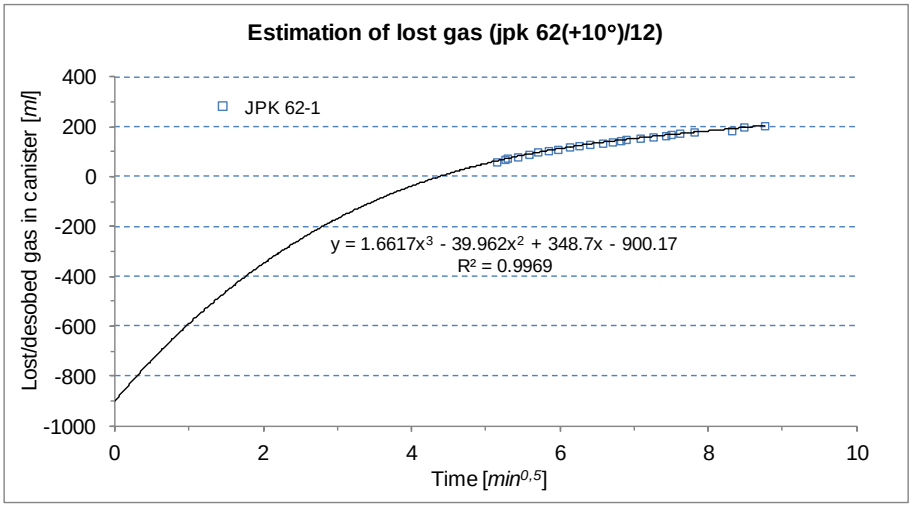
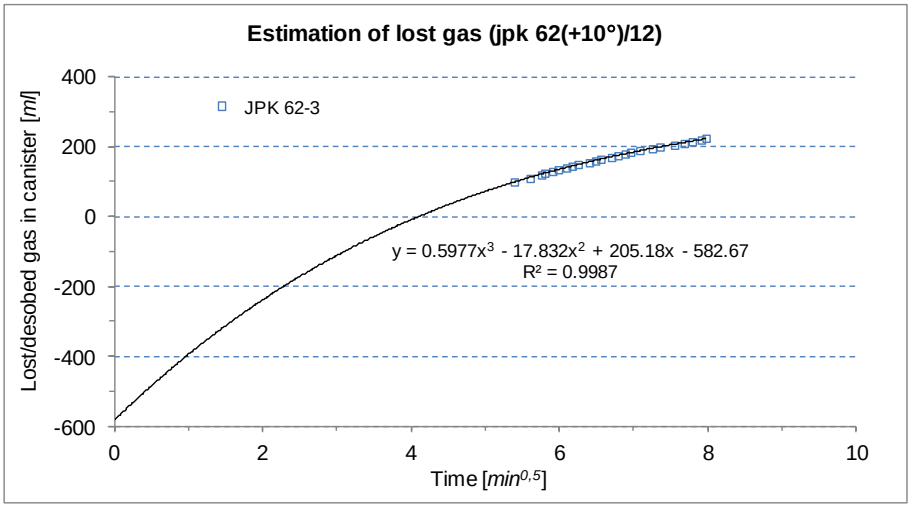


Figure 5.9: Estimation of lost gas volume with the USBM method (Sample JPK 62-3).



Sample JPK 62-1



Sample JPK 62-3

Figure 5.10: Estimation of lost gas volume by fitting to a 3rd order polynomial.

Based on these observations and previous gas content measurements from drill cuttings, research in this field has focused on defining a modified lost gas determination methodology based on lithotypes and other coal properties. Attempts have been made to fit the desorption data using higher order polynomial in order to yield a greater lost gas volume. It was found that, for the samples considered here, a 3rd order polynomial would give rise to lost gas volumes ranging from 239 to 900 ml, and the corresponding gas contents in the range of 4.01 to 5.44 m^3/tonne. These are broadly comparable to the gas contents estimated from the measured isotherms (Table 5.3). Examples of fitting of the desorption data with a 3rd polynomial are given in Figure 5.10.

Chapter 6

Design and implementation of active seismic monitoring campaigns

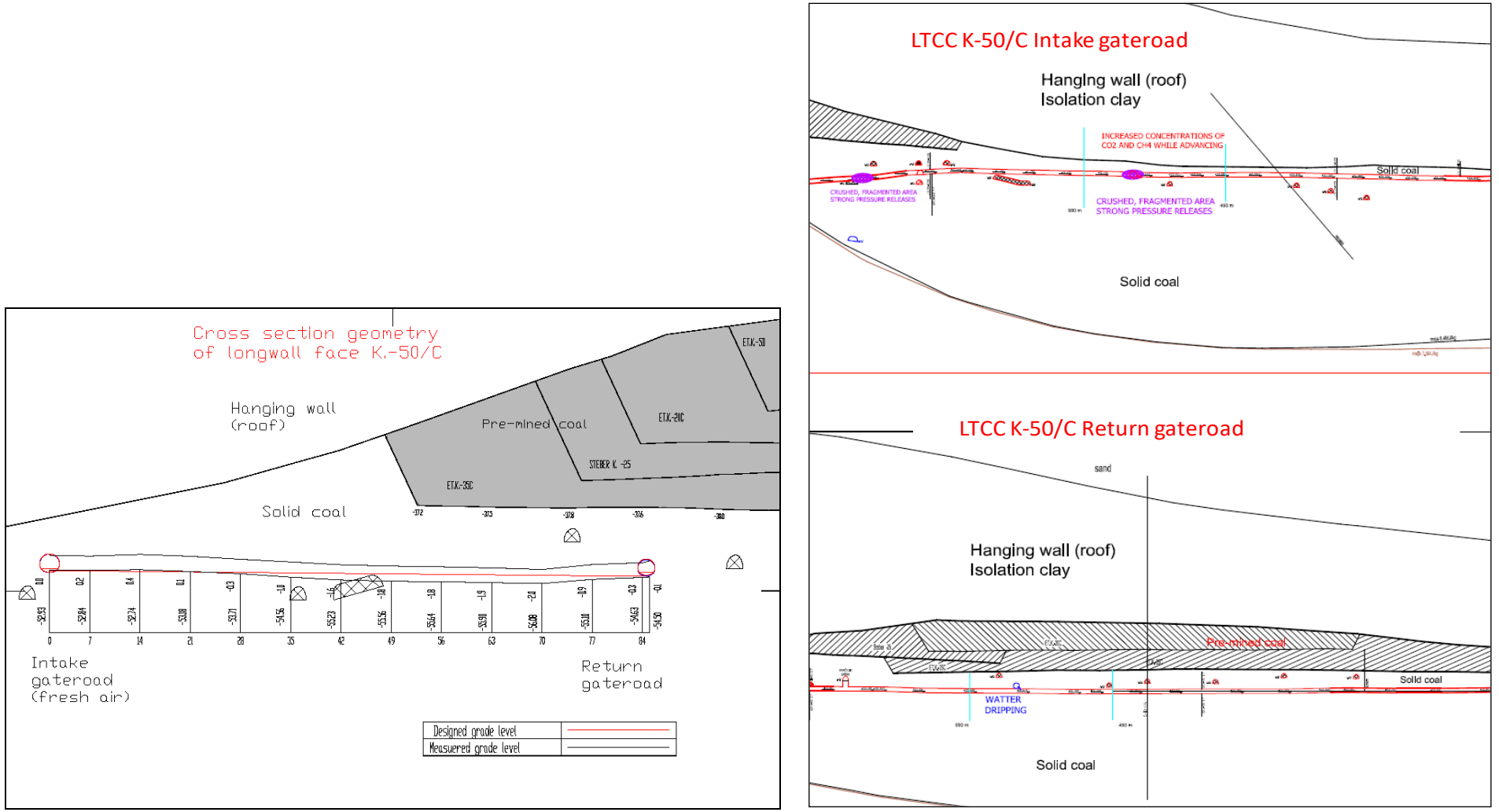
During the RFCS funded research project CoGasOUT, one of the objectives of the active seismic tomography implemented at Coal Mine Velenje was to identify the differences and the effect of working under mined out areas (as is the case in most Longwall Top Coal Caving faces) and under solid coal blocks (in the early stages of LTCC operations) on the development of outburst conditions.

Historical records of mining at Velenje have shown increased gas emissions and higher rock stresses in areas where mining is performed for the first time. Active seismic tomography performed by KUTEC was a part of the CoGasOUT project and, during the project period, two longwall panels were chosen for investigation and the research into the differences between structural properties of pre-mined and virgin coal areas.

The methodology used included creation of seismic sources by blasting or seismic vibrating hammer in longwall panels' return air gateroad and signal capture by three-chanel geophones in parallel locations in intake air gateroad over the panel section of 100 m. Site preparation included preparation of technical designs with the purpose of providing safe technical solutions and safety measures for the use of non-flame proof equipment in the coal mine which is classified as gassy (methane). The technical designs prepared included the details of borehole drilling for mechanical seismic source, blasting management for secondary seismic source and the niches prepared for seismic receivers in the chosen area of the longwall panels C K. -50 and B k. -130.

Boreholes for mechanical seismic source (vibrating hammer) in the longwall panel required stability for a longer time period. A special borehole construction was designed by drilling a 2 m long horizontal borehole, installing a 169 mm protective steel casing and applying coupling by cement mixture injection. The second seismic source was provided with an explosive charge (Slavit, 200g) in short blasting boreholes under the horizontal borehole prepared for the vibrating hammer. Every blast was prepared by drilling a borehole into the side-floor of the gateroad and activated for the recording. The receiver locations were prepared as shallow niches in parallel location to seismic sources in the longwall panel side of the gateroad.

The safety measures implemented included constant ventilation air measurements (methane concentration below 0.5 %); removal of non-flame proof equipment when measurements were not performed; automatic power supply safety switch and safety training for the non Velenje personnel.



a) b)

Figure 6.1: (a) Cross section A-A' along the face line, (b) Longitudinal sections taken along the intake and return gateroads of the longwall district C K.-50.

6.1 Active seismic tomography

Underground coal extraction activities can significantly alter the in-situ stress field around mine openings. Mining-induced stresses may lead to fracture initiation, or the reactivation of pre-existing faults. It has been found that the variation of applied stress on rock mass can positively affect the P-wave velocity (Maxwell and Young, 1996). In addition, the creation of fractures during the process of rock failure can dramatically reduce the P-wave velocity perpendicular to the loading direction (Scott et al., 1993). Furthermore, seismic velocity is characterised by rockmass properties such that local variations in coal lithology would affect P-wave velocity as:

$$v_P = \sqrt{\frac{K + 4G/3}{\rho}} \tag{6.1}$$

where v_p is the P-wave velocity, K is bulk modulus, G is the shear modulus, and ρ is the density of the rock.

Solving velocity tomograms is a classic problem of inversing travel time data. Assuming that n rays are recorded by a receiver, there is a vector of travel time $\boldsymbol{T}$ ($n\times1$). By spatially discretising the study area into an m number of grids, the slowness vector $\boldsymbol{S}$ ($m\times1$) for all grids has the following relationship with travel time $\boldsymbol{T}$:

$$\boldsymbol{T}=\boldsymbol{D}\boldsymbol{S} \tag{6.2}$$

To solve $\boldsymbol{S}$,

$$\boldsymbol{S}=(\boldsymbol{D}^T\boldsymbol{D})^{-1}\boldsymbol{D}^T\boldsymbol{T} \tag{6.3}$$

Where $\boldsymbol{D}$ ($n\times m$) is the matrix of ray path and its data represent the distance of each ray at each grid to the receiver point. In order to effectively solve $\boldsymbol{S}$, iterative methods, such as Algebraic Reconstruction Techniques (ART), Simultaneous Iterative Reconstruction Technique (SIRT), conjugate gradient, and least squares method, can be used (Mendecki, 1997).

Time-lapse seismic tomography measurements at Coal Mine Velenje were jointly conducted by K-UTEC Salt Technologies (Germany) and the mine staff in a 100 m-long section of the K. -50/C LTCC panel as shown in Figure 3. The seismic sources and receivers were placed along two gateroads. The horizontal distance between the two gateroads was 141 m. The boreholes required for the sources and receivers were planned and drilled in advance, before the installation of conveyors and other mining equipment in the main (intake) gateroad. In total, 40 receiver and 40 source boreholes, which were spaced regularly at ~2.5 m, were prepared in the intake and return gateroads, respectively. During the surveys, 120 receiver components located on 40 receiver points (each point equipped with x-, y- and z- components) were used. X-component represents the P-wave velocity parallel to the gateroad, y-component represents the P-wave velocity perpendicular to the gateroad, and z-component represents vertical direction. For the generation of P-waves, explosive sources in small boreholes were used. The seismic wave recording equipment consisted of geophones, signal transceivers and a system control/recording computer.

6.2 Active seismic tomography at longwall panel C k.-50

The first programme of seismic tomography surveys aimed at taking advantage of the unique characteristics of LTCC face C k. -50 where the longwall panel is retreating partly under a mined out zone and partly under solid roof coal for some distance (Figure 6.1). Figure 6.2 presents the position of the seismic tomography zone where the NW part of the longwall panel is located directly under solid (virgin) coal and intact roof strata whereas the SE part is located under mined out coal and caved roof strata.

The objective of the research was the determination of structural differences of coal mass in the longwall panel via rock stress distribution created by the effect of longwall face advance. Research included a number of separate campaigns of tomography measurements, from which two were successful.

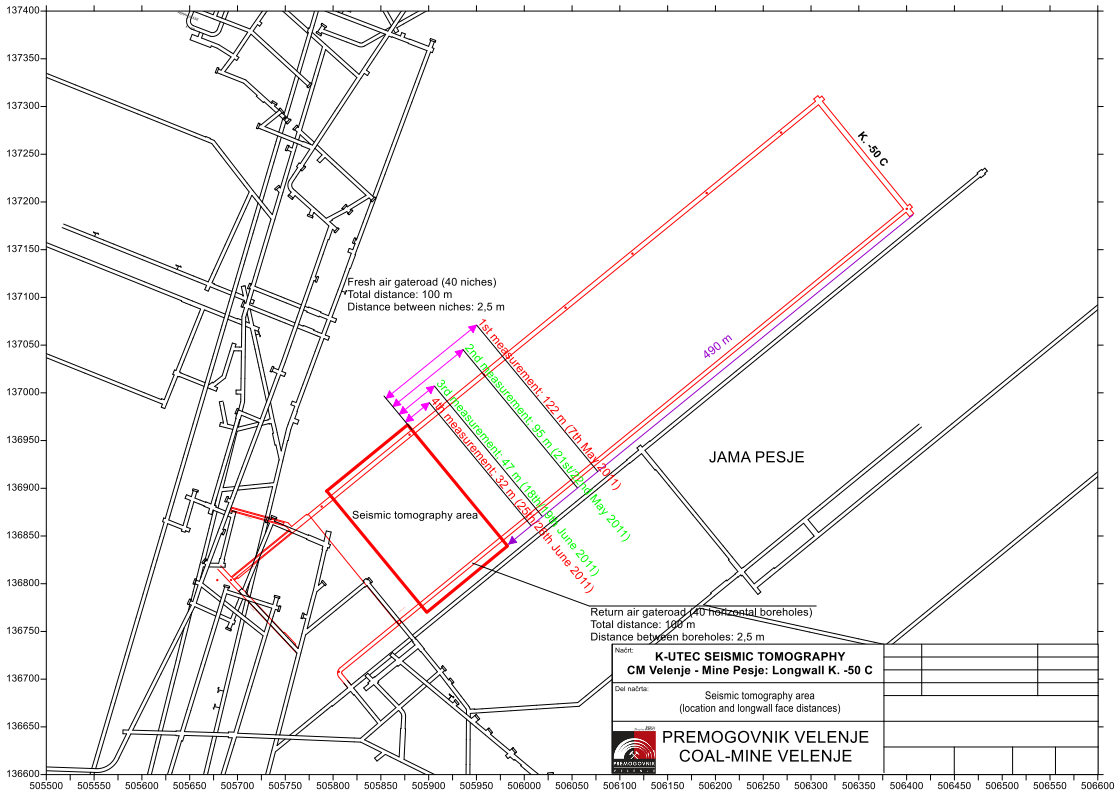


Figure 6.2: Mine outline with longwall panel C k. -50 (Mine Pesje – Coal Mine Velenje). Seismic tomography area is marked with red rectangle.

A 100 m section of the longwall panel C k. -50, close to the face completion line, was set up for tomography measurements as shown in Figure 6.2, which also overlapped with the microseismic monitoring zone, described in Chapter 7. The seismic sources and receivers were placed along the two gate roads. The horizontal distance between the two gateroads was 141 m. The boreholes required for the sources and receivers were planned and drilled in advance, before the installation of conveyors and other mining equipment in the main (intake) gateroad. In total, 40 receiver and 40 source boreholes, which were spaced regularly at 2.5 m, were prepared in the intake and return gateroads respectively.

During the surveys, 120 receivers located on 40 receiver points (each equipped with one x-, y- and z-component) were used. For the generation of P-waves, explosive sources in shallow boreholes were used. Figure 6.3 shows the seismic tomography team on site and the geophone layout in the gateroad. The seismic wave recording equipment consisted of geophones, signal transceivers and system control/recording computer. During the lifetime of longwall C. k -50, four surveys were attempted and two seismic tomography measurement campaigns were successful (face position with respect to the tomography zone indicated in green text in Figure 6.2), others having to be interrupted due to excessive gas levels in the longwall district. The first (baseline) survey was carried out during 21st/22nd May 2011. During this first campaign the nearest receiver was 95 m away from the longwall face, which was advancing towards the tomography zone. For the second successful measurement carried out during 18th/19th June 2011, this distance was 47 m. The seismic velocities generated from seismic sources measured in the two campaigns ranged from 1.55 km/s to 2.15 km/s.



(a) (b)

Figure 6.3: (a) Seismic tomography measurement team from the Coal Mine Velenje and K-UTEC), (b) Geophone layout for seismic tomography measurements.

As an example, Figures 6.4 and 6.5 present the P-wave velocity tomograms of the 1st and 2nd measurements for the x component when the longwall face was 95 m and 47 m away from the tomography zone respectively. Figure 6.6 presents the velocity difference tomogram for the x component, plotted by taking the difference between the 2nd and 1st measurements (e.g. P_{x2}-P_{x1}). The tomograms produced by the three components were reasonably consistent, reflecting the overall stress concentrations on both sides of the panel (NW under the solid roof coal and the SE under caved roof) with slight differences caused by lithology and anisotropy effects.

Note that a relatively high velocity zone was detected diagonally across the centre of the study area by the 1st campaign. During the time of the first campaign, the 100 × 141 m tomography zone was relatively far from the face-line and almost unaffected by the mining-induced abutment stresses, which suggests that the P-wave velocity variations reflect the lithological conditions within the study zone. No notable faults were detected. Therefore, the relatively high seismic velocity zone detected is believed to be a xylite-dominated zone. Naturally, even higher seismic velocities would have been expected if this zone contained pure xylite.

Although the results after the first tomography campaign were not conclusive, the tomograms supported the hypotheses that, as compared to the SE part under caved roof, the NW part of the longwall face under solid roof should experience higher abutment pressures when the face is at some distance from the tomography zone. With the longwall face 47 metres from the tomography zone, the area nearest to the approaching face in the NW half of the panel has the lowest P-wave velocities, suggesting fracturing of the coal under extreme abutment stresses, a slightly higher (medium) velocity behind this area which may suggest the initial stages of fracture formation, and a high velocity zone beyond this indicating compacted coal under stress build up. The SW half of the tomograms on the other hand, suggest that the seam under a relatively thin slice of top coal and caved roof only experiences a mild stress abutment, enough to compact the coal seam (but not fracture) leading to high P-wave velocities in the front and lower (medium) P-wave velocities beyond this area due to a slight increase in the stress.

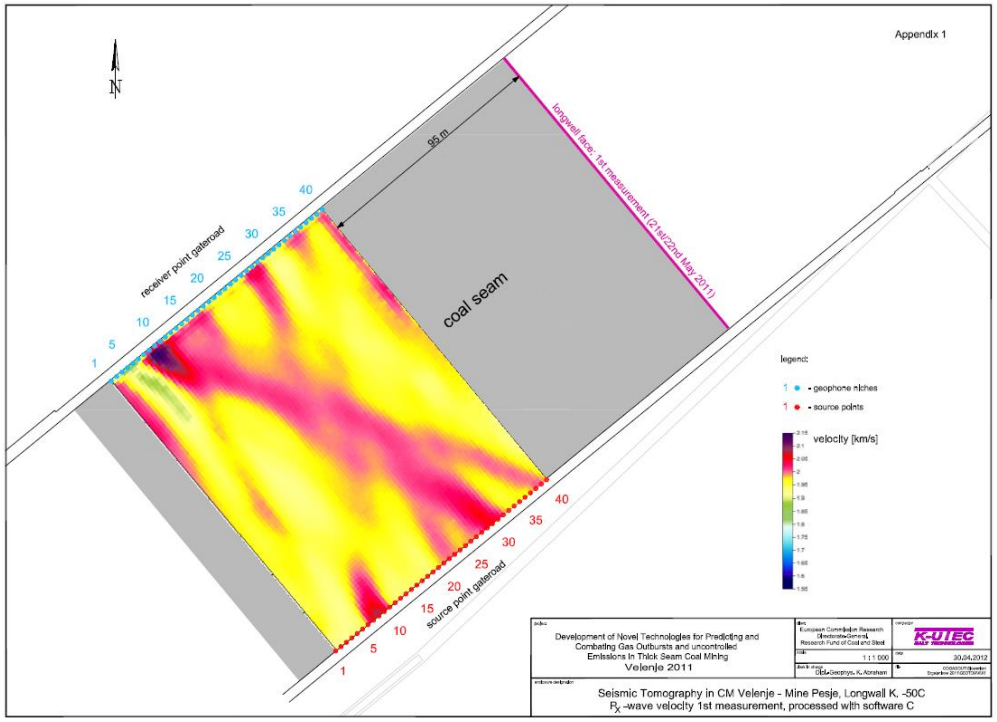


Figure 6.4: Longwall panel C k.-50 P-wave velocity tomogram for the 1st measurement during the2011 campaign (x component) (Courtesy of K-UTEC and the CoGasOUT Project).

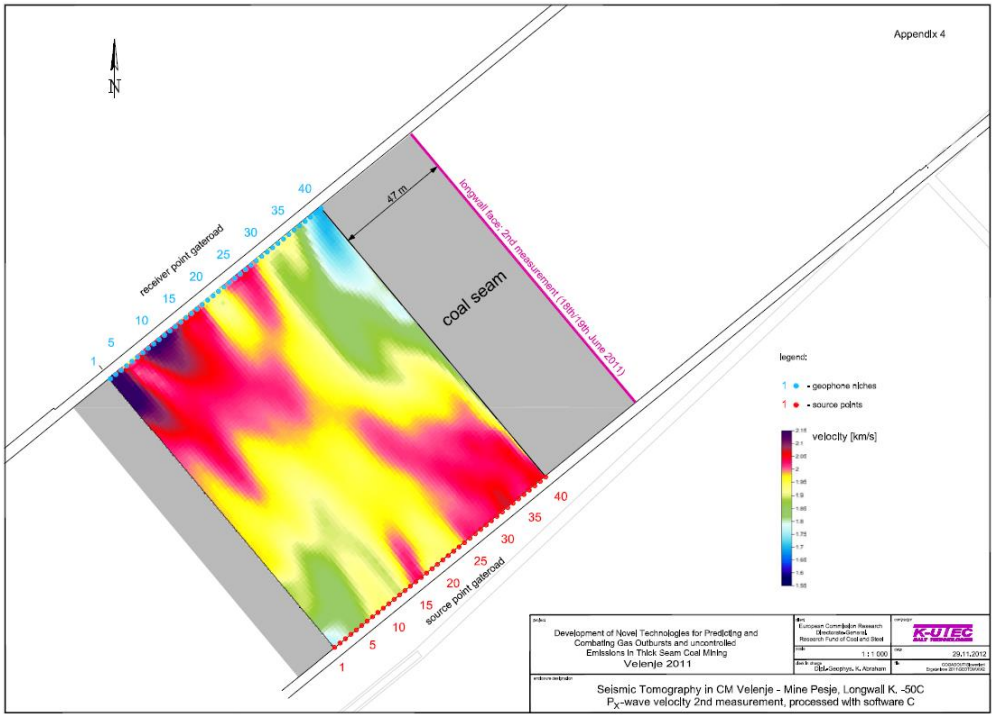


Figure 6.5: Longwall panel C k.-50 P-wave velocity tomogram for the 2nd measurement during the 2011 campaign (x component) (Courtesy of K-UTEC and the CoGasOUT Project).

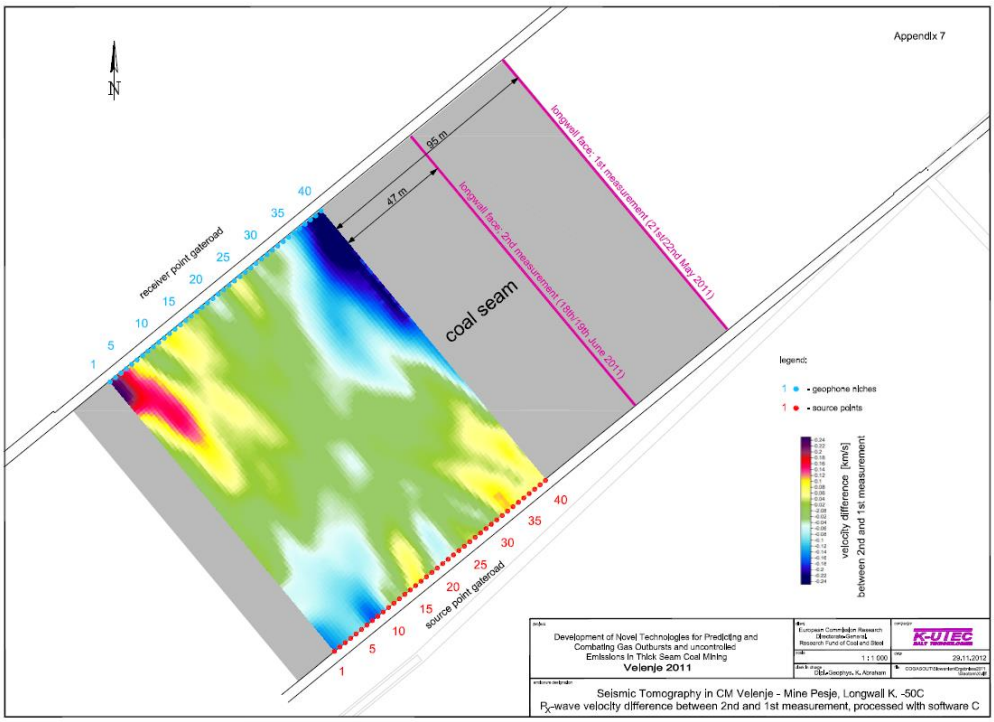


Figure 6.6: Longwall panel C k.-50 P-wave velocity difference between 2nd and 1st measurements in 2011 (x component) (Courtesy of K-UTEC and the CoGasOUT Project).

6.3 Active seismic tomography at longwall panel B k.-130

The second repeat seismic tomography campaign at Coal Mine Velenje was carried out at LTCC face B k.-130 in 2012 (Figure 6.7).

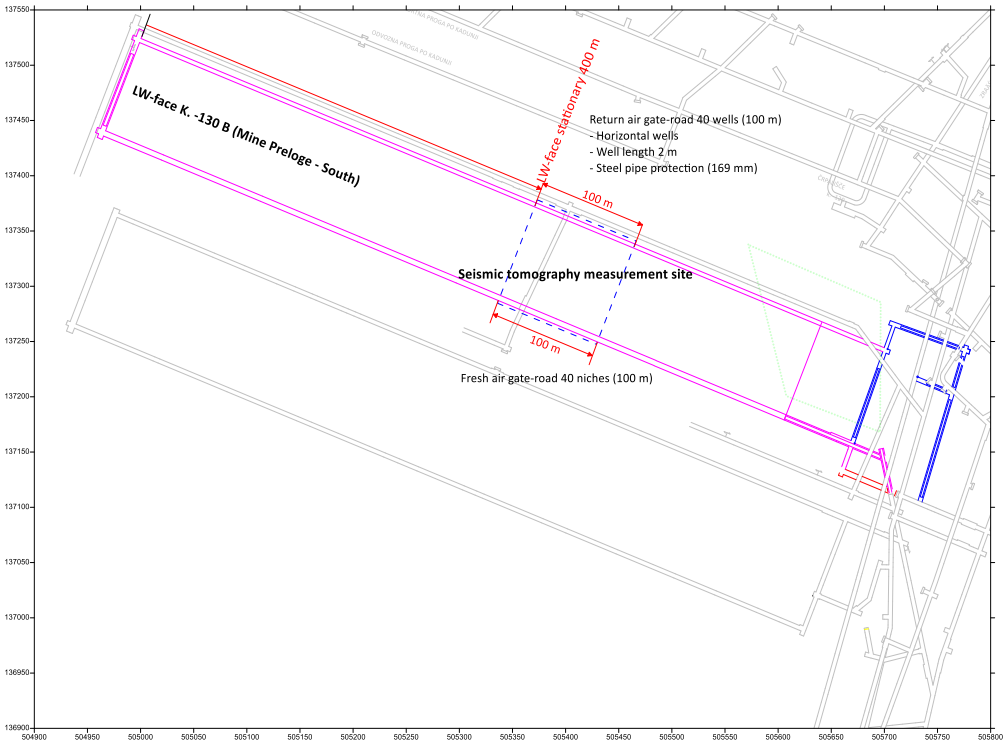


Figure 6.7: Mine outline with longwall panel B k. -130 (Mine Preloge – Coal Mine Velenje). Seismic tomography area is marked with dashed blue rectangle.

Compared with the first set of measurements in longwall face C k.-50 in 2011, there were two significant differences in the coal panel measurement area:

- a large fault plane was crossing the coal panel within the measurement area with further smaller but significant faults running parallel to the face line further back (Figure 6.8).
- the whole measurement area was under a caved waste at the bottom level of the coal seam.

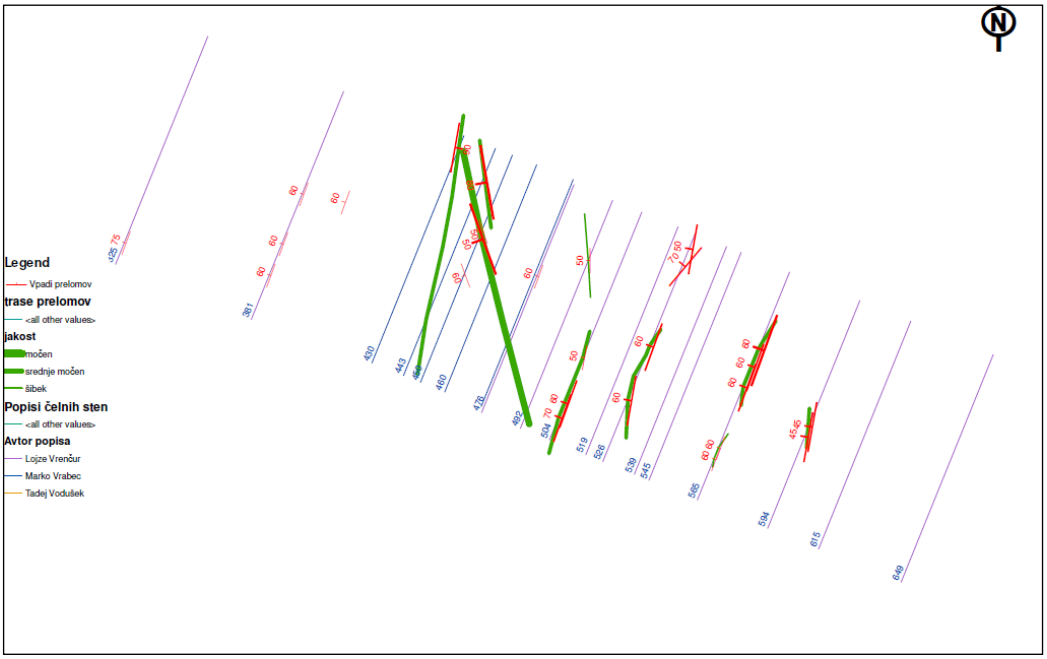


Figure 6.8: Structural map of longwall B k.-130 showing the faults identified (Scale 1:1,000).

Figures 6.9 and 6.10 present the P-wave velocity tomograms of the 1st and 2nd measurements for the P-wave component y when the longwall face was situated 87 m away and 1.5 metres inside the tomography zone respectively. Overall, the results of the P-wave seismic tomography campaign have shown up to 600 m/s decrease in P-wave velocities within close proximity of the longwall face, a sign of significant fracturing, increased permeability and gas flow. Figure 6.11 present the velocity difference tomogram for the y component, plotted by taking the difference between the 2nd and 1st measurements (e.g. P_{y2}-P_{y1}).

The tomograms produced by the three components were reasonably consistent, reflecting the overall stress regime with slight differences caused by lithology. Overall, the results of the P-wave seismic tomography campaign have shown decreasing P wave velocities within close proximity of the longwall face as shown for all 3 components in the second tomography data when the longwall face is very close to the measurement zone.

One very important observation from the 2nd measurement campaign in 2012 was that there is no anisotropy in the seismic data. This can be attributed to the longwall face B k. -130's position within the coal seam, as the whole longwall panel was under a thin slice of uniform Top Coal with caved roof above the whole footprint of the longwall panel. The effect of stress abutment and reduction in P-wave velocity was uniform and along the full face width. Indicating the overriding role of stress changes and thus its effect on gas pressure and seismic velocities compared to that of lithology within the stress abutment zone.

A second important feature of the 2012 tomography measurements was the existence of a large fault running across the longwall panel which was cut through by the longwall face before the 2nd tomography campaign. Figure 6.9 clearly identifies the fault with a distinct P-wave velocity difference at two sides of the fault plane during the first campaign when the longwall face is far enough not to affect the stress regime. This is due probably to lithology and/or gas pressure. The effect of the two relatively smaller faults further in to the measurement zone is also clear. On the other hand, once the

longwall face is close to the fault, or partly cut through it, the influence of the stress abutment overrides the fault effect and there is a uniform distribution of P-wave velocity in the front abutment zone, indicating significant fracturing, increased permeability and gas flow (Figure 6.10).

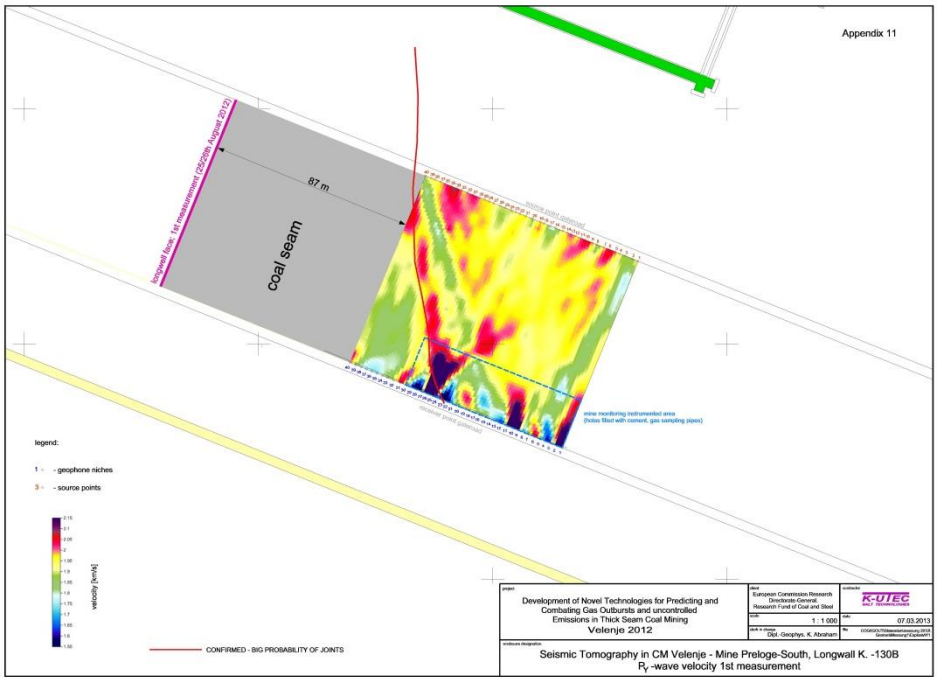


Figure 6.9: P-wave velocity tomogram of the 1st measurement at longwall face B k.-130 (y component) (Courtesy of K-UTEC and the CoGasOUT Project).

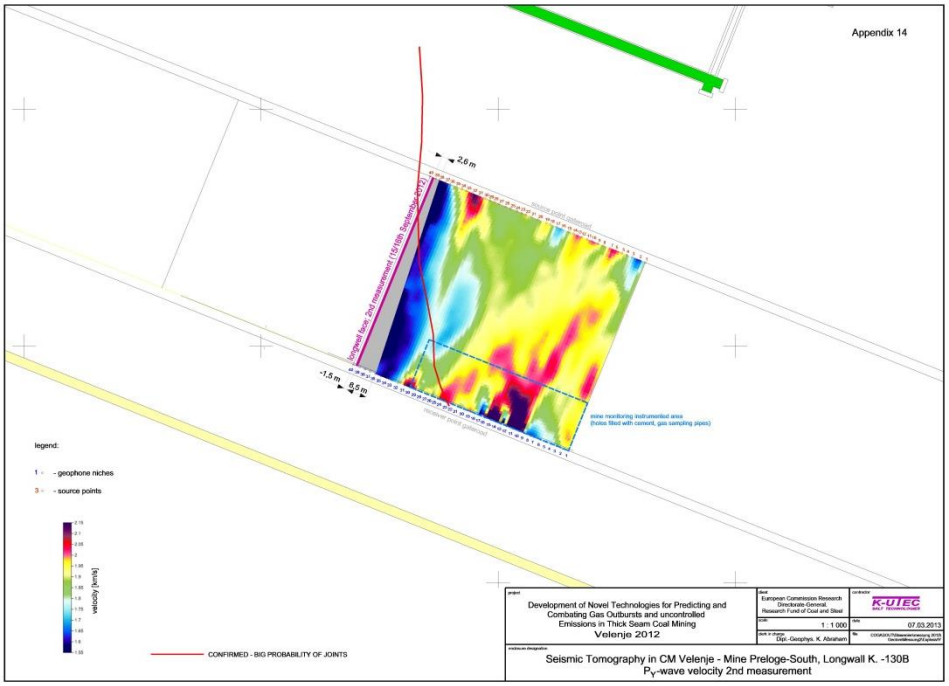


Figure 6.10: P-wave velocity tomogram of the 2nd measurement at longwall face B k.-130 (y component) (Courtesy of K-UTEC and the CoGasOUT Project).



Figure 6.11: B k.-130 P-wave velocity difference between 2nd and 1st measurements in 20112 (y component) (Courtesy of K-UTEC and the CoGasOUT Project).



Figure 6.12: The Vp/Vs ratio difference tomogram between 2nd and 1st measurements at longwall face B k.-130 taken during the 2012 campaign (Courtesy of K-UTEC and the CoGasOUT Project).

In order to generate controlled S-waves, a high energy borehole S-wave vibrator was used. The results of the second tomography campaign using the S-wave vibrator with pressure-on mechanism during 2012 were very successful. In general, the S-wave velocity increased up to 400 m/s as the longwall face approached towards the tomography zone. This increase was notable around 70 - 77m ahead of the longwall face, confirming the same observations from geotechnical measurements, indicating the forming of stress abutment, and an increasing gas pressure combined with changes in gas mixture. With the successful S-wave tomography, the V_p/V_s ratio tomograms and the ratio differences between the two 2012 campaigns were also analysed, which confirmed the same

observations made from P-wave tomograms, that a fractured zone with increased permeability and gas flow may be formed 40 m ahead of the longwall face.

6.4 Conclusions from the seismic tomography campaigns

The repeat (time-lapse) seismic surveys performed at longwall faces C k.-50 and B k.-130 in Coal Mine Velenje were completed successfully and demonstrated the viability of this method underground, yielding valuable results by correlating stress zones, gas pressure and flow ahead of an advancing LTCC face with seismic velocities. It was clearly shown that the changing stress regime in the vicinity of an advancing longwall face can be identified through seismic tomography and the methodology can identify distinct zones of stress and lithological changes, as well as structural anomalies and their behaviour within a coal panel. The changes in both P- and S-wave velocities correlated with the enhanced permeability and gas flow zones in the dimensions of which were also confirmed during the drainage trials, presented in Chapter 8.

The mechanised longwall layout and production/face advance rate at Coal Mine Velenje is comparable to that practiced at most other mechanised hard coal mines in Europe and it is believed that the methodology demonstrated is independent of the characteristics of particular coals or seams and is transferable to other coal mines in Europe. The methodology, which was successfully demonstrated in the CoGasOUT project, would be also effective and useful in identifying lithological changes, as well as structural anomalies within a longwall district, which may be a precursor for a potential outburst condition and be used and analysed hand in hand with continuous microseismic monitoring.

Chapter 7

Design and implementation of passive seismic monitoring campaigns

In parallel with the active seismic investigations, passive seismic monitoring campaigns as part of the CoGasOUT project were carried out at Coal Mine Velenje. The objective of this work was to evaluate the potential use of passive microseismic monitoring and passive tomography for detection of overstressed and fractured zones, which may lead to coal and gas outburst, or uncontrolled gas emissions. Research concerned with assessing the validity and application potential of the following techniques:

- Development of underground microseismic networks to monitor gas and coal outburst;
- Microseismic monitoring and development of a methodology to interpret seismic events for identifying high gas emission and outburst risk conditions;
- Assessment of the correlation between emission of total gas, CH_4, CO_2, daily advance of longwall face and parameters of recorded micro seismic events during extraction of coal in thick seams;
- Passive tomography methodology in underground coal longwall panels;
- Detection of locations prone to coal-gas outburst and uncontrolled gas emission according to passive tomography study.

7.1 Microseismic monitoring

Both fracture initiation and fault reactivation involve the change of elastic energy in a rockmass, which are generally accompanied by the radiation of some energy in the form of seismic waves (Cook, 1964). Fracture initiation around mine openings is predominately caused by tensile failure (Cai, 1998). The potential energy (E_c) released from this type of failure is of low magnitude and can be described by (Griffith, 1921; Broek, 1986):

$$E_c = \frac{(1-\mu^2)\pi\sigma_n^2 a^2}{E} \tag{7.1}$$

where a is the half length of the crack, E is the Young's modulus, μ is the Poisson's ratio, σ_n is the normal stress acting on the crack.

Fault reactivation as a result of shear failure occurs some distance from the mining activities and the potential energy (E_f) released is associated with larger magnitude (Gibowicz and Kijko, 1994):

$$E_f = \frac{1}{2}\Delta\sigma DA + \sigma_f DA \tag{7.2}$$

where A is the surface area of the fault, D is the average fault slip, $\Delta\sigma$ is the stress drop between the initial stress and the final stress σ_f after faulting.

The measured seismic energy is a relatively small fraction of the total energy released (E_c or E_f). The energy released during failure can also be consumed in overcoming the cohesion of crack tips/faults or attenuated during wave transmission. In the absence of attenuation, the radiated seismic energy

(E_r) can be computed based on the time-integrated values of P-wave and S-wave seismograms, $u_P(t)$ and $u_S(t)$ respectively (Shearer, 2009):

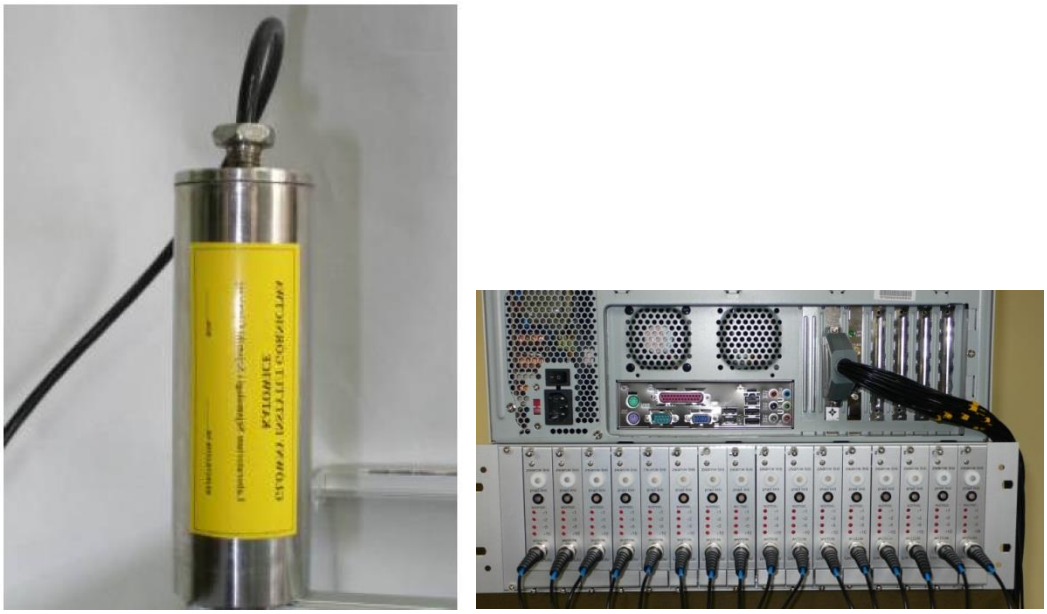
$$E_r = 4\pi\rho v_P r^2 \frac{< U_{Pm}^2 >}{U_P^2} \int_{t_1}^{t_2} |u_P(t)|^2 \, dt + 4\pi\rho v_S r^2 \frac{< U_{Sm} >}{U_S} \int_{t_1}^{t_2} |u_S(t)|^2 \, dt \qquad (7.3)$$

where r is the distance between the source and receiver, ρ is the density of medium, v_P and v_S are P-wave and S-wave velocities of the medium, U_P^2 and U_S^2 are the radiation pattern terms, and $<U_{Pm}^2>$ and $<U_{Sm}^2>$ are the mean values for P-wave and S-wave. t_1 and t_2 are times bounding a group of P-wave and S-wave.

Microseismic monitoring does not only record the scale of energy released during fracturing or faulting, but also locate the hypocentre of a failure episode by assessing the P-wave and S-wave arrival times at geophones. Ideally, the geophones should be placed in a non-planar array, but this is sometime restricted by the engineering conditions, such as that in underground longwall panels where access to the coal seam is limited to the gateroads.

7.2 Microseismic monitoring campaigns at Coal Mine Velenje

The underground microseismic monitoring campaign at Coal Mine Velenje was jointly conducted by the Department of Geology and Geophysics of Central Mining Institute (GIG) in Poland and the mine staff. GIG has designed a flameproof automated seismic observation system (SOS) for underground installation in coal mines (Mutke, 2013). An entire SOS includes a number of low frequency underground geophones combined with seismic signal transmitters in the form of current signals via transmission lines, and a surface DLM-SO Receiving Station which is connected with the Seismic Recording System (see Figure 7.1). The hardware allows for automatic triggering and recording of mining induced seismic events. The MULTILOK and SEISGRAM software, which are integrated into the SOS seismic system, enable data acquisition and data processing so as to provide information about source parameters and location of seismic events. The 32-channel Seismic Observation System (SOS) was designed as flame-proof equipment.



(a) (b)

Figure 7.1: Microseismic monitoring equipment: (a) The low frequency DLM-2001 geophone probe and (b) DLM-SO surface data receiver.

At Coal Mine Velenje, the flameproof automated Seismic Observation System (SOS) was first installed in March 2011 (Figure 7.2). The system was constructed as a 32 channel data transmission system

working with 8 three component velocity sensors and 8 one component velocity sensors. Each probe was fixed into floor coal with a 1.5 m long anchor as depicted in Figure 7.3(a). Cement was used to ensure the coupling between probes and coal. Microseismic data recorded by the probes were sent to surface via the data transmission system as illustrated in Figure 7.3(b). The seismic sensors were installed at two longwall faces in the mine as (Figure 7.2):

- At longwall panel C k.-50 four three component sensors and four one component-vertical sensors were installed at the same area where the seismic tomography work was carried out.
- At longwall panel A k.-130/A four three component sensors and four one component-vertical sensors were installed.

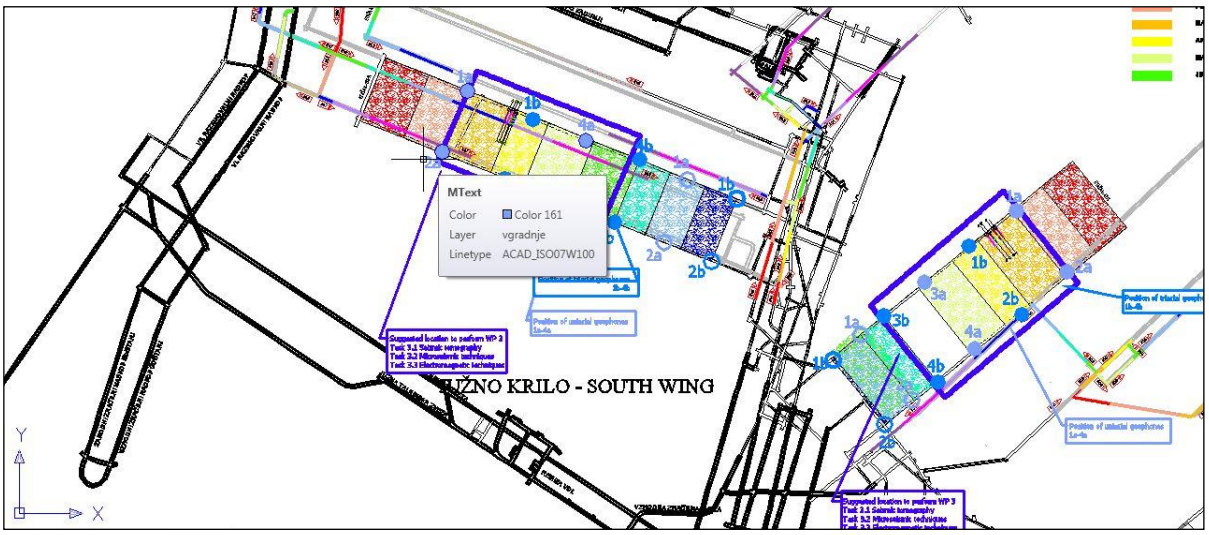
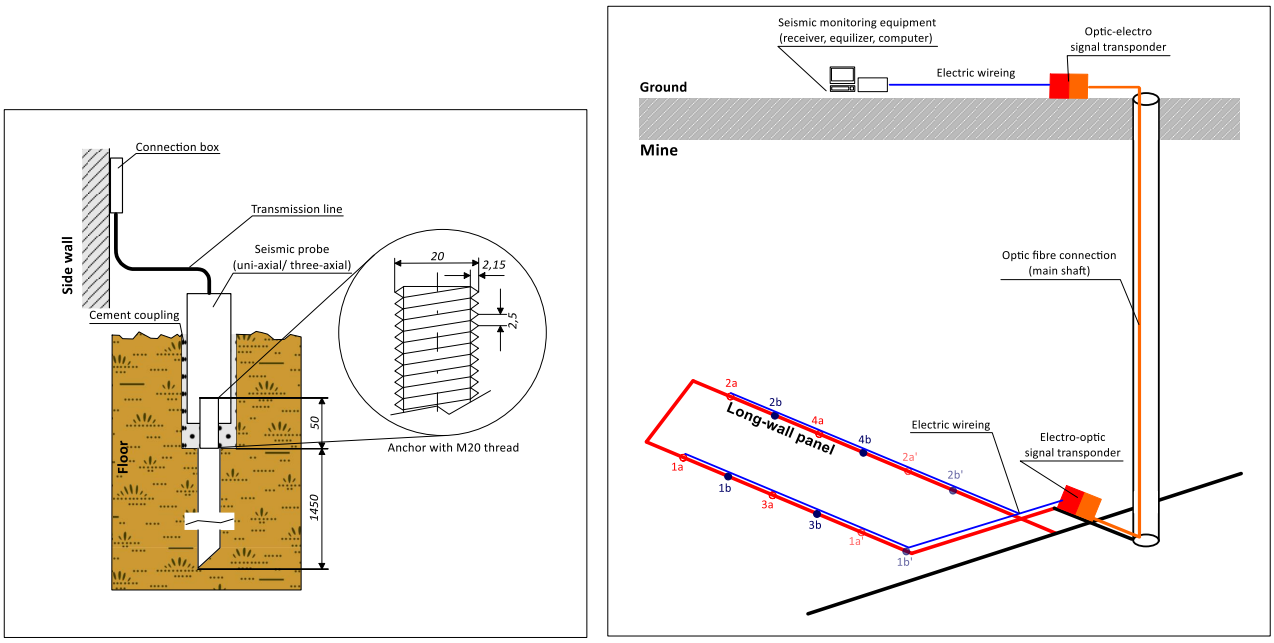


Figure 7.2: The distribution of the seismic stations and the spatial configuration of the sensors used for microseismic study in longwall faces C k.-50 and A k.-130 at Coal Mine Velenje.



(a) (b)

Figure 7.3: Schematic of (a) the geophone probe installation, (b) the data transmission system.

The seismic events have been transmitted through the internet to the GIG data centre. At Coal Mine Velenje, 2,784 seismic events were recorded at longwall panels C k.-50 and A k.-130 during the

monitoring period from 27 April 2011 to 31 August 2011. The largest seismic event reached a seismic energy as high as $6x10^6$ J (local magnitude of about 2.5).

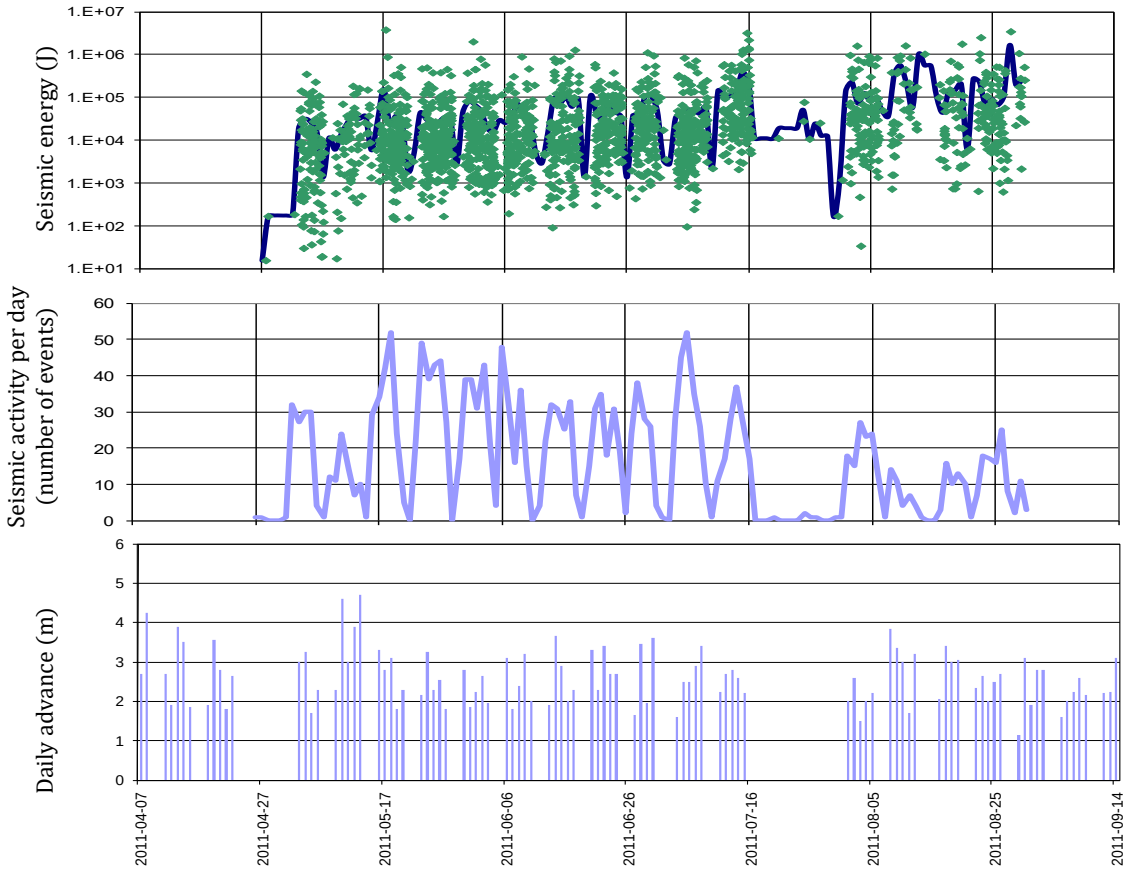


Figure 7.4: Daily seismic activity, seismic energy and face advance at the longwall panel K-50/C in coal mine Velenje during the period 7 July to 14 September 2011 (Courtesy of GIG and the CoGasOUT Project).

The analysis of the microseismic monitoring data has suggested that the dominant source mechanism (Wiejacz, 1994) for the seismic events was uniaxial compression or tensile stresses associated with the failure of coal seam and, thereby, increase the fracture zones in the coal seam and the possibility of intensive migration of gases.

Analysing the correlation between daily face advance, seismic activity and seismic energy recorded at longwall panel C k.-50 at Coal Mine Velenje it was found out that nearly no seismic activity took place over the weekends or during other periods of no production at the face (Figure 7.4); the correlation between longwall face advance and seismic activity was clearly identifiable.

7.2.1 Use of passive tomography in detecting areas prone to outbursts and uncontrolled emissions

Using the seismic events recorded during the monitoring periods Bent-ray tomography P wave velocity images (Lurka, 2009) were obtained for Coal Mine Velenje longwall districts studied. As shown in Figures 7.5 and Figure 7.6, particularly notable was the effect of faces C k. -50 and A k. -130 movement and the migration of high and low P-wave velocity zones in both longwall districts in the direction of mining over the monitoring period, confirming the effectiveness of the methodology in identifying potential high gas emission and/or stress build-up sites. The high P-wave velocity regions were identified as high abutment stress zones and the relatively lower P-wave velocity zones were associated with highly fractured zones where more intensive gas emission may be expected.

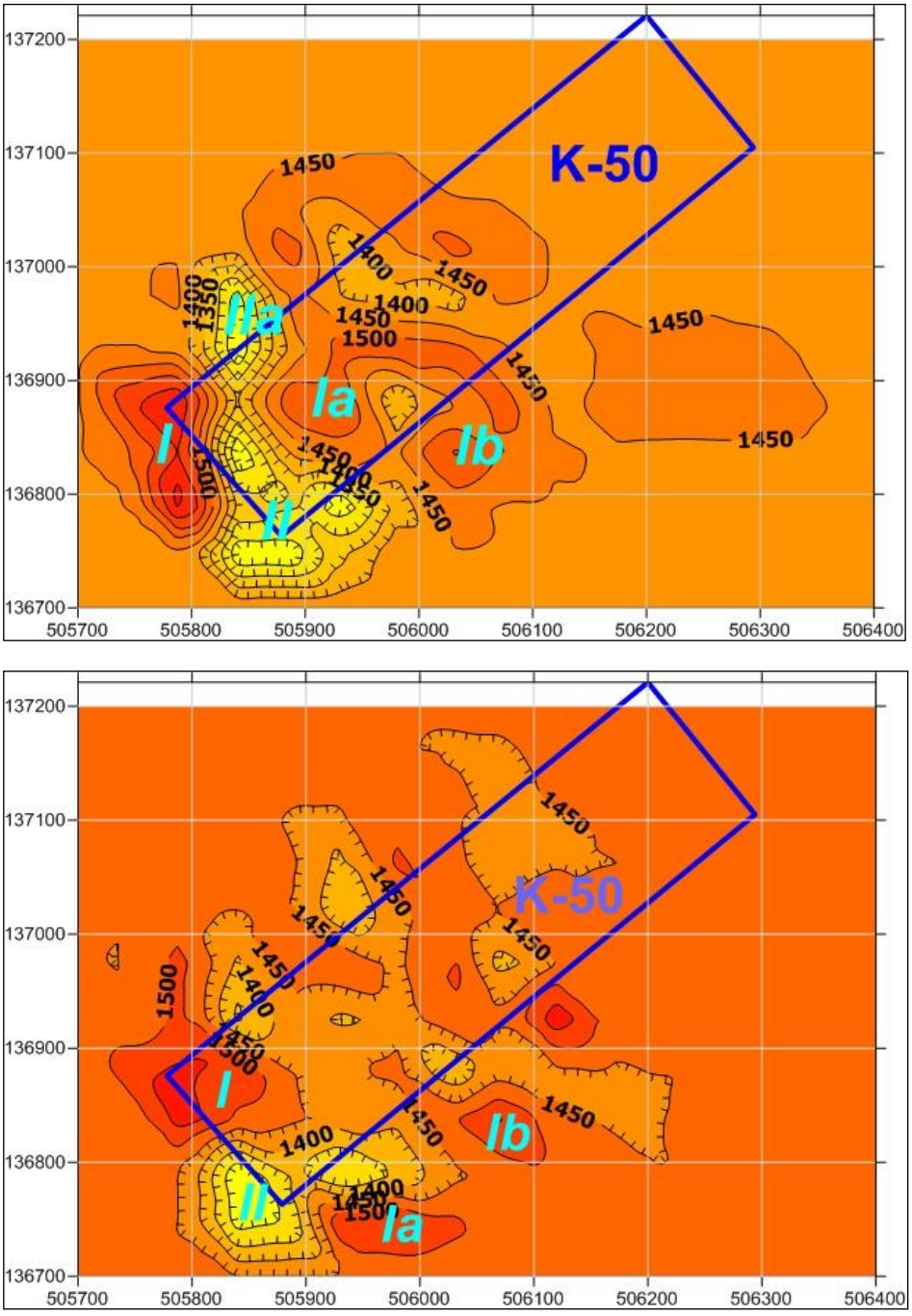


Figure 7.5: Bent-ray tomography P wave velocity images obtained using seismic events recorded during consecutive monitoring periods at longwall C k.-50 in Coal Mine Velenje (units m/s) (Courtesy of GIG and the CoGasOUT Project).

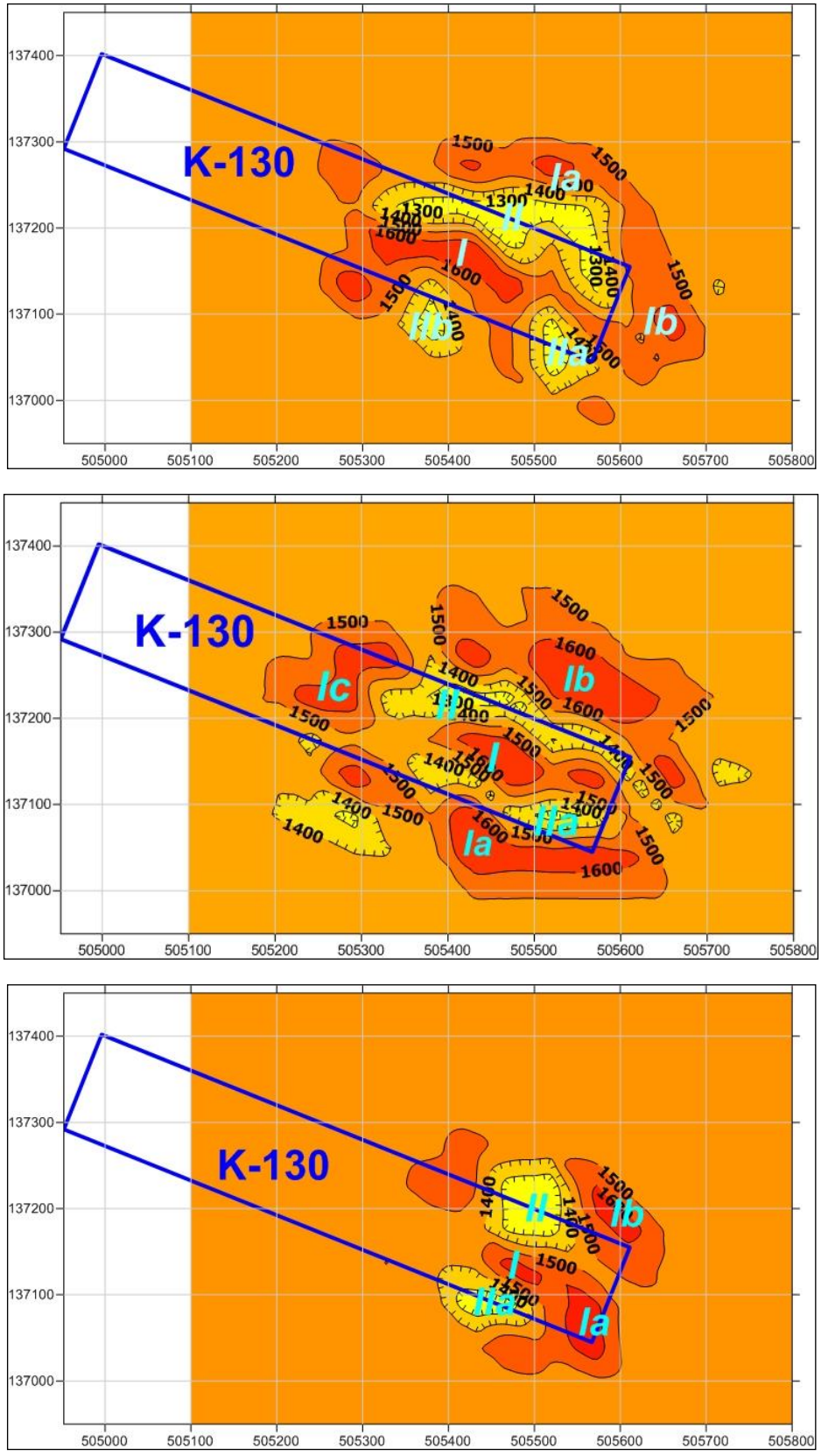


Figure 7.6: Bent-ray tomography P wave velocity images for longwall A k.-130 in Coal Mine Velenje during three consecutive months as face retreated towards the SE direction (units m/s) (Courtesy of GIG and the CoGasOUT Project).

7.2.2 Analysis of microseismic monitoring data to predict build-up of uncontrolled emissions

Following the completion of the microseismic monitoring at Coal Mine Velenje, Imperial College carried out a detailed analysis of the processed microseismic data provided by GIG. Specifically, the analysis included the spatial distribution of the microseismic events with respect to the advancing coal face, the histogram of the weekly energy released and its temporal evolution. Recognising that microseismic events occur as a result of the fracturing of coal/rock surrounding the mine openings, a methodology was developed to use the fractal dimension, estimated from the spatial density of the recorded microseismic incidents, to characterise the seismic energy build-up ahead of the face, and correlate this with high gas emission events.

Coal production at C k.-50 started in November 2010 and ended in October 2011. The face advance rate at the C k.-50 panel was approximately 11~12 metres per week. Gas concentration and the ventilation airflow were monitored by using 3 sensors (Figure 7.7) throughout the production at this panel. Microseismic events induced by the movement of the coal face were recorded from 27 April to 30 August 2011. In an effort to gain an understanding of the induced microseismicity due to mining activity, the microseismic data was plotted and analysed on a weekly basis.

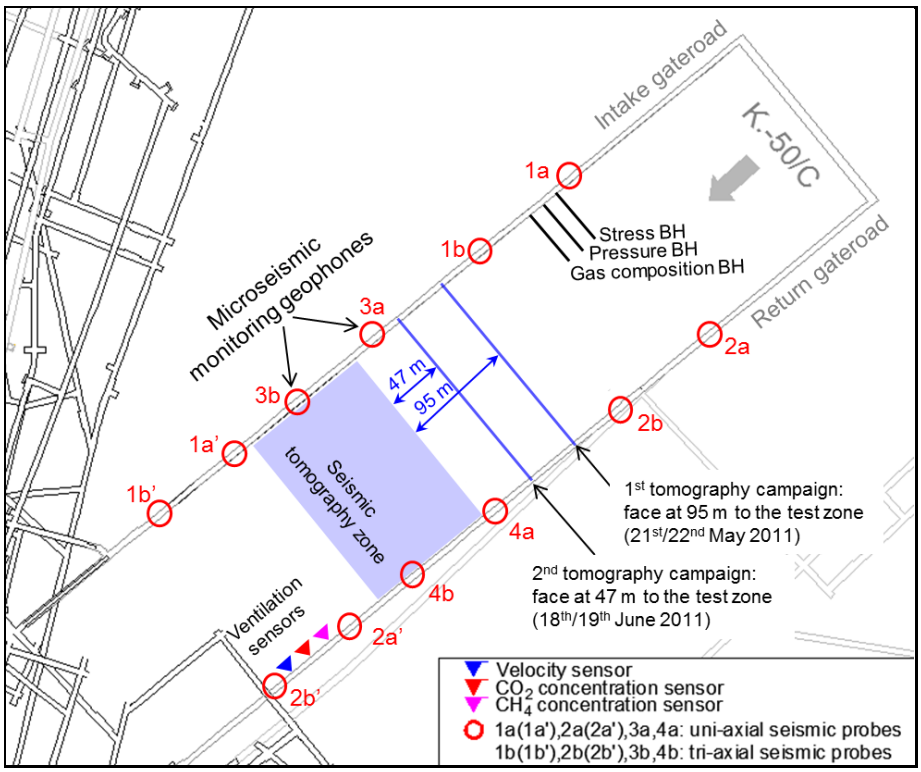
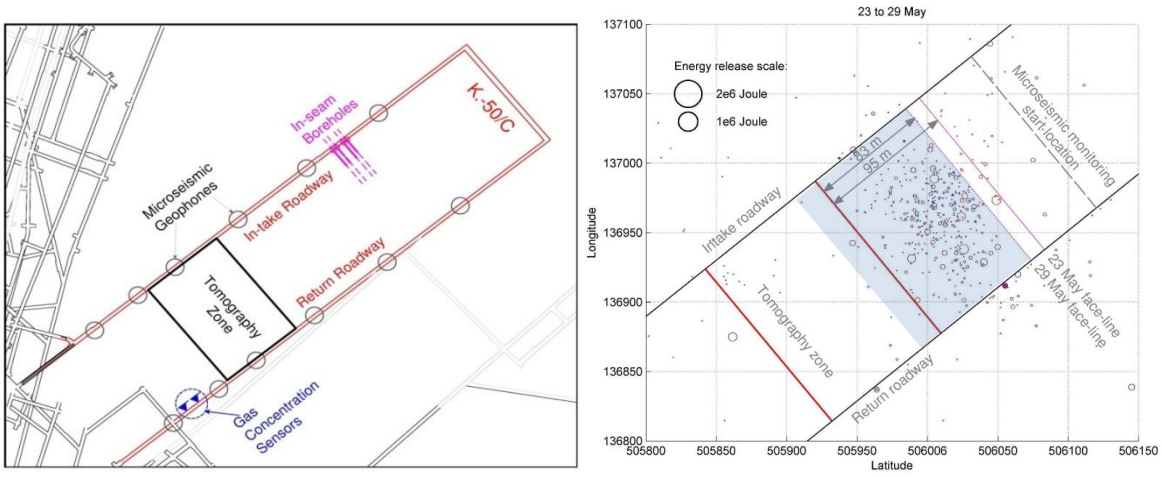


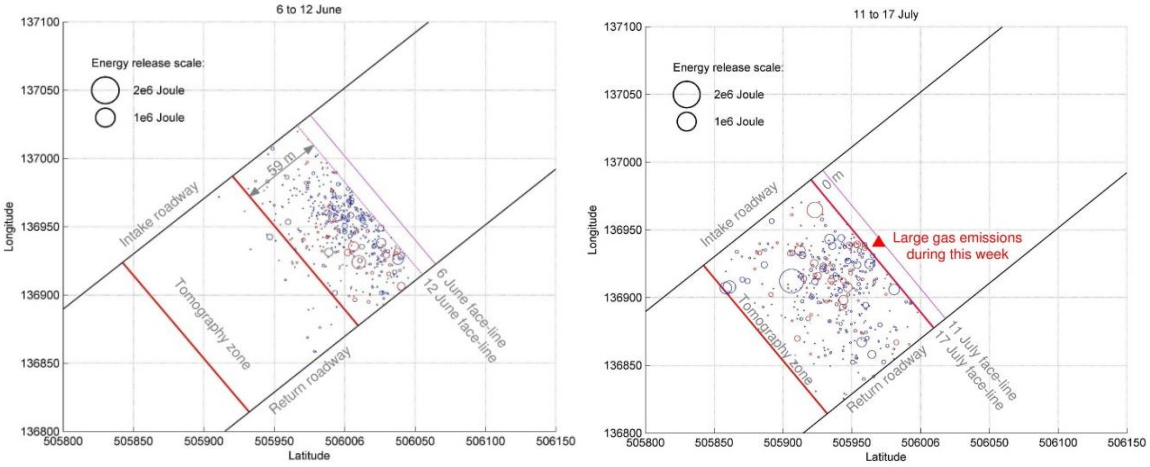
Figure 7.7: Seismic stations and the configuration of sensors used for microseismic monitoring and ventilation measurements at LTCC panel C k. -50 in Coal Mine Velenje.

Figure 7.8b illustrates an example plot of the spatial distribution of microseismic events. In the figure, red and blue circles denote the events recorded during week 23 to 29 May 2011 and in the previous weeks (2 to 22 May 2011) respectively, with the size of the circle reflecting the energy intensity released by a microseismic event. Analysis of the spatial distribution of the microseismic events have shown that most of the microseismic activity occurred within 70m ahead of the advancing face, clustering and forming a cloud of events building up in numbers and energy intensity in the same area for some time, and then moving on to a new location notably ahead of the old events, further away from the coal face in a periodic cycle. As shown in Figure 7.8b and Figure 7.9, one such build-up of seismic events and energy led to a very high gas emission event at longwall face C k.-50 during 14-15 July 2011, and that the face had to be vacated and gas cleared out for some time.



a) b)

Figure 7.8: (a) The deployment of monitoring techniques in C k. -50 LTCC panel at Coal Mine Velenje (b) an example plot of the spatial distribution of microseismic events at the longwall panel

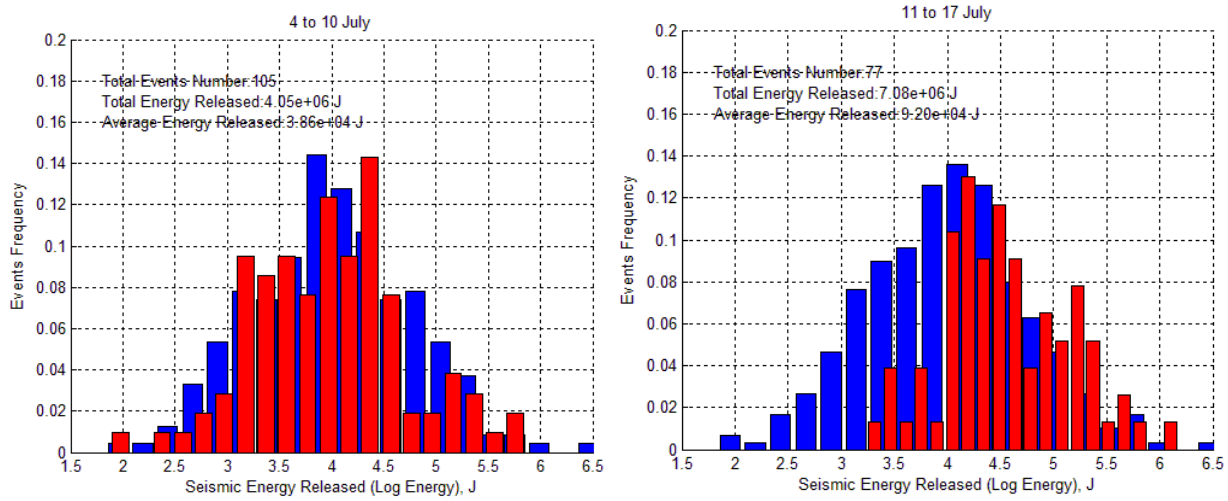


a) 6 to 12 June 2011 b) 11 to 17 July 2011

Figure 7.9: Spatial evolution of microseismic events leading to an episode of increased gas emission.

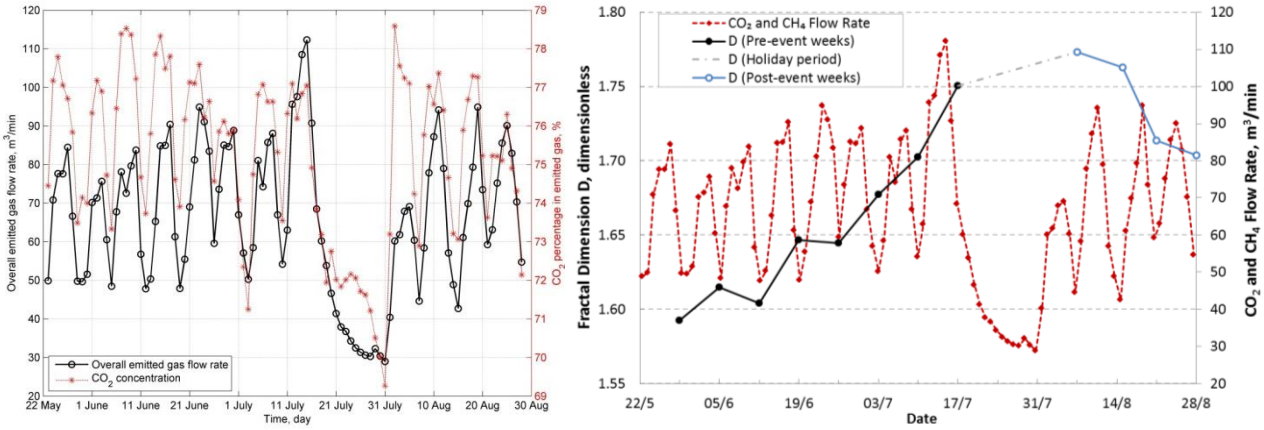
In Figure 7.10, the red bars indicate the statistics of the new events occurred during the reference week, while blue bars indicate that of events occurred during previous production weeks. Unlike it was during the week 6 to 12 June 2011, a notable shift of the red bars to the right (higher energy levels) marks the observed excessive gas emission event in the week 11 to 17 July 2011.

As fractal dimension is an effective measure to characterise the fracture patterns in rock failure process (Zhao et al., 1993; Poliakov et al., 1994; Balankin, 1997), Imperial College researchers computed the fractal dimension (D) of the recorded weekly microseismic events in order to characterise the fracture network induced by coal extraction at the face during the CoGasOUT project. It was noted that the fractal dimension corresponding to the weekly seismic events displayed a positive correlation with the monitored gas emission rate in the district (Figure 7.11). It can be seen that the fractal dimension increased steadily, from just less than 1.60 to 1.75, over the 8 weeks period leading to the heightened gas emission rate. This increase in the fractal dimension suggests that the mining induced fractures evolved towards forming a two-dimensional network over the period, extending further away from the face, and thus potentially an increasingly larger mining disturbed area becoming available as both a source for gas emission which was experienced on 14-15 July 2014.



a) 6 to 12 June 2011 b) 11 to 17 July 2011

Figure 7.10: Histograms and periodic advance of seismic energy released in a production week.



a) b)

Figure 7.11: (a) Gas flow rate and gas concentrations measured during 22 May – 30 August 2011 period, and (b) evolution of fractal dimension versus the flow rate of emitted gas during 22 May – 28 August 2011 in C k. -50 LTCC panel at Coal Mine Velenje.

7.3 Conclusions from the microseismic monitoring campaigns

The data obtained from ventilation environment monitoring and microseismic monitoring at the LTCC panels were analysed and integrated. The following observations were made:

- The gas emission pattern follows closely the weekly coal production schedule at the mine, being much lower at weekends or holidays.
- The onset of microseismic events ahead of an advancing LTCC face tended to be localised over relatively stronger zones, such as the xylite-rich coal.
- A marked increase (by ~ 80% in two hours) in gas emission at the study LTCC face coincided with the period where there was heightened microseismic activity.

- A detailed analysis of the microseismic events during the week of excessive gas emissions suggests the spatial and temporal clustering of microseismic events at the heterogeneous zone indicated by seismic tomography as discussed in Chapter 6
- Although the number of events recorded during the week when excessive gas emissions interrupted production was relatively smaller, the total energy released during this week reached a maximum.

As discussed earlier in Chapter 4, a comprehensive borehole gas pressure and composition monitoring programme around production faces at Coal Mine Velenje has shown that, an extensively fractured zone within ~40 m of the LTCC faces in the upper mining levels of the seam contributes significantly to the gas emissions in a longwall district. The active seismic tomography campaigns described in Chapter 6 also suggested that, a relatively strong xylite- rich zone a barrier in front of a high gas content but relatively weaker detrite-rich zone and cause increased gas emissions or gas outbursts at the mine. Although no coal or gas outbursts have been observed during the microseismic monitoring period at the two LTCC faces monitored, the strong correlation between the episode of excessive gas emission and the increased microseismic activity improves our confidence in using microseismic monitoring as a tool for the early detection of mining conditions which may lead to gas and/or coal outbursts.

Chapter 8

Design and implementation of gas drainage trials at Coal Mine Velenje

Main objectives of underground gas drainage trials at Coal Mine Velenje was an investigation into the technology required to achieve drainage to reduce gas content and pressure in the lignite before and during longwall coal extraction. Trials were oriented towards single long-wall panel drainage pilots with testing of drainage boreholes, pipe-line, gas vacuum pump and monitoring equipment. Gas drainage pilot trial set-up was assembled as sections of pipeline for gas transfer, vacuum pump with closed water cycle, water-gas separation installation and monitoring equipment for performance evaluation and safety requirements.

It should also be noted that the design of the drainage borehole layout was based on the experience and learning achieved through coal seam gas composition, pressure, stress monitoring and the active and passive seismic monitoring campaigns as described in previous chapters.

8.1 Drainage system and monitoring equipment during pilot drainage trials (Longwall panel F k. -65)

A schematic of the pilot gas drainage trials' layout used at LTCC panel F k. -65 is presented in Figure 8.1. The drainage boreholes were all drilled in coal, in relative positions with respect to the retreating longwall panel in Mine Pesje. A number of different depths and directions of drilling were chosen for a coupled analysis of drainage performance and in seam stress/gas pressure measurements when operating in different sections of the longwall panel regarding the face position. The design parameters of the drainage boreholes prepared are presented in Table 8.1. Locations of all the drainage and monitoring boreholes are presented in Figure 8.2. As the longwall face advanced over boreholes R1 and R2 before the start of drainage trials could be started, additional (back-up) boreholes R5 and R6 were also drilled. A schematic presentation of a drainage borehole installation is shown in Figure 8.3.

Table 8.1: Drainage bore-hole design parameters.

Borehole	Y	X	Z	Inclination (°) (from horizontal)	Depth (m)
R1 (+2°)/13	505,821.7	137,530.5	-72.5	2°	50
R2 (+20°)/13	505,799.9	137,509.9	-75.0	20°	30
R3 (+2°)/13	505,766.0	137,478.0	-81.2	2°	50
R4 (-30°)/13	505,760.2	137,472.6	-83.5	- 30°	30
R5 (+20°)/13	505,719.3	137,433.9	-90.2	20°	30
R6 (+2°)/13	505,712.0	137,427.1	-92.0	2°	50

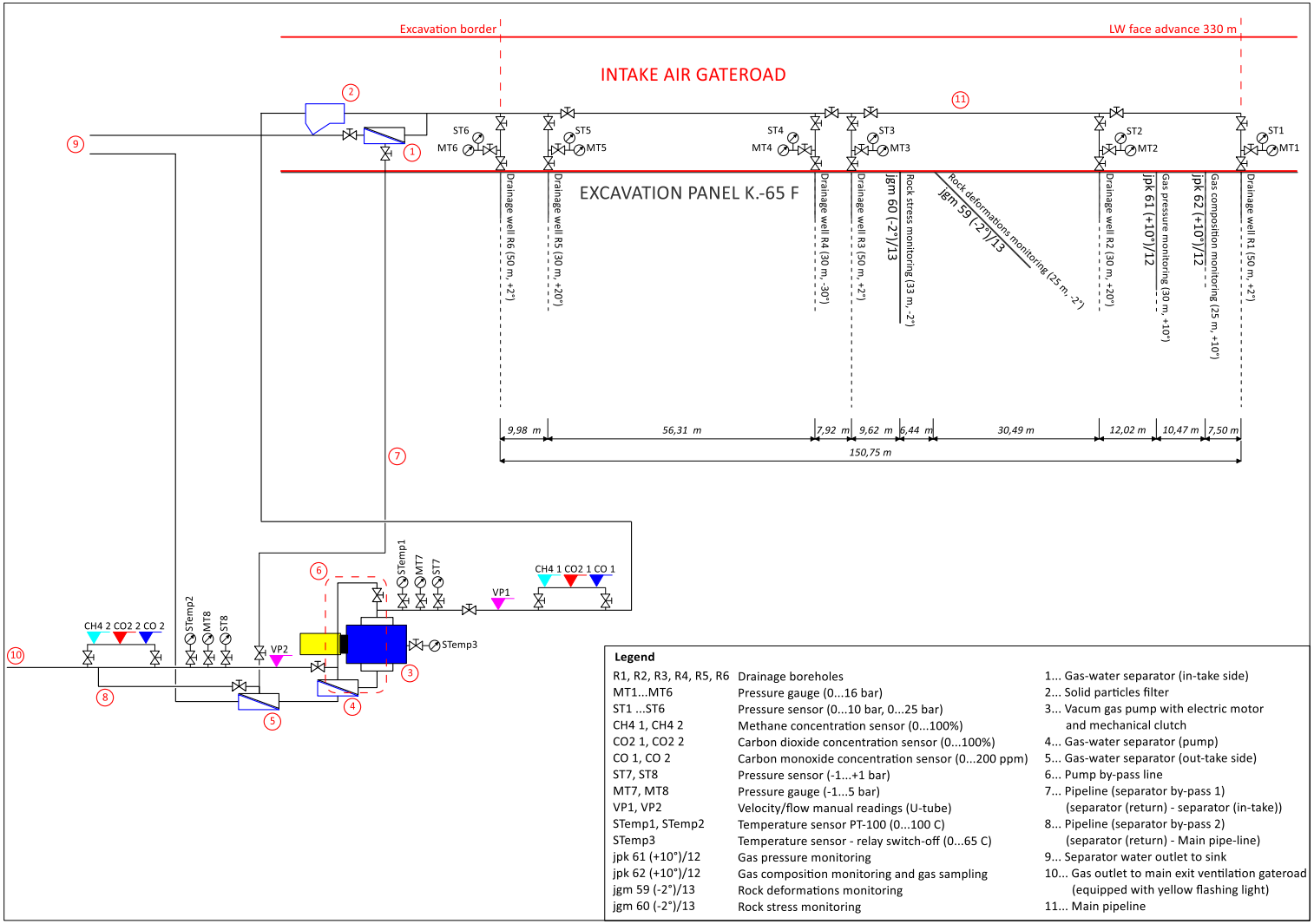


Figure 8.1: A schematic of the pilot gas drainage trial system in Coal Mine Velenje.

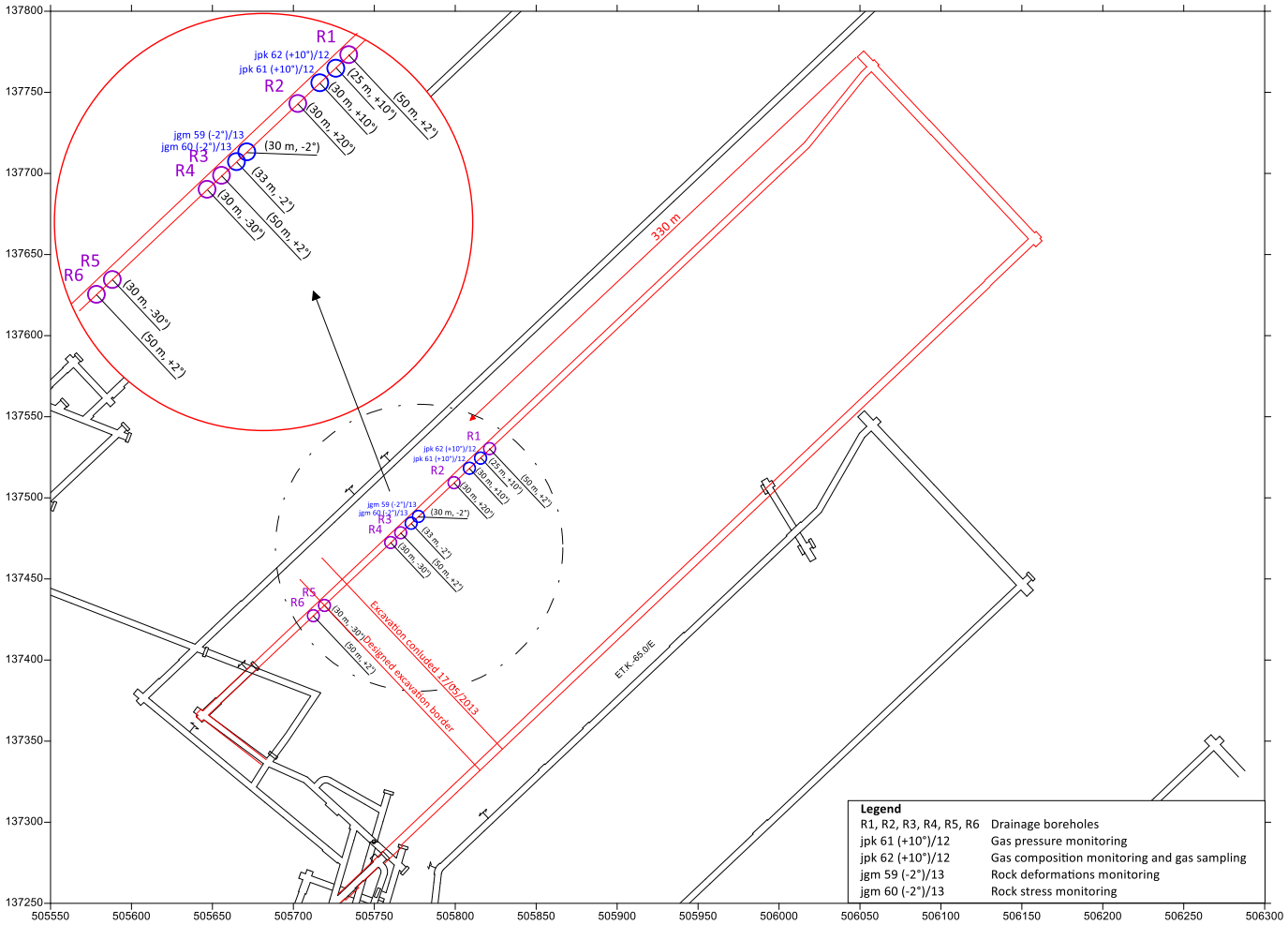


Figure 8.2: Locations of gas drainage and seam gas pressure-composition,rock stress and deformation monitoring boreholes at LTCC panel F k. -65.

Drainage pipeline, as the main component of gas transportation system, was located along the intake gateroads to longwall face and then led to the main return ventilation roadways for safety. Connections to boreholes were provided with T-sections on the pipeline, followed by ∅2'' antistatic plastic or rubber hose with mounted valves on both ends (Figures 8.4a) and 8.4b).

The full length of the pipeline was tested for leakages at overpressure of 5 bars before its use. A fully mechanical, water-cycle vacuum pump, Nash 2BE1 203, which is certified for gas and petroleum industry use, was further certified for mine use and installed as part of the drainage system. In preparation for the underground trials, the pump was equipped with required sensors and other safety elements as shown in Figure 8.5.

Gas drainage trials were performed under strict regulations applied at the mine. Safety equipment was installed at all crucial elements and sections of the gas drainage system. All equipment used was certified as intrinsically safe and approved for mine use, except for the gas vacuum pump, which was operating under strictly controlled conditions concerning gas concentrations in the gateroad, gas concentrations of drained gas, pressure in the pipeline and water (working media) temperature.

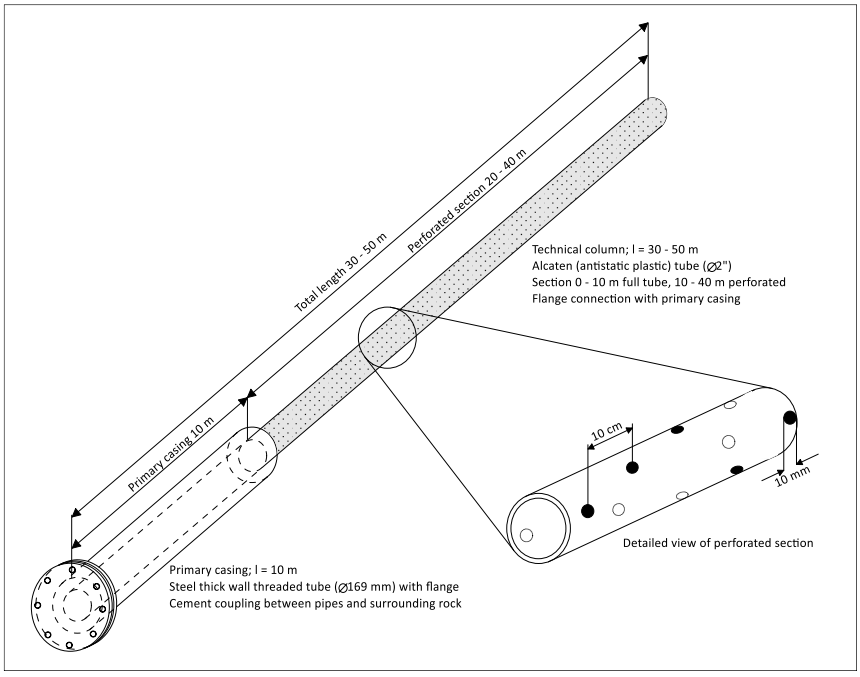
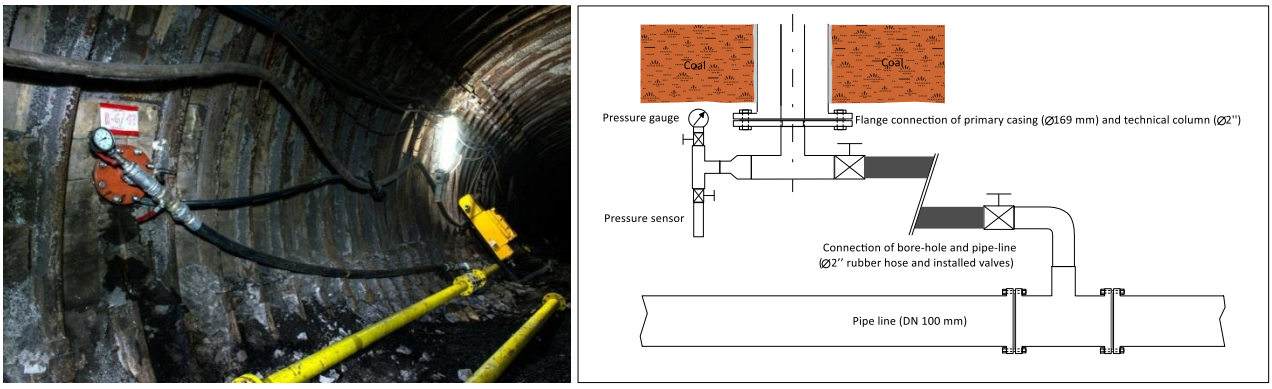


Figure 8.3: Schematic representation of a drainage borehole construction.



(a) (b)

Figure 8.4: Connection between drainage borehole and pipeline with 2'' rubber hose and valves and the gas pressure monitoring equipment.

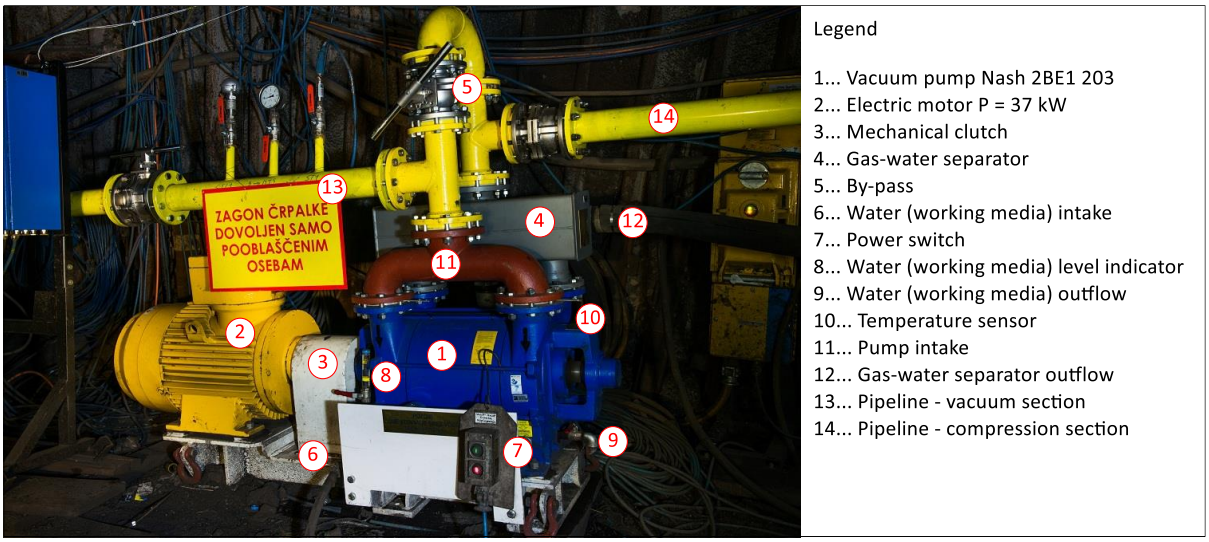


Figure 8.5: (a) Gas vacuum pump Nash 2BE1 203 used in gas drainage trials, (b) the whole drainage control and monitoring system along the main gateroad.

8.1.1 Pilot gas drainage trials and data analysis

As required by the mine safety regulations, the pilot drainage trials were conducted as experimental work under continuous surveillance. Continuous automated gas drainage was not allowed by law and the gas extraction procedures were repeated for short periods of time and performance recorded and analysed. In addition to the mine's fixed monitoring network of gas sensors, the project had to provide additional sensors and follow a specified procedure during the drainage trials. Figure 8.6 presents the layout of the drainage boreholes drilled at longwall face F k.-65.

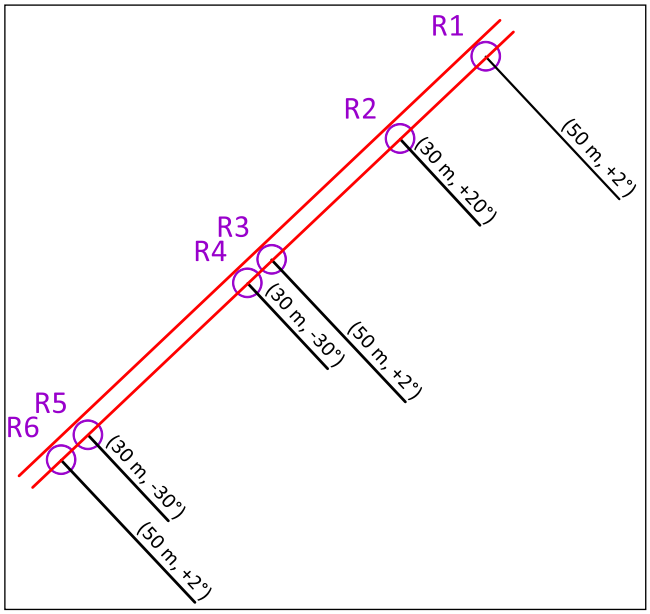


Figure 8.6: Detailed layout of the drainage boreholes at longwall face F k. -65.

Table 8.2: Details of the drainage cycles implemented and the performance achieved during the pilot trials using boreholes R3 and R4..

Date	LW face position (m)	LW face distance to borehole (m)	Time trial started (h/min/sec)	Time trial ended (h/min/sec)	Duration (h/min/sec)	*Suction pressure (kPa)	*Concentration (vol %)				Total flow rate (m^3/h)	CH_4 flow rate (m^3/h)	CO_2 flow rate (m^3/h)	Air flow rate (m^3/h)
							CH_4	CO_2	Air	CH_4 in air				
Borehole R3														
27/02/2013	329.0	69.4					35.00	22.00	43.00	44.87	Less than detectable rate	Less than detectable rate	Less than detectable rate	Less than detectable rate
27/02/2013	351.2	47.2					37.00	24.00	39.00	48.68	Less than detectable rate	Less than detectable rate	Less than detectable rate	Less than detectable rate
11/03/2013	354.5	43.9					37.00	24.00	39.00	48.68	Less than detectable rate	Less than detectable rate	Less than detectable rate	Less than detectable rate
15/03/2013	367.2	31.8	10:35:50	10:36:30	00:00:40	-28.00	20.70	43.25	36.05	36.48	186.00	38.51	80.44	67.05
20/03/2013 10:35	367.2	31.8	10:42:10	10:53:00	00:10:50	-29.00	17.37	43.81	38.82	30.92	157.61	30.47	76.87	68.27
20/03/2013 10:42	377.0	31.0	11:10:10	11:20:00	00:09:50	-28.00	20.05	37.59	42.37	32.12	188.90	36.98	70.04	81.88
23/03/2013	379.0	29.0	09:54:40	10:35:10	00:40:30	-21.00	19.41	44.65	35.94	35.07	142.41	27.62	63.47	51.33
25/03/2013	386.0	22.0	09:09:10	09:39:50	00:30:40	-20.00	19.66	46.38	33.96	36.67	205.34	40.37	95.23	69.74
27/03/2013	388.0	20.0	10:27:00	10:46:40	00:19:40	-24.00	20.22	46.39	33.39	37.72	181.31	36.64	84.07	60.60
29/03/2013	394.0	14.0	08:40:50	10:29:40	01:48:50	-20.00	14.51	44.19	41.30	26.00	185.19	26.96	81.87	76.36
02/04/2013	396.0	12.0	08:50:00	09:20:20	00:30:20	-21.00	18.76	45.95	35.30	34.70	193.06	36.23	88.71	68.12
03/04/2013	399.0	8.0	08:41:50	12:20:40	03:38:50	-20.00	16.93	44.87	38.20	30.70	141.59	23.96	63.44	54.20
05/04/2013	402.5	4.5	09:36:00	09:39:00	00:03:00	-	2.30	5.80	91.90	2.44	50.00	1.15	2.90	45.95
Borehole R4														
20/03/2013	367.2	39.7	11:03:50	11:15:20	00:11:30	-31.85	19.16	42.20	38.64	49.58	131.36	25.04	55.19	51.12
27/03/2013	386.0	29.9	10:18:40	10:48:20	00:29:40	-22.77	20.21	41.70	38.09	53.07	153.30	30.85	63.82	58.62
29/03/2013	388.0	27.9	10:02:40	10:23:00	00:20:20	-20.34	21.94	44.56	33.50	65.49	149.00	32.69	66.40	49.91
02/04/2013 10:43	394.0	21.9	10:43:00	10:59:40	00:16:40	-23.67	20.03	37.03	42.94	46.64	167.84	33.52	62.03	72.29
02/04/2013 11:01	394.0	21.9	11:01:20	11:31:00	00:29:40	-18.58	17.25	36.98	45.77	37.68	164.96	28.49	61.02	75.45
03/04/2013	396.0	19.9	09:33:50	10:09:00	00:35:10	-21.72	18.61	36.86	44.53	41.79	172.97	32.34	63.88	76.76
05/04/2013	399.0	15.9	12:28:40	12:56:10	00:27:30	-22.84	18.33	37.74	43.93	41.72	154.59	28.01	57.96	68.62
08/04/2013	402.5	12.4	09:48:50	10:25:00	00:36:10	-17.13	20.16	41.45	38.39	52.51	139.83	28.32	58.03	53.48
10/04/2013	407.0	7.9	09:46:00	10:01:00	00:15:00	-0.29	14.79	41.42	43.80	33.76	60.33	8.93	25.02	26.38

*The suction pressure and gas concentrations listed are mean values obtained from the continuous monitoring data during the pilot drainage trials.

The drainage borehole R3 was designed to investigate the drainage/pre-drainage performance of in seam horizontal boreholes and drilled at +2° from the horizontal plane, and 50 metres long. Drainage borehole R4, on the other hand, aimed at investigating drainage from the floor, and drilled at -30° from the horizontal plane, and 30 metres long. Table 8.2 provides a detailed outline of the drainage cycles implemented and the performance achieved during the pilot trials using boreholes R3 and R4.

Trials with drainage borehole R3 were performed in 13 separate campaigns in relation to longwall face advance (Table 8.2). Initial trials, when the longwall face was over 44 metres form borehole R3, have recorded gas flow rates below detectable limits due to low permeability of the seam around the borehole. Figures 8.7 and 8.8 summarise the overall gas concentration and gas component flow rates at different dates as the longwall face moved towards the drainage borehole R3.

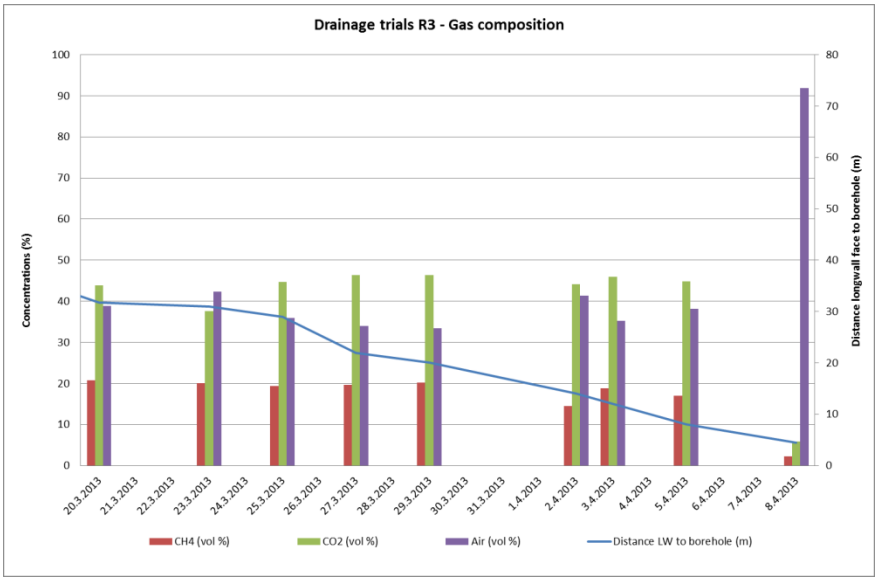


Figure 8.7: Gas concentration measurements in the pipeline during drainage trials in borehole R3.

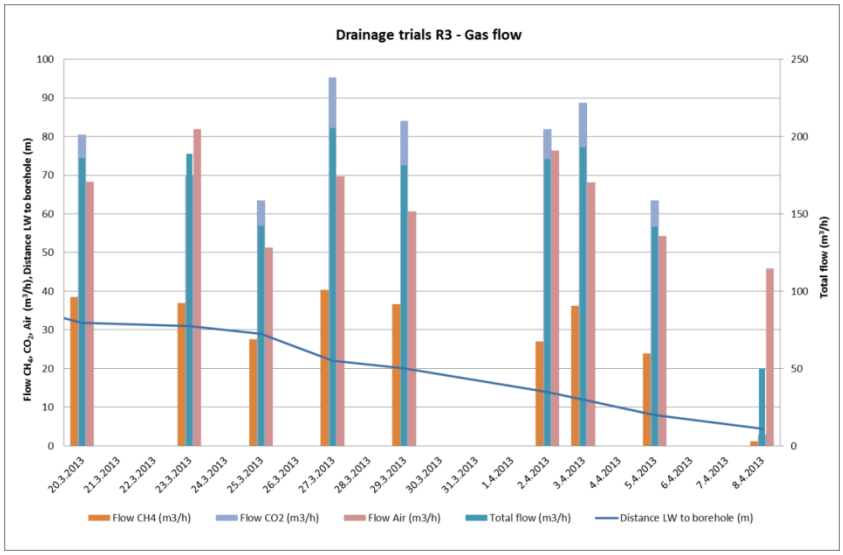


Figure 8.8: Flow measurements in the pipeline during drainage trials in borehole R3.

As the longwall face moved closer to the borehole, a slight increase in the CO_2 concentration and flow rate was observed. This was accompanied by a slight decrease in the CH_4 levels. It was also noted that the air concentration in the drained gas increased significantly due to leakage of ventilation air in to the borehole through enhanced fractures and permeability within the crushed zone towards the end of the trials when the longwall face reached within 5 metres of the R3 drainage borehole. As Figure 8.8 illustrates, the total flow rate of drained gas varied between 141 to 205 m^3/h, reaching its highest value as the longwall face was around 20 metres from the borehole R3.

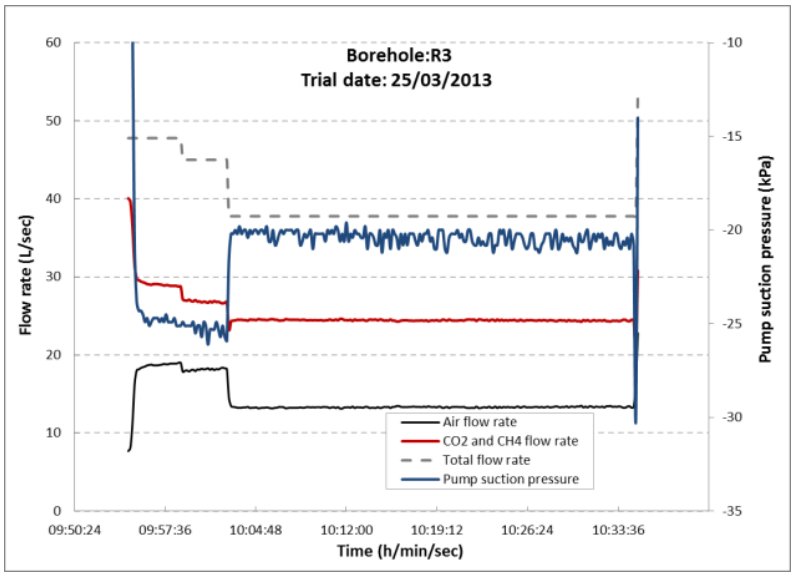


Figure 8.9: Flow rate response of different gas components to changes in the suction pressure in borehole R3.

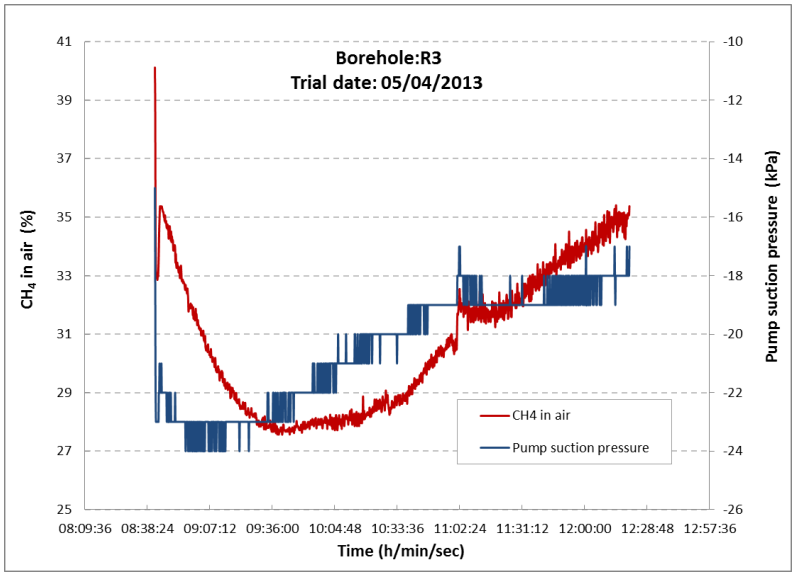


Figure 8.10: Flow rate response of different gas components to changes in the suction pressure in borehole R3.

Drainage performance of the individual boreholes were analysed closely and the effect of suction pressure on performance, especially the CH_4 concentration in the system, were investigated. Figure 8.9 presents the flow rate response of different gasses to the changes in suction pressure and distance from the longwall face in borehole R3. It was clear that

increased suction pressure increases the flow rate of air in to the borehole, thus the total gas flow rate in the system. In the same manner, lower suction pressures lead to an increase in the drained CH_4 concentration which needs to be kept significantly above the explosive range for safety, as well as drainage efficiency (Figure 8.10).

Trials with the drainage borehole R4 were performed in parallel to trials in R3, with some delay during the initial tests with R3. A total of 9 separate drainage tests were carried out while recording the longwall movement towards R4 (Table 8.2). Observations have shown lower average methane concentration compared to those observed in borehole R3 (14 – 22%), while the carbon dioxide concentrations were much closer. Once again, the total flow rate of gases in borehole R4 reached a maximum at around 20 metres distance from the longwall face.

Compared to the in-seam borehole R3, the length of R4 was limited to 30 metres (rather than 50 metres), which would have affected the area covered by the borehole, thus a lower gas drainage capacity observed. Figure 8.11 compares the performance of boreholes R3 and R4 (in-seam versus floor boreholes) per metre of borehole drilled. As also noted during the numerical modelling work in the frame of CoGasOUT project (Durucan et al., 2014), borehole R4 had an earlier production enhancement than R3, which occurred when the face was 40 metres away from R4.

This was most likely because the fractured zone in the floor coal covered a larger area ahead of the face compared to that of the panel being mined, confirming the accuracy of the predictions made by numerical modelling. Furthermore, the floor borehole R4 appears to be more efficient than R3 (longwall panel) in capturing CO_2 and CH_4. Given the same drilling length, the drained gas flow rates in borehole R4 were much higher than that in borehole R3.

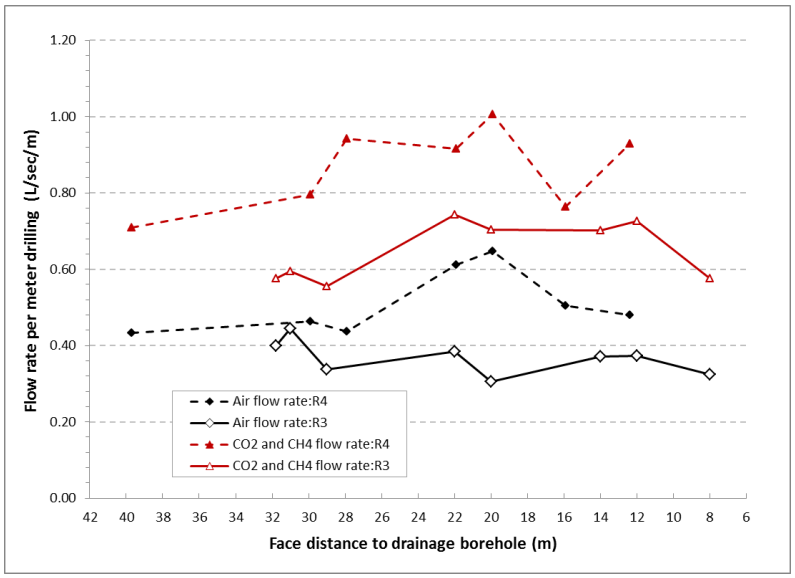


Figure 8.11: Borehole performance comparison between R3 and R4 .

This can be explained by the fact that the coal seam around borehole R4 may have been more severely fractured by the abutment stress and resulted in a much higher permeability. Unfortunately, Coal Mine Velenje experienced a number of rock burst incidents within close proximity of longwall panel F k. -65 during 2013, which resulted in premature abandonment of the district for safety. This limited the number of drainage

trials carried out at the mine. Nevertheless, one short trial was carried out with borehole R5, which was designed and drilled exactly same as borehole R4 as a floor drainage borehole. Unlike boreholes R3 and R4, drainage trials with R5 yielded a higher methane concentration compared to carbon dioxide. It was not possible to carry out further drainage trials with borehole R5 due to the rock burst incidents and the earlier than planned termination of production at longwall face F k. -65.

Along with single borehole drainage trials, 7 trials with multiple boreholes were also planned and 3 of these fully completed before the rock burst incident. As can be seen in Figure 8.12, the flow rates, as well as gas purity, rose significantly. This is believed to be the result of enhanced drainage performance due to draining a larger fractured area in front of the longwall face (up to 40 metres from the boreholes). Flow rate and purity of the gas components increased as the longwall face approached the boreholes.

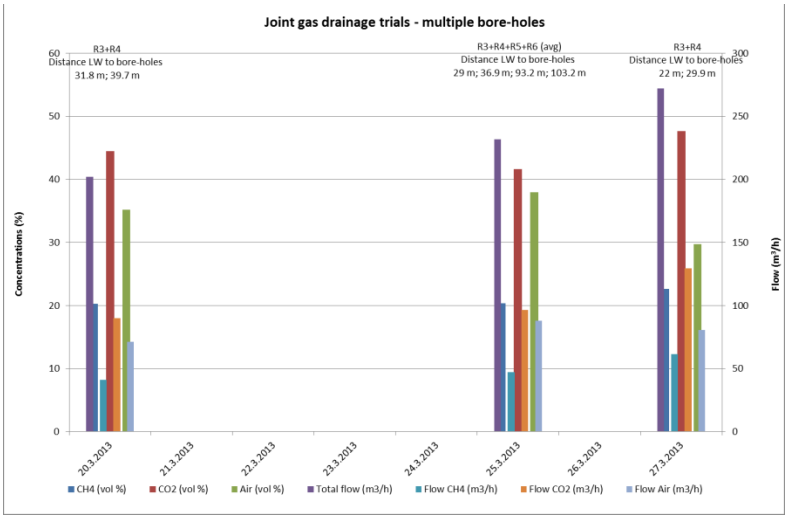


Figure 8.12: Gas concentration and flow rate measurements in the pipeline during multiple borehole drainage trials.

Borehole interference tests were conducted on 20th March, 2013, when the longwall face was 31.8m and 39.7m away from boreholes R3 and R4 respectively. The first two trials were single borehole trials with one borehole open and the other shut. R3 was open at the first trial and R4 was open for the second. Both trials lasted around 11 minutes. The third trial was a combined borehole drainage trial with both R3 and R4 open and operated for 10 minutes at the same suction pressure as the first two trials, which was -31 kPa.

Compared to the first single borehole drainage trials, the third trial with multiple borehole drainage has shown a considerable increase in the drained gas flow rate, which was 23.3% higher than that of R3 alone, or 85% higher than that of R4 on its own (Figure 8.13). Since the spacing between these two boreholes was only 8 m, competition in capturing the seam gas was clearly observed during the third trial. This was indicated by the gas flow rate of the third trial being lower than the sum of flow rates for R3 and R4 alone, which would have been nearly 50 l/s.

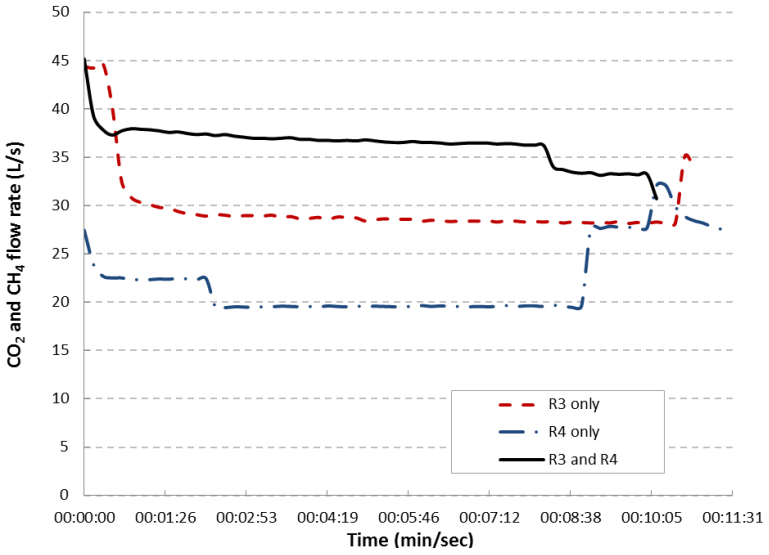


Figure 8.13: Flow rates of drained gas during borehole interference testing (CO_2 and CH_4).

At Coal Mine Velenje, the pilot gas drainage trials were designed and successfully implemented at the longwall panel F k. -65. The procedure followed aimed at evaluating the performance of drainage boreholes drilled at different angles in to the longwall panel, top coal and floor coal, as well as evaluating the effect of suction pressure, borehole length and spacing. The analysis of the results have suggested that gas drainage at Coal Mine Velenje is feasible and should help reduce the risk of gas outbursts if successfully applied in draining the floor area of a LTCC face (the top coal for the next level LTCC faces).

8.2 Full scale gas drainage trials (Longwall panel D k. -65)

At Coal Mine Velenje, full scale drainage trials at Longwall panel D k. -65 followed a limited number of preliminary single borehole drainage trials at longwall face F k. -65. In the previous single borehole drilling, the borehole lengths used were maximum 50 metres. In case of longwall panel D k. -65, lengths of six drainage boreholes were extended up to 70 metres (Figure 8.14), but with same structure as in initial trials (Figure 8.3). Furthermore, these demonstration trials were extended to run continuously throughout the three production shifts.

Gas drainage trials targeted the longwall panel (coal seam) and goaf gas drainage and excluded neighbouring rock formations (clay in the roof strata). Designed drainage boreholes were all drilled in coal in relative positions according to geometry of excavation panel D k.-65 F in Mine Pesje. Various directions and depths of drilling were chosen for analysis of drainage performance when active in different sections of the coal panel with respect to the longwall face position.

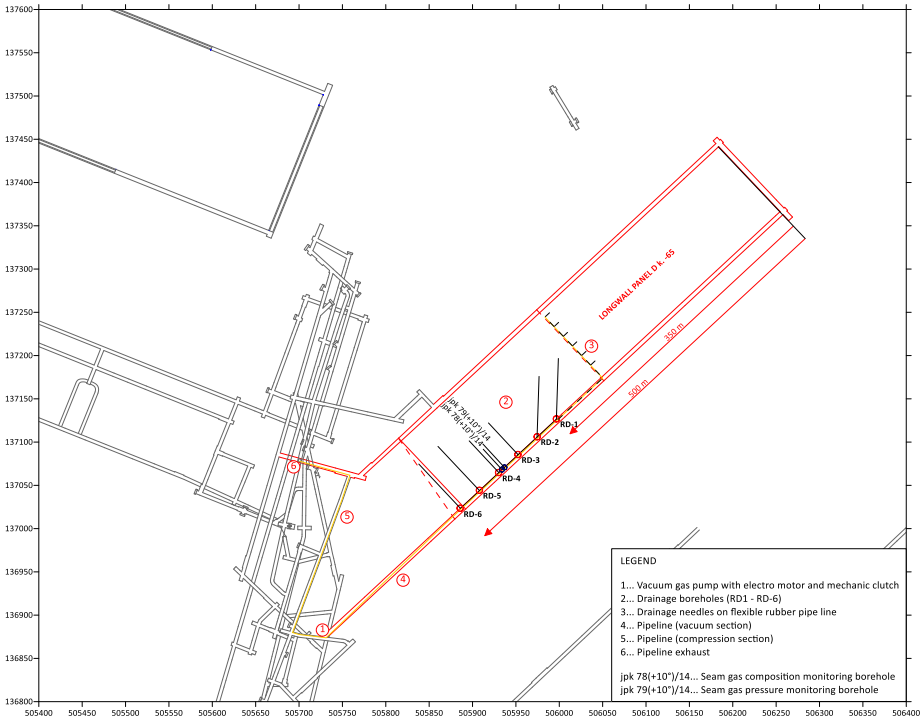


Figure 8.14: Longwall panel D k. -65 outline with main gas drainage installation locations.

Table 8.3: Drainage bore-hole design parameters.

Bore-hole	Y	X	Azimuth (°)	Inclination (°) (from horizontal)	Length (m)
RD-1	505,996	137,126	2	-30	70*
RD-2	505,974	137,106	2	-30	70*
RD-3	505,952	137,085	317	+5	50
RD-4	505,930	137,064	317	+5	50
RD-5	505,908	137,044	317	-5	70
RD-6	505,885	137,023	317	-5	70

The sequence of drilling (coring) included:

- drilling for primary casing (∅100 mm, re-drilled with ∅180 mm; depth 10 m),
- insertion of primary casing (∅169 mm steel tube; length 10 m; installed flange),
- cement coupling of primary casing with surrounding coal, cement coupling drying,
- technical column drilling (∅100 mm, until final depth 30/50 m),
- insertion of perforated antistatic plastic drainage tube with installed flange,
- coupling and sealing of primary casing and technical column,
- borehole to pipeline connection installation.

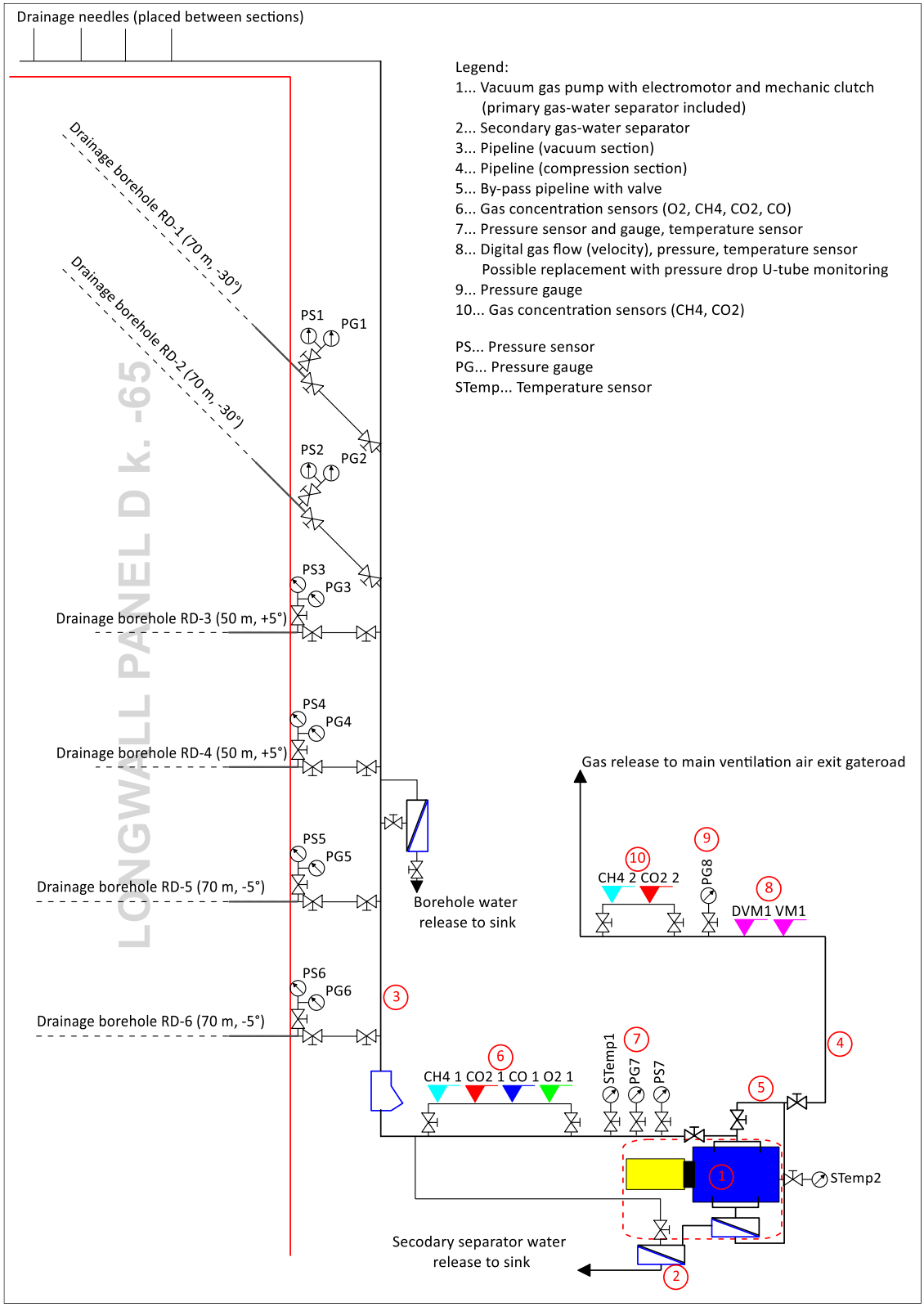


Figure 8.15: Gas drainage system at longwall panel D k. -65. Drainage includes boreholes in panel and steel perforated needles placed between sections of hydraulic shield support. Needles were placed in the goaf (behind shield support) for collecting released gas from consolidating coal.

The drainage pipeline was assembled from steel pipes, connected with flange and sealant. The whole length of pipeline was 670 m with diameter ∅100 mm (340 m vacuum section, 330 m compression section), with a separate section of adjustable ∅2" armoured rubber pipeline for steel needles on longwall face (Figure 8.15).

The vacuum pump (Nash 2BE1 203), used for gas drainage was a fully mechanical, water-cycle pump which was converted at the mine for use underground with the necessary additional technical documentation to meet the safety conditions and risk assessment. In order for safe working and data monitoring, further additional sensors and switches were installed on the pump and pipeline (Figures 8.16 and 8.17).

Goaf drainage system was designed as flexible armoured rubber pipeline attached to fixed main pipeline with connectors for drainage needles along longwall face (Figure 8.15). Needles were made from 2 meter ∅1" steel tubes with perforated ends to be placed in goaf behind sections of hydraulic steel shield supports

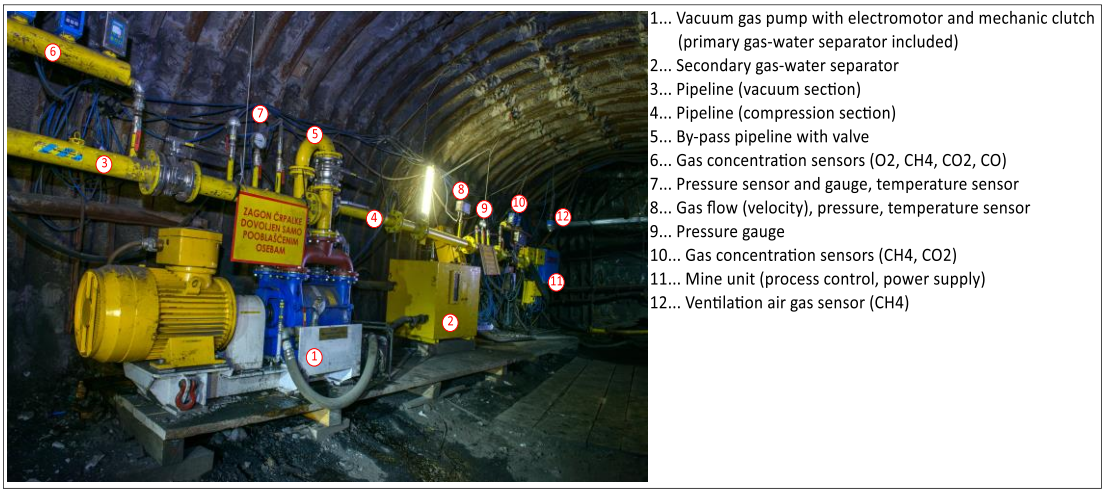


Figure 8.16: Gas drainage equipment configuration at longwall panel D k. -65.



(a) (b)

Figure 8.17: a) Drained gas concentration sensors (from left: CO_2 (0 – 100 %), CH_4 (0 – 100 %), CO (0 – 200 ppm)); b) Drained gas pressure and temperature monitoring (from left: pressure sensor (-1 to 1 bar), pressure gauge (-1 to 5 bar), temperature sensor (0 - 100°C)).

The gas drainage trials at longwall panel D k. -65 were carried out sequentially as continuous drainage, ultimately running throughout the 3 working shifts. When compared

to the gas composition and purity achieved in the preliminary trials, short term drainage with single boreholes, continuous drainage system produced a significant improvement in gas purity (~70%) and drainage efficiency in the whole system. The drainage trials showed most effective drainage from the upper part of the panel or the top coal, which is in contact with the isolative clay layer in 1st level mining. Drainage quantities when boreholes were most active averaged around 400 – 600 m^3/h with peaks at nearly 1,000 m^3/h.

One of the main segments for gas drainage in Coal Mine Velenje is the vacuum pump (Nash 2BE1 203), which was chosen according to its capacity, handling and costs (Figure 8.16). Nash 2BE1 203 is fully mechanical, water-cycle vacuum pump with certification for gas and petroleum industry use, therefore, additional technical documentation was required in order to define all safety conditions and risk assessment. The main parameters of vacuum pump Nash 2BE1 203 as listed by the manufacturer is presented in Table 8.4.

Table 8.4: Drainage bore-hole design parameters.

Nash 2BE1-203	
Power requirements (electro-motor)	P = 37 kW
Rated speed	N = 985 min-1
Speed (span)	N = 740 – 1300 min-1
Temperature of water (gas transfer media)	T = 0 – 65°C
Water (gas transfer media) flow	< 200 mbar; 2,6 m^3/h > 600 mbar; 0,9 m^3/h 200 … 600 mbar; 1,7 m^3/h
Allowed maximum vacuum pressure (absolute)	33 mbar
Allowed maximum compression pressure (absolute)	900 … 1100 mbar

Gas vacuum pump requires inflow of water as working media when in operation. Vacuum conditions are established with water cycle in pump rotor. As a result, a share of water is continuously transferred into compression section of the pipeline. As a prevention element, gas-water separator is installed between pump and compression section of the pipeline, followed by additional (secondary) separator. Level of water in secondary separator is controlled by constant outflow of water to sink (Figure 8.16).

8.2.1 Full scale gas drainage trials and data analysis

Gas drainage trials at longwall panel D k. -65 were planned to be carried out as full time drainage. Initial period of testing and setting was organized as one-shift work, which was followed by two- and three shifts work. Average effective time of gas drainage during a one shift trial was 5-6 hours, during two shifts 10-14 hours and during three shifts up to 20 hours of trial time. Below is the sequence of drainage trials carried out at longwall panel D k. -65. Contrary to pilot trials, full scale trials were oriented towards maximum gas drainage performance in order to provide results for further decisions about including gas drainage into working cycle of coal excavation process.

Full scale gas drainage trials were prepared and performed according to the timeline below:

- The equipment installation was completed by 16th January 2015, when test gas drainage started as short term trials under full supervision.
- A comprehensive technical and safety revision of drainage system took place on 20th January 2015.

- Drainage trials reconvened on 3rd February 2015 when authorised persons started with educative trials and equipment tests.
- From 3rd February to 23rd February 2015 the drainage system was operating in 1st shift, from 24th February to 3rd March in 1st and 2nd shifts and until temporary halt on 30th March in all three shifts.
- Gas drainage was stopped on 30th March due to return gateroad support repair work.
- Maximum drainage quantities during drainage trials reached 989 m^3/h (Borehole RD-3 closest to the longwall face, average ratio of $CO_2/CH_4 = 70/30$).
- Average drainage quantities during trials ranged between 200 and 600 m^3/h.
- As experienced in earlier gas composition monitoring campaigns, composition of drained gas mostly followed the same pattern. At distances between longwall face and activated borehole at about 30 – 25 meters from the face, methane concentration exceeded carbon dioxide concentration ($\sim CO_2/CH_4 = 35/65$). After the longwall face approached the drainage borehole, gas composition ratio changed in favour of carbon dioxide.
- Needles for longwall goaf gas drainage were also included in the system during trials with the use of 2 needles, followed by 4 and 6 needles in different sections of the longwall face. No efficient drainage of goaf gas has been recorded as gas mixture purity detected at gas sensors was very low.
- Calculations of drained gas volumes showed minor reduction of gas emissions at longwall face during production. Comparison during excavation of coal in areas without drainage and area of drainage showed reduction for 3 – 5%.
- Comparison between pilot and full scale trials showed improved drainage capacity by drainage borehole length enlargement. It is more like that distribution of drainage boreholes in both sides of panel with increased density in different orientations would increase drainage capacity and reduction of gas emissions on the longwall face.

Gas drainage trials required several organisational, safety technical and maintenance activities as the process is not defined by Slovene mining legislation. In Table 8.5, most important data, describing the organisation and chronology are presented.

Table 8.5: Chronology and organisation of full scale gas drainage trials (Longwall panel D k. -65).

	Time period	Boreholes	Other activities
Trials one shift	16.1. – 20.1.2015	RD-1 – RD-6	Equipment test, Safety revision
	21.1 – 2.2.2015		Instructions, Safety maintenance
	3.2. – 10.2.2015	RD-1 – RD6	Gas drainage, Longwall face drainage
	11.2. – 15.2.2015		Pump maintenance RD-1 Disconnected
	16.2. – 18.2.2015	RD-2 – RD-6	Gas drainage, Longwall face drainage RD-2 Disconnected
	18.2 – 23.2.2015	RD-3 – RD-6	Gas drainage,
Trials two shifts	24.2. – 3.3.2015	RD-3 – RD-6	Gas drainage, Longwall face drainage
Trials three shifts	4.3. – 9.3.2015	RD-3 – RD-6	Gas drainage, Longwall face drainage
	10.3. – 30.3.2015	RD-4 – RD-6	Gas drainage, Longwall face drainage

8.2.1.1 Data analysis for drainage trials carried out as one shift per day

Drainage trials until 10th February included all drainage boreholes and none of drainage needles at longwall face. Drainage was performed only in 1st shift with effective drainage time between 4 to 6 hours of operating the vacuum pump. Boreholes closest to the longwall face during this period were RD-1 and RD-2 which were drilled at an angle of 45° towards the longwall face with negative (-30°) inclination in order to capture seam gas which was being released from the floor section of the panel (Figure 8.15).

Average drainage rates ranged between 200 and 600 m^3/h with the same trend of gas composition as described earlier (Figures 8.18 and 8.19). When compared to the gas composition and concentrations experienced in the preliminary single borehole drainage data shown in Figure 8.7 earlier, it is clear that improved designs with longer term drainage was more efficient in draining higher purity (~70%) gas mixture).

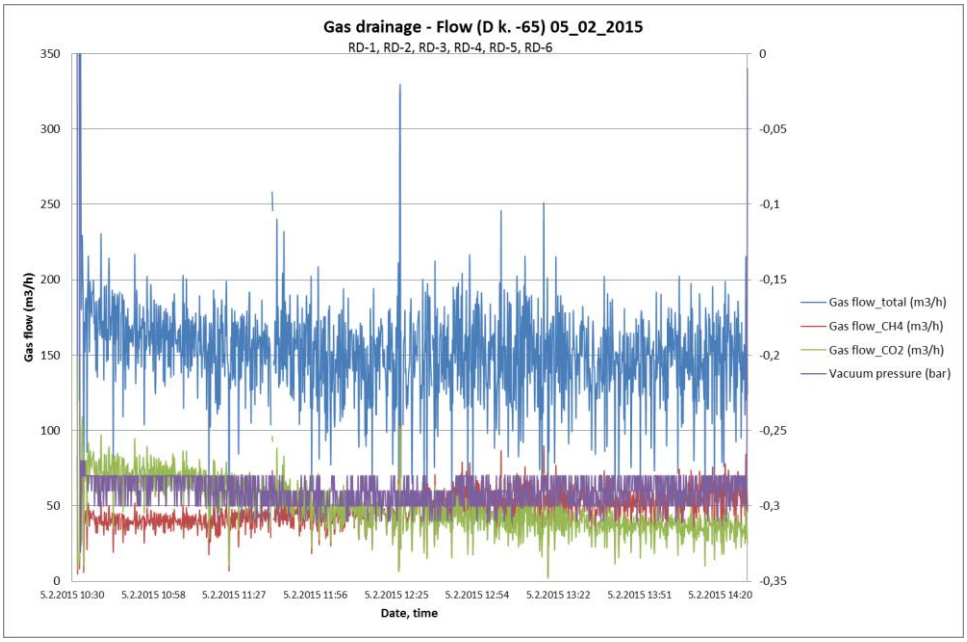


Figure 8.18: Gas flow analysis of trials by operating boreholes RD-1, RD-2, RD-3, RD-4, RD-5, RD-6 (1st shift drainage) at longwall panel D k. -65.

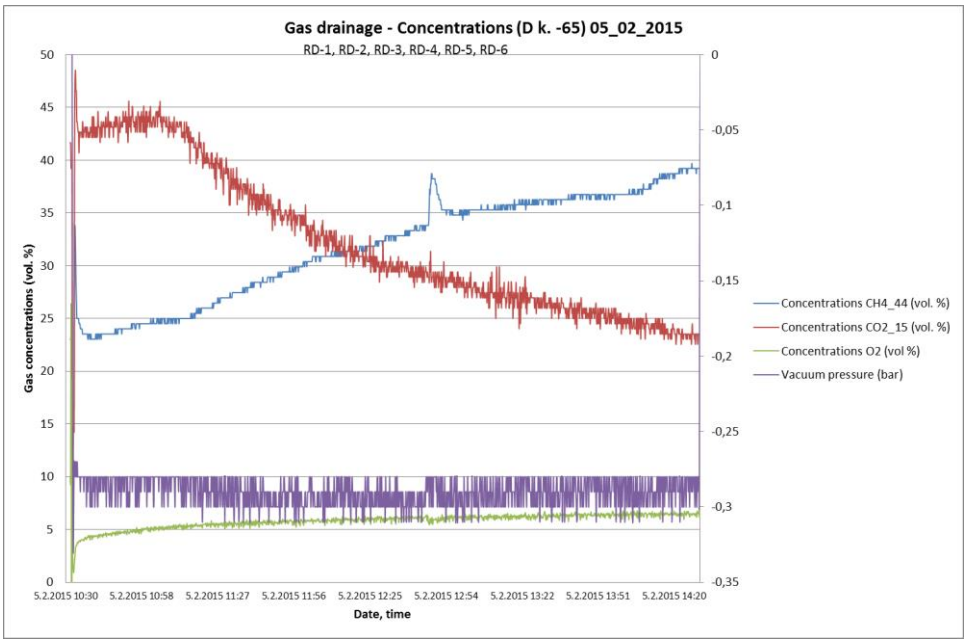


Figure 8.19: Composition of drained gas during trials of operating boreholes RD-1, RD-2, RD-3, RD-4, RD-5, RD-6 (1st shift drainage) at longwall panel D k. -65.

8.2.1.2 Data analysis for drainage trials carried out as two and three shifts per day

Most efficient drainage trials so far were after the activation of drainage borehole RD-3, which was drilled towards the contact between coal and clay overburden. Previous analysis of gas composition and gas pressure had shown an indication of increased gas accumulations around that contact. Drainage rates after the activation of borehole RD-3 have averaged at 400 – 600 m³/h and reached the maximum quantities of 989 m³/h, and

an overall efficient drainage performance. Similar efficiency was recorded during activation of borehole RD-4 (averages of 300 – 400 m³/h), Figures 8.20 and Figure 8.21.

At this period, the work schedule was extended to full time gas drainage and effective gas drainage time was increased to 3 shifts and average 20 hours, which increased daily gas drainage efficiency remarkably. Figure 8.22 and Figure 8.23 presents a detailed analysis of drainage achieved over three shifts in one day only.

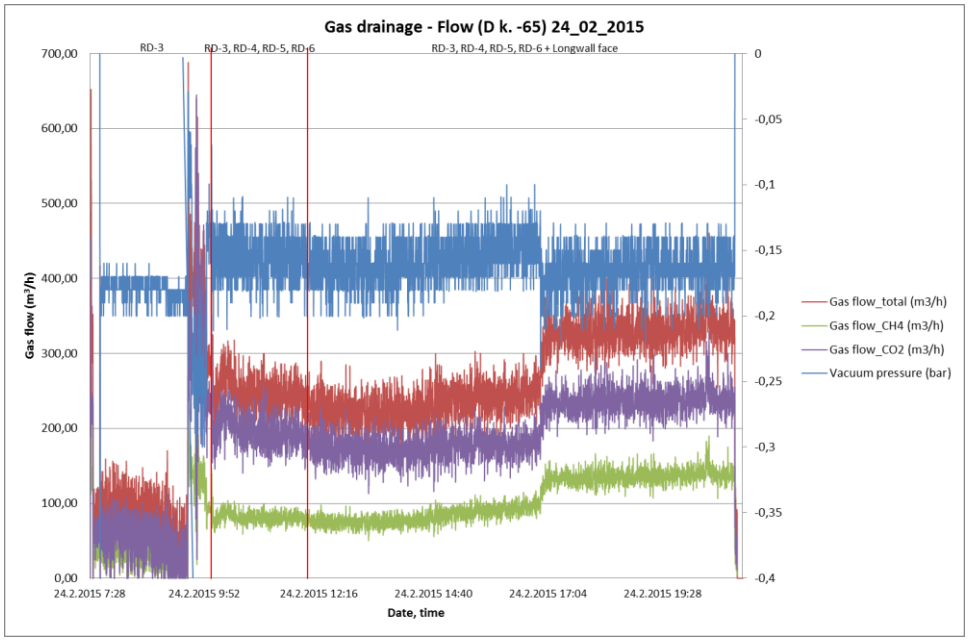


Figure 8.20: Gas flow analysis of trials of operating boreholes RD-3, RD-4, RD-5, RD-6 (1st and 2nd shift drainage) at longwall panel D k. -65.

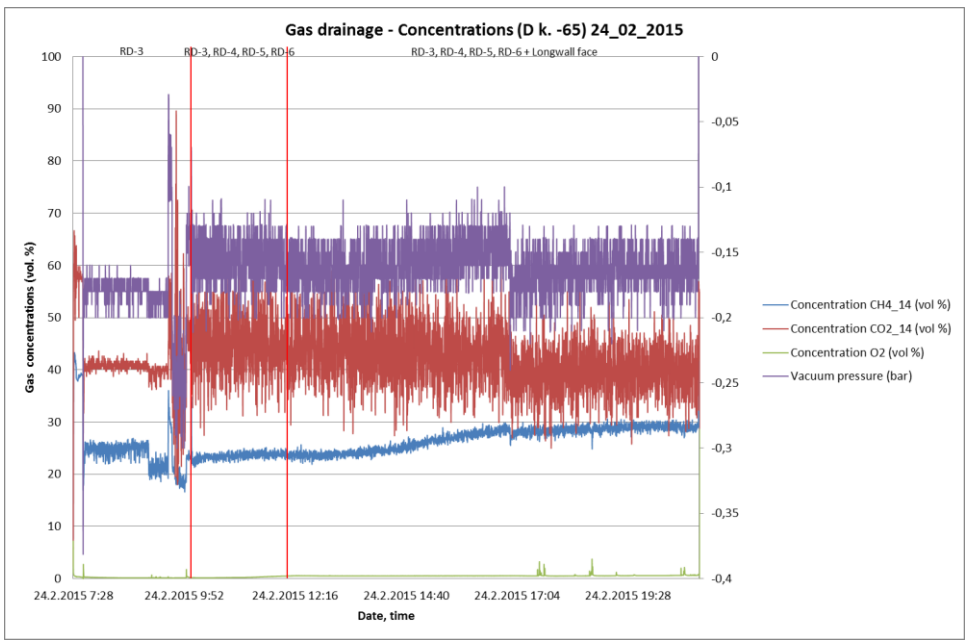


Figure 8.21: Composition of drained gas during trials of operating boreholes RD-3, RD-4, RD-5, RD-6 (1st and 2nd shift drainage) at longwall panel D k. -65.

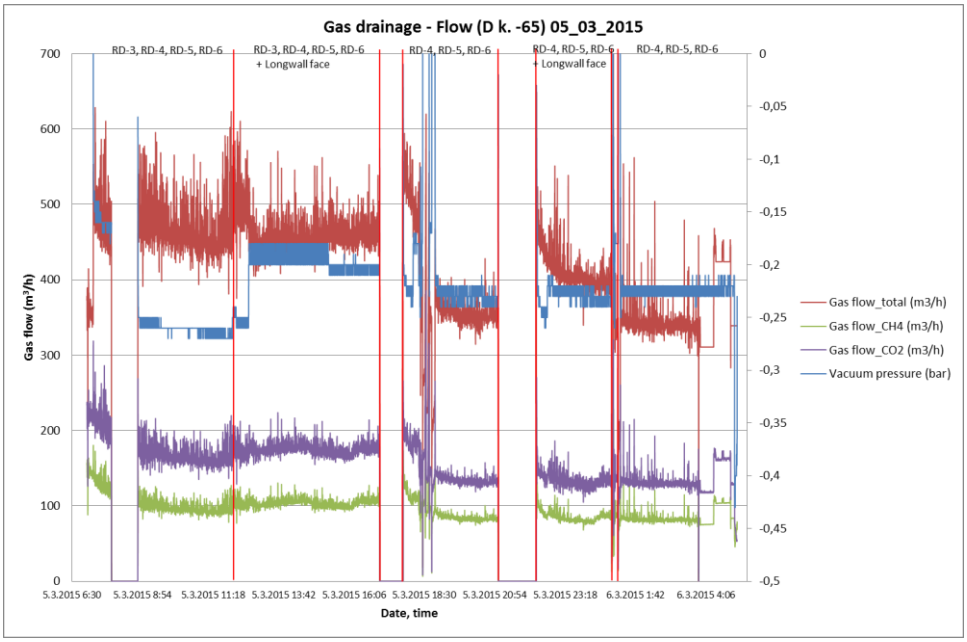


Figure 8.22: Gas flow analysis of trials of operating boreholes RD-3, RD-4, RD-5, RD-6 with activation of borehole RD-4 and longwall face needle drainage system (three shift drainage) at longwall panel D k. -65.

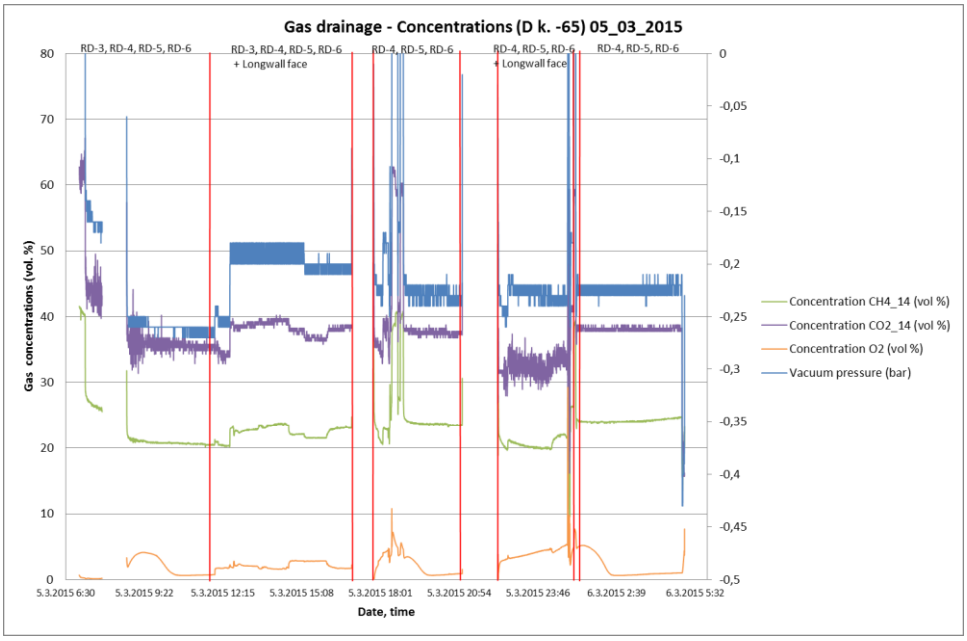


Figure 8.23: Composition of drained gas during trials of operating boreholes RD-3, RD-4, RD-5, RD-6 (three shift drainage) at longwall panel D k. -65.

8.2.2 Conclusions of full scale gas drainage trials

Gas drainage trials at longwall panel D k. -65 was designed to target a larger area of longwall panel and also sections above and below panel (longer boreholes and borehole's orientation).

Before drainage started, the gas concentrations at longwall face D k. -65 were exceeding the maximum allowed concentrations in most of working days, therefore, the selection of this panel for the demonstration trials was justified and most effective. The drainage boreholes were not tested as single boreholes, but were all connected to the drainage system during the trials. Therefore analysis refers to period of time when specific borehole was most active for the whole drainage system.

Drainage results showed most effective drainage from the upper part of the panel or the top coal, which is in contact with the isolative clay layer. Drainage quantities when boreholes RD-3 and RD-4 (borehole length 50 m) were most active averaged around 400 – 600 m^3/h with peaks at nearly 1,000 m^3/h.

Period of most active boreholes RD-1 and RD-2 (borehole length 70 m), which were drilled bellow the longwall panel with a 45° angle towards longwall face, provided relatively efficient drainage (200 – 400 m^3/h) from the solid floor, which would provide pre-drainage for the next (2^{nd}) level LTCC face.

Drainage needles at longwall face were placed between sections of hydraulic shied support with a purpose to collect gas that was released from goaf. In early stages, the system included two needles, followed by upgrade to 6 needles in part of the longwall face closes to the return gateroad, where gas concentrations were exceeding allowable limits. Preliminary results of needles' drainage performance showed no or low effect on gas concentration in the return gateroad.

Chapter 9

Conclusions

Gas composition, pressure and stress changes induced by multi-level coal extraction in LTCC faces have been investigated through borehole measurements at different mining levels of an ultra-thick coal seam at Coal Mine Velenje.

The monitored borehole gas concentration data suggested that the initial free gas at first level panels is predominantly CH_4. After pressure relief induced by mining in the upper levels, CO_2 becomes the primary gas component of the free gas in lower level panels. This is consistent with the knowledge that coal has a higher adsorption affinity to CO_2 than CH_4, and CO_2 is much strongly held in coal matrix and will not be released unless the seam gas pressure is reduced significantly.

As also confirmed by the mine's past experience, the first mining level is expected to experience the highest rate of gas emission both from the mined coal and the floor level due to high initial in-situ gas pressure. On the other hand, for LTCC panels operating at lower mining levels, gas inflow from both the floor coal and the roof goaf may form a considerable share of overall gas emissions. The concentration of CO_2 in the gas emitted to the ventilation air is expected to increase progressively as the mining reaches lower level of the ultra-thick seam.

Borehole monitoring carried out before the drainage trials have started has suggested that a near face fracturing zone, which is ~40 m ahead of a LTCC face, is believed to play a significant role in contributing to the gas emissions at the face. It was also confirmed that the gas emission into the LTCC face is very sensitive to the rate of fracturing experienced due to stress relief and the size of fractured zone in the floor coal at multi-level mining layouts.

In the frame of research projects CoGasOUT and GHG2E funded by the European Commission monitoring data obtained by the author once again confirmed the earlier observations that in virgin and moderately disturbed areas methane stored in the Velenje lignites readily releases and migrates due to mining associated stress and permeability changes, however, the CO_2 stored in the coal remains in the seam and requires further fracturing and significantly more enhanced flow paths in order to start its release and migration. Therefore, gas outburst risk at Velenje would be higher in areas of higher CO_2 concentration as the seam gas, as well as in areas of increased stress disturbance due to mining or geological features (Durucan et al., 2012; Durucan et al., 2013).

In general, in seam gas pressures measured in the boreholes varied between 4-6 bars gauge and an increased pressure zone is observed at around 70 to 30 metres from the face, after which the pressure started to decline and reached the flowing gas pressure at around 5 metres from the longwall face. In the case of borehole jpk 79 (+10°)/14, the monitoring borehole was surrounded by xylite (core log), which provides a locally isolated area, similar to those where gas is stored under even higher pressures and can cause gas outburst by affecting the sealing coal mass.

In conclusion, the pressure decline zone suggests extensive fracturing and failure of coal around the borehole due to changing stress conditions. This usually is accompanied by a sharp increase in stress measured in all the cells monitored, where the increased abutment stresses peak.

At Coal Mine Velenje, the pilot gas drainage trials were designed and successfully implemented at the longwall panels F k. -65 and D k. -65. The second gas drainage trials at longwall panel D k. -65 was designed to cover larger area of longwall panel and also sections above and below the panel (longer boreholes and borehole's orientation). In both cases the procedure followed aimed at evaluating the performance of drainage boreholes drilled at different angles in to the longwall panel, top coal and floor coal, as well as evaluating the effect of suction pressure, borehole length and spacing. The analysis of the results have suggested that gas drainage at Coal Mine Velenje is feasible and should help reduce the risk of gas outbursts if successfully applied in draining the floor area of a LTCC face (the top coal for the next level LTCC faces).

9.1 Main conclusions

The lessons learned from the drainage trials can be summarised as follows:

- Drainage pump suction pressure is of critical importance for drainage efficiency and increased gas purity. High suction pressure may lead to increased total drained volume, however this may compromise the purity of drained methane or CO_2 by increasing air leakage from the ventilation system. Further testing should aim at optimising the suction pressure applied.

Due to the low permeability of Velenje lignite, the initial total gas flow rate was too low to be measured unless the coal seam is highly fractured. The enhanced total gas flow rate ranged between 132 – 205 m^3/h in boreholes R3 and R4 throughout the period of pilot trials, while the original total gas flow rate was less than 3 m^3/h and very difficult to measure.

- The drainage trials and performance assessment have confirmed the role off stress and fracturing in increasing the permeability and flow rate of gas at some distance ahead of an advancing face.
- It was observed that enhanced permeability zone for horizontal in-seam boreholes in LTCC faces may start at around 30 metres from the longwall face, while -30° inclined floor boreholes may experience permeability enhancement as far as 40 metres ahead of the coal face.
- Drainage capacity of a single drainage borehole is largely dependent on the length of borehole and its perforated section.
- Given a same borehole length, more gas could be captured from the floor boreholes than that from the in-seam horizontal boreholes. Floor boreholes seem to have an advantage over horizontal boreholes in controlling seam gas since the former may benefit from a longer and higher permeability enhancement.
- Borehole interference has been observed from two neighbouring boreholes with 8 m spacing. Compared with single borehole drainage, increased total gas flow rate and decreased air concentration were observed when these two neighbouring boreholes were operated at the same time.
- Drainage results have shown that most effective drainage would be from the upper part of the panel or the top coal, which is in contact with the isolative clay layer. Drainage quantities when 50 m long boreholes were most active averaged around 400 – 600 m^3/h with peaks at nearly 1,000 m3/h.

- Drainage boreholes which were drilled bellow the longwall panel with a 45° angle towards longwall face provided relatively efficient drainage (200 – 400 m^3/h) from the solid floor, which would provide pre-drainage for the next (2^{nd}) level LTCC face.
- Joint analysis of borehole monitoring and drainage trials data has shown that drainage system efficiency depends on different coal properties and technical features as:
    - Distance between longwall face and nearest drainage borehole and influence on the following borehole,
    - Degree of fracturing at the coal panel (permeability ranges),
    - Length and orientation of drainage borehole,
    - Lithotype of coal,
    - Applied suction pressure,
    - Maintenance of the drainage system.

Research described in this thesis led to an improved understanding of the impact of longwall face advance on the seam gas flow behaviour around LTCC panels with respect to the distance to the face line. As a result, three distinct gas behaviour zones were defined:

- Zone 1 (longwall face > 40m away)
  Fractures in the longwall panel are not developed to the level of a connected network. Seam gas pressure measured represents (or close to) the in situ pressure. Coal permeability is low and gas drainage is confined to a limited region around the drainage boreholes.
- Zone 2 (longwall face between 40 – 5m from the face line)
  Fractures in the longwall panel are developed as a consequence of stress front affecting the relevant section. As stress is transformed into deformation the seam gas pressure is reduced, indicating enhanced permeability and gas flow through the fracture network created. Gas drainage efficiency is increased and reaches its maximum.
- Zone 3 (longwall face within 5m)
  The longwall panel in this section is significantly fractured, connections between drainage borehole and the longwall face are established, and consequently drainage efficiency is reduced as seam gas in the drained volume is replaced by ventilation air.

References

Ahsan, M. (2006). Gas flow and retention characteristics of coal seams for enhanced coalbed methane recovery and carbon dioxide storage. *Department of Earth Science and Engineering. Imperial College London, 225.*

Airey, E.M. (1968). Gas emission from broken coal: An experimental and theoretical investigation. *International Journal of Rock Mechanics and Mining Sciences 5, 475-494.*

Airey, E.M. (1971). A theory of gas emission in coalmining operations. Proc. 14th Int. Conf. Directors of Safety in Mines Research. Donetsk, USSR.

Balankin, A.S. (1997). Physics of fracture and mechanics of self-affine cracks. *Engineering Fracture Mechanics, 57(2), 135-203.*

Beamish, B.B., Crosdale, P.J. (1998). Instantaneous outburst in underground coal mines: An overview and association with coal type. *International Journal of Coal Geology, 35, 27-55.*

Brezigar, A (1986). Premogova plast Rudnika lignita Velenje. *Geologija – Razprave in poročila 28/29, 319-336.*

Broek, D. (1986). Elementary engineering fracture mechanics. *Springer.*

Cao, Y.X., He, D.D., Glick, D.C., (2001). Coal and gas outbursts in footwalls of reverse faults. *International Journal of Coal Geology 48, 47-63.*

Choi, S.K., Wold, M.B. (2002). Numerical modelling of outburst mechanisms and the role of mixed gas desorption. *CSIRO Petroleum ACARP Project No.C9023, December, Australian Coal Association Research Program. 37p.*

Curl, S. J. (1978). Methane prediction in coal mines. *Rep. ICTIS/TR 04. London: IEA Coal Research, 80 pp.*

Diaz A.M.B., Gonzalez N.C. (2007): Control and prevention of gas outbursts in coal mines, Riosa-Olloniego coalfield, Spain. *International Journal of Coal Geology 69, 253–266.*

USEPA (2009). Coal Mine Methane Recovery: A Primer. Retrieved from: https://nepis.epa.gov/Exe/tiff2png.cgi/P1004T87.PNG?-r+75+-g+7+D%3A%5CZYFILES%5CINDEX%20DATA%5C06THRU10%5CTIFF%5C00000511%5CP1004T87.TIF

Diamond W.P., Schatzel S.J. (1998). Measuring the Gas Content of coal: A Review. *International Journal of Coal Geology 35, 311–331.*

Diamond W.P., Schatzel S.J., Garcia F., Ulery J.P. (2001). The Modified Direct Method—A Solution for Obtaining Accurate Coal Desorption Measurements. *Proc. Int. Coalbed Methane Symposium, Tuscaloosa, Alabama, May 14–18, University of Alabama, Paper 0128, 331–342.*

Dubiński J. (1989). Sejsmiczna metoda wyprzedzającej oceny zagrożenia wstrząsami górniczymi w kopalniach węgla kamiennego. *Prace Naukowe Głównego Instytutu Górnictwa.*

Dunn, B. W., Vertical well degasification in advance of mining – a potential gas management method for reducing high gas emissions and outbursts. *International Symposium-Cum-Worksop on Management and Control of High Gas Emissions and Outbursts in Underground Coal Mines, Wollongong, 20-24 March, 2004, p. 267-275.*

Durucan, S. (1981). *An investigation into stress-permeability relationship of coal and flow patterns around working longwall faces.* (Doctoral dissertation).

Durucan, S., Edwards, J.S., (1986). The effects of stress and fracturing on permeability of coal. *Mining Science and Technology 3 (3), 205-216.*

Durucan, S., Ahsanb, M., Shi, J.Q. (2009). Matrix shrinkage and swelling characteristics of *European coals. Energy Procedia 1 (1), 3055-3062.*

Durucan, S., Korre, A., Shi, J.Q., Syed, A., Brenkley, D., Jozefowicz, R., …, Paulik, S. (2012). *Development of Novel Technologies for Predicting and Combating Gas Outbursts and Uncontrolled Emissions in Thick Seam Coal Mining,* Mid-term technical implementation report, CoGasOUT, RFCR-CT-2010-00002. London.

Durucan, S., Korre, A., Shi, J.Q., Syed, A., Brenkley, D., Jozefowicz, R., …, Paulik, S. (2013). *Development of Novel Technologies for Predicting and Combating Gas Outbursts and Uncontrolled Emissions in Thick Seam Coal Mining,* Annual Report, CoGasOUT, RFCR-CT-2010-00002. London.

Durucan, S., Korre, A., Shi, J.Q., Syed, A., Brenkley, D., Jozefowicz, R., …, Paulik, S. (2014). *Development of Novel Technologies for Predicting and Combating Gas Outbursts and Uncontrolled Emissions in Thick Seam Coal Mining,* Final Report, CoGasOUT, RFCR-CT-2010-00002. London.

Durucan, S., Korre, A., Shi, J.Q., Syed, A, Si, G., Jamnikar, S.,…, Zavšek, S. (2014). *Greenhouse Gas Recovery from Coal Mines and Coalbeds for Conversion to Energy,* Deliverable N. 4.1 Report on the field and laboratory experiments at Velenje. ENERGY.2010.5&6.2-1, London.

Durucan, S., Korre, A., Shi, J.Q., Syed, A, Si, G., Jamnikar, S.,…, Zavšek, S. (2014). *Greenhouse Gas Recovery from Coal Mines and Coalbeds for Conversion to Energy,* Final Report. ENERGY.2010.5&6.2-1, London.

Esterhuinzen, G.S., & Karacan, C.O. (2005). Development of Numerical Models to Investigate Permeability Changes and Gas Emissions around Longwall Mining Panel. Retrieved from: http://www.cdc.gov/niosh/mining/UserFiles/works/pdfs/donmt.pdf.

Farmer, I., Pooley, F., 1967. A hypothesis to explain the occurrence of outbursts in coal, based on a study of West Wales outburst coal. *International Journal of Rock Mechanics and Mining Sciences & Geomechanics Abstracts. Elsevier, 189-193.*

Friedel, M.J., Scott, D.F., Williams, T.J. (1997). Temporal imaging of mine-induced stress change using seismic tomography. *Engineering Geology, 46, 131-141.*

Gibowicz, S.J., Kijko, A. (1994). An introduction to mining seismology. *Academic Press: London, 397p.*

Gray, I. (1987). Reservoir engineering in coal seams, part 1-the physical process of gas storage and movement in coal seams. *SPE Reservoir Engineering 2 (1), 28-34.*

Griffith, A.A. (1921). The phenomena of rupture and flow in solids. *Philosophical transactions of the royal society of London. Series A, containing papers of a mathematical or physical character, 163-198*.

Hanson D.R., Vandergrift T.L., DeMarco M.J., Hanna K. (2002). Advanced techniques in site characterization and mining hazard detection for the underground coal industry. *International Journal of Coal Geology, V.50, Issues 1-4, pp. 275-301.*

Hargraves, A.J., Upfold, R.W. (1985). Aspects of laboratory simulations of instantaneous outbursts. *In: Green, A.R. (Ed.), Safety in Mines Research. A.A. Balkema, Rotterdam, pp. 129– 137.*

Hargraves, A.J. (1993). Update on instantaneous outbursts of coal and gas. *Proc. Australas. Inst. Min. Metall. 298 (2), 3 – 17.*

Harpalani, S. (1999). Compressibility of coal and its impact on gas production from coalbed reservoirs. *In: Amadei, Dranz, Scott, Smeakkie (Eds.), Rock Mechanics for Industry, 301-308.*

Lama, R.D., Bodziony, J. (1998). Management of outburst in underground coal mines. *International Journal of Coal Geology 35, 83-115.*

Jeromel, G. (2010). *Constitutive model of multiple hanging wall caving in underground coal mining*. (Doctoral dissertation).

Kanduč, T., Pezdič, J. (2005). Origin and distribution of coalbed gases from the Velenje Basin, Slovenia. *Geochemical Journal 39, 397-409*.

Kidybinski A. (1980). Significance of in situ strength measurements for prediction of outburst hazard in coal mines of Lower Silesia. *Proc. Symp. on the occurrence, prediction and control of outbursts in coal mines. Aust Inst Min Metall, Melbourne pp193–201.*

Kissell, F.N., McCulloch C.M., Elder C.H. (1973). The Direct Method of Determining Methane Content of Coalbeds for Ventilation Design. *U.S. Bureau of Mines, Report of Investigations 7767, 17 p.*

Kočar, F., Veselič, M., Ribičič, M., Mramor J. (1987). Kriteriji varnega odkopavanja premoga pod vodonosnimi plastmi v jamah RLV. *Interno gradivo, Titovo Velenje, Rudnik lignita Velenje.*

Kočar, F., Veselič, M., Ribičič, M., Mramor, J. (1989). Safety criteria of coal excavation under aquifer layers in Velenje Coal Mine. *Mining and metallurgy quarterly: periodical for geology, mining and metallurgy, 36, Vol. 2, 421-438.*

Kowalczuk, J., Szwejkowski, J. (1975). Relation between anomaly of seismic velocity and state of stress around geological structures. *Scientific Bulletins Academy of Mining and Metallurgy, No 467, Geology, p.2 (in Polish).*

Kormendi, A., Bodoy, L., Hermann, L., Dianisda, L., Kalman, T. (1986). Seismic measurements for safety in mines. *Geophysical Prospecting, 34, 1022-1037.*

Lenart, M. (1996). Velenjska odkopna metoda, RP – 36/95 LM, *Premogovnik Velenje*.

Likar, J. (1995). *Analysis of sudden outbursts of coal and gas in coalmines.* (Doctoral dissertation)

Lunarzewki, L.W. (2001). Gas Drainage Practices. *Coal Operators´ Geotechnology Colloquium, University of Wollongong & the Australasian Institute of Mining and Metallurgy, 34-44.*

Lurka A. (2009). Selected theoretical and practical problems of passive tomography in underground mining. *Prace Naukowe GIG (Sc. Work of GIG), nr 879 (in Polish).*

Majewska Z., Marcak H. (1989). The relationship between acoustic emission and permeability of rock under stress. *Mining Science and Technology, 9.*

Markič, M. (2009). *Petrology and genesis of the Velenje lignite* (Doctoral disertation).

McKavanagh, B., Enever, J., (1978). Developing a microseismic outburst warning system, *Proceedings of the 2rd conference on acoustic emission/microseismic activity in geological structures and materials. Pennsylvania, 211-225.*

Maxwell, S.C., Young, R.P. (1996). Seismic imaging of rock mass responses to excavation. *Int. J. Rock Mech. Min. Sci. Geomech. Abstracts 33, No.7, 713-724.*

Morcote, A., Mavko, G., Prasad, M. (2010). Dynamic elastic properties of coal. *Geophysics, 75(6), E227, doi:10.1190/1.3508874.*

Mutke, G. (2013). Registration of seismic foci under mining coal seam – The experience of polish mines. *Acta Geodyn. Geomater 10(2), 147–153*.

Noack, K. (1998). Control of gas emissions in underground coal mines. *International Journal of Coal Geology, 35(1-4), 57-82.*

Ozdemir, E. (2009). Modeling of coal bed methane (CBM) production and CO_2 sequestration in coal seams. *International Journal of Coal Geology, 145-152.*

Palmer, I., Mansoori, J. (1998). Permeability depends on stress and pore pressure in coalbeds, a new model. *SPE Reservoir Evaluation and Engineering 1 (6), 539-544.*

Pan, Z., Connell, L. D. (2012). Modelling permeability for coal reservoirs: A review of analytical models and testing data. *International Journal of Coal Geology 92 (2012), 1-44.*

Paterson, M.S., & Wong, T-F. (1978). Experimental rock deformation - The brittle field. *Berlin: Springer.*

Poliakov, A.N. B and Herrmann, H.J., Podladchikov, Y.Y., Roux, S. (1994). *Fractal plastic shear bands. Fractals, 1994. 2(04). 567-581.*

Rakovec, I. (1968). O mastodontih iz Šaleške doline. *Razprave IV. razr. SAZU, 11/8, 299-350.*

Ren, T., Edwards, J. (2000). Three-dimensional computational fluid dynamics modelling of methane flow through permeable strata around a longwall face. *Mining Technology 109 (1), 41-48.*

Rogers, R., Ramurthy, K., Rodvelt, G., Mullen, M. (2007). Coalbed Methane: Principles and Practices. *Oktibbeha Publishing Co. LLC.*

Schatzel S.J., Karacan C.Ö., Krog R.B., Esterhuizen G.S. and Goodman G.V.R. (2008). Guidelines for the Prediction and Control of Methane Emissions on Longwalls. *Department of Health and Human Services Centers for Disease Control and Prevention National Institute for Occupational Safety and Health Information Circular 9502, DHHS (NIOSH) Publication No. 2008–114.*

Scott, D.F., Williams, D. (2004). Geophysical methods to detect stress in underground mines. *Spokane Research Laboratory, NIOSH.*

Seher, A. (1995). Zgodovina premogovnika Velenje. 1. knjiga. *Velenje Coal Mine.*

Shi, J.-Q., Durucan, S. (2005). A model for changes in coalbed permeability during primary and enhanced methane recovery. *SPE Reservoir Evaluation & Engineering 8, 291-299.*

Shi, J.Q., Durucan. S. (2009). Exponential growth in San Juan basin Fruitland coalbed permeability with reservoir drawdown-model match and new insights. *SPE Reservoir Evaluation and Engineering 13 (6), 914-925.*

Si, G. (2015). *An investigation into gas emission and outburst control in thick seam coal mining,* (Doctoral dissertation).

Shepherd, J., Rixon, L., Griffiths, L. (1981). Outbursts and geological structures in coal mines: a review. *International Journal of Rock Mechanics and Mining Sciences & Geomechanics Abstracts. Elsevier, 267-283.*

Šercelj, A. (1968). Pelodna stratigafija velenjske krovnine plasti z ostanki mastadontov. *Razprave Slov. akad. znan. in umet., 4. razred, 11/8, 337-397, Ljubljana*.

Thill, R.E. (1973). Methods for Monitoring Failure in Rock. *University Park 14th Symposium on Rock Mechanics.*

Thoksoz, M.N., Cheng, C.H., Timur, A. (1976). Velocity of seismic Waves in porous rocks. *Geophysics Society of Exploration Geophysicists, V. 41, No.4, 621-645.*

Unver, B., Yasitli, N. (2006). Modelling of strata movement with a special reference to caving mechanism in thick seam coal mining*. International Journal of Coal Geology 66, 227-252.*

Wang, K., Xue, S. (2008). Gas Drainage Practices and Challenges in Coal Mines of China. *Coal Operators` Conference, University of Wollongong & the Australasian Institute of Mining and Metallurgy, 178-185.*

Watanabe, T., Sassa, K. (1996). Seismic tomography and its application to rock mass evaluation. *Int. J. Rock Mech. Min. Sci. Geomech. Abstracts 33, No.5, 467-477.*

Westman, E.C., (2001). A correlation between seismic tomography, seismic events and support pressure. *Rockmechanics in the National Interest, Tinucci & Heasley, 319-326, Swets& Zeitlinger*.

Westman, E.C., Heasley, K.A., Swanson, P.L. Paterson, S. (2001). A correlation between seismic tomography, seismic events and support pressure. *Proceedings 38th Rock Mechanics Symposium, Washington DS, July 7-10, 319-326.*

Whittaker, B.N. (1974). An appraisal of strata control practice. *Transaction if the Institution of Mining and Metallurgy, 134 (166), 9-24.*

Whittles, D.N., Lowndes, I.S., Kingman, S.W., Yates, C., Jobling, S. (2006). Influence of geotechnical factors on gas flow experienced in a UK longwall coal mine panel. *International Journal of Rock Mechanics & Mining Sciences, 43, 369-387.*

Wiejacz, P. (1994). The SMT software, Inst. Geophys. *Pol. Acad. Sc. (unpublished report).*

Wikipedia (2016).Retrieved from https://en.wikipedia.org/wiki/Category:Coal_mining_disasters_by_country

Williams, R.J., Weissman, J.J. (1995). Gas emission and outburst assessment in mixed CO_2 and CH_4 environments. *ACIRL Underground Mining Seminar Brisbane.*

Wold, M.B., Choi, S.K. (1999). Outburst mechanisms: coupled fluid flowgeomechanical modelling of mine development. *CSIRO Petroleum ACARP Project No.C6024, December, Australian Coal Association Research Program. 58p.*

Wold, M.B., Connell, L.D., Choi, S.K. (2008). The role of spatial variability in coal seam parameters on gas outburst behaviour during coal mining. *International Journal of Coal Geology 75, 1-14.*

Xia, Y. and Xu K. (2004). Engineering techniques of gas drainage under suction while driving gate roadways in an underground mine with serious outburst. *International Symposium-Cum-Worksop on Management and Control of High Gas Emissions and Outbursts in Underground Coal Mines, Wollongong, 20-24 March, 2004, 283-287.*

Xue, Z. (2005). Effects of coal matrix swelling on seismic wave monitoring of CO_2 in coal seams. *Coal and Safety, 26, 11-18.*

Yu, G, Vozoff, K, & Durney, D. (1993). The influence of confining pressure and water saturation on dynamic elastic properties of some Permian coals. *Geophysics, 58, No. 1, 30-38.*

Zavšek, S. (2004). *Model for research of structural and petrographical changes of the Velenje lignite depending on various stress states and presence of gases.* (Doctoral dissertation)

Zavšek, S., Richter, T., Pippig, U., Weller, A., Nordsiek, S., …, Lorenz, K. (2008). Results of the international PROINNO-EUREKA project VELGASPREVENT-EDITORIAL. *International workshop on Mine (Green-House) gases CO_2, CH_4, Mine Safety, Prevention, Managing and Utilization, Velenje, 91-99.*

Zhao, Y., Huang, J. and Wang R. (1993). Fractal characteristics of mesofractures in compressed rock specimens. *International journal of rock mechanics and mining sciences & geomechanics abstracts.*

Zheng, Z., Khodaverdian, M., McLennan, J.D. (1991). Static and dynamic testing of coal specimens. *SCA Conference Paper, No. 9120*.

Žerdin, F., 2003: Restructuring in Slovenian coal mines. – Prestrukturiranje premogovniškega gospodarstva v Sloveniji. *RMZ – Materials and Geoenvironment 50/2, 543-553.*

Bibliography

Publications Related to the Thesis

Si, G., Jamnikar, S., Lazar, J., Shi, J. Q., Durucan, S., Korre, A., Zavšek, S. (2015). Monitoring and modelling of gas dynamics in multi-level longwall top coal caving of ultra-thick coal seams, part I: Borehole measurements and a conceptual model for gas emission zones. *International Journal of Coal Geology, 144, 98-110.*

Si, G., Shi, J. Q., Durucan, S., Korre, A., Lazar, J., Jamnikar, S., Zavšek, S. (2015). Monitoring and modelling of gas dynamics in multi-level longwall top coal caving of ultra-thick coal seams, Part II: Numerical modelling. International Journal of Coal Geology, 144, 58-70.

Si, G., Durucan, S., Jamnikar, S., Lazar, J., Abraham, K., Korre, A., Shi, J. Q., Zavšek, S., Mutke, G., Lurka, A. (2015). Seismic monitoring and analysis of excessive gas emissions in heterogeneous coal seams. *International Journal of Coal Geology, 149, 41-54.*

Conference Paper

Jamnikar, S., Sedlar. J., Zavšek, S., Zadnik, I. (2015). Razplinjevanje odkopnega stebra in zarušenega dela za odkopom v Premogovniku Velenje. *Zbornik 12. znanstvenega posvetovanje rudarjev in geotehnologov ob 44. Skoku čez kožo, Ljubljana, 23-29.*

Jamnikar, S., Sedlar. J., Zavšek, S., Golob, L. (2012). Results of coal gas desorption experiments, laboratory sorption experiments on lignite samples and in-situ seam gas pressure - rock stress measurements. Proceedings of the *4th Jožef Stefan International Postgraduate School Students Conference, 25. maj 2012, Ljubljana, Slovenija, 22-32.*

Jamnikar, S., Sedlar. J., Zavšek, S., Golob, L. (2013). Execution and results of RFCS funded project CoGasOUT. *Proceedings of the 5th Jožef Stefan International Postgraduate School Students Conference, 22-31.*

Jamnikar, S., Zavšek, S., Lah, R. (2008). CO_2 and CH_4 drainage and utilization. Mine (green-house) gases CO_2, CH_4, mine safety, prevention, managing and safety, prevention, managing and utilization, International workshop Velenje '08.

Sedlar, J., Zavšek, S., Jamnikar, S., Žula J., Uranjek, G., Golob, L. (2011). Execution of RFCS CoGasOUT project. *4th Balkan Mining Congress, 18th-20th October 2011, Ljubljana, Slovenia, 681-686.*